AD-A185 003 NEARSHORE SAND TRANSPORT(U) CALIFORNIA UNIV SAN DIEGO 1/3
LA JOLLA T E WHITE 1987 N00014-75-C-0300

UNCLASSIFIED F/G 8/3 NL

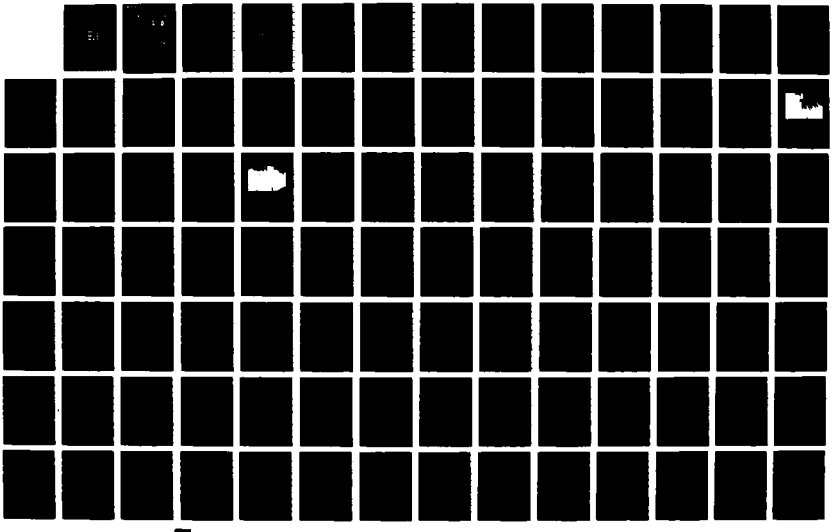

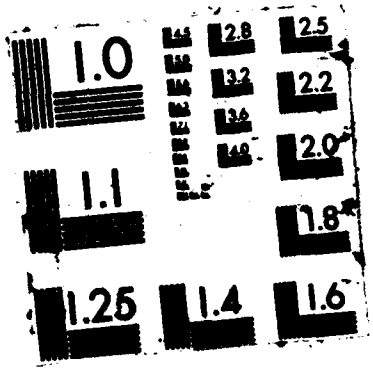
1.0
1.1
1.25
1.4
1.6
1.8
2.0
2.2
2.5
2.8
3.2
3.6
4.0

6

NEARSHORE SAND TRANSPORT

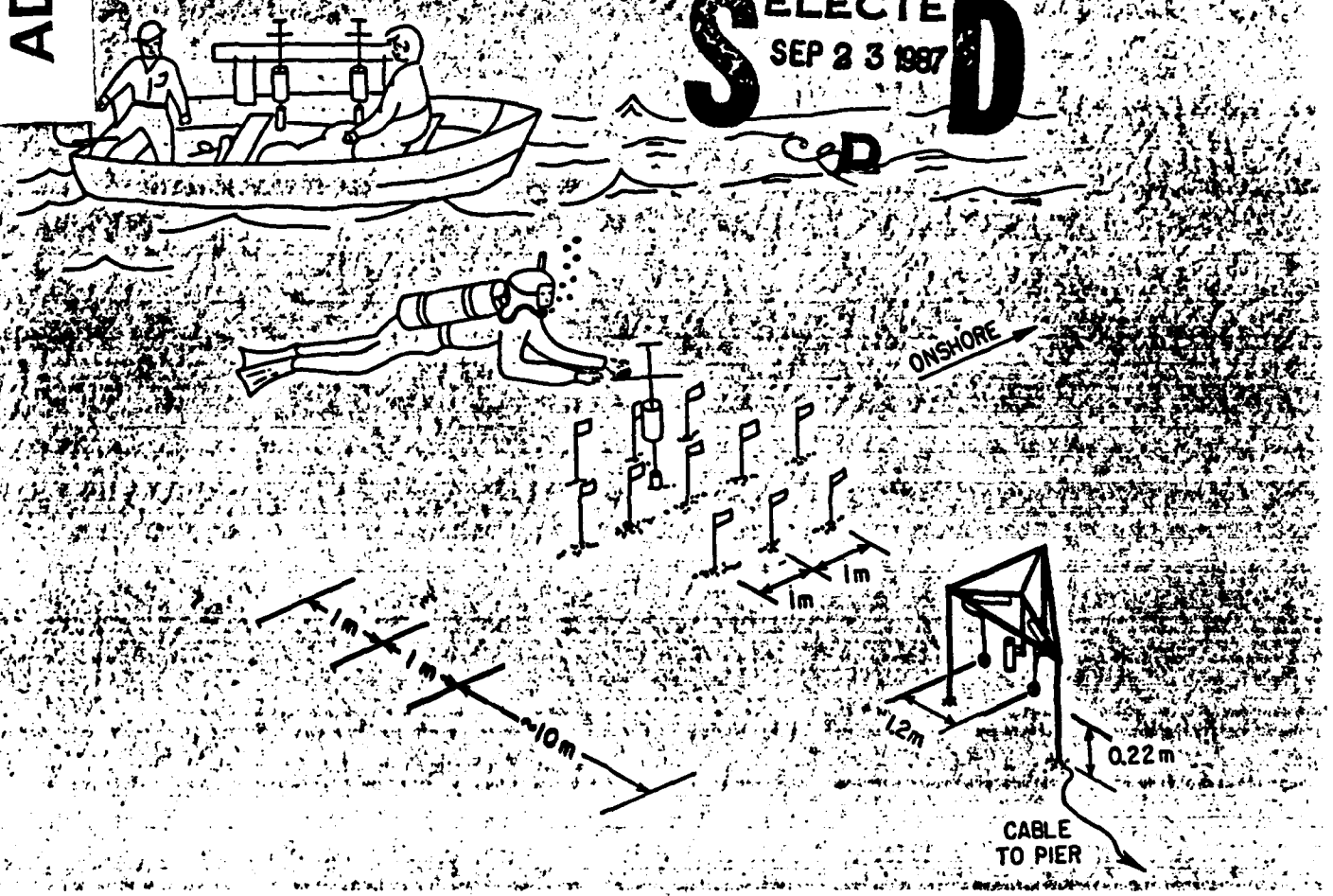

THOMAS E. WHITE

1987

UNIVERSITY OF CALIFORNIA

SAN DIEGO

Nearshore Sand Transport

A dissertation submitted in partial satisfaction of the requirements for the degree Doctor of Philosophy in Oceanography

by

Thomas Ellis White

Committee in charge:
Professor Douglas L. Inman, Chairman
Professor Joseph R. Curray
Professor Robert T. Guza
Professor Myrl C. Hendershott
Professor Daniel B. Olfe

1987

Contract N00014-75-C-0300

The dissertation of Thomas Ellis White is approved, and it is acceptable in quality and form for publication on microfilm:

Chairman

University of California, San Diego

1987

To Mom and Dad

TABLE OF CONTENTS

Section	Page
List of symbols	viii
List of figures	xii
List of tables	xiv
Acknowledgments	xvi
Vita and publications	xviii
Fields of study	xix
Abstract	xx
1. INTRODUCTION	1
1.1 Transport regimes	2
1.2 Transport kinematics	8
1.3 Bedload, suspended load, and total load	11
2. THEORETICAL CONSIDERATIONS	16
2.1 Tracer theory	16
2.1.1 Transport velocity	17
2.1.2 Transport thickness	20
2.1.3 Tracer recovery	25
2.2 Dimensional analysis	26
2.3 Bedload models	33
2.3.1 u^3 models:	37
Meyer-Peter and Mueller's unidirectional-flow model (1948)	37
Yalin's unidirectional-flow model (1963)	41
Bagnold (1963)	43

Bailard and Inman (1981) 48

Kobayashi (1982) 51

2.3.2 u^4 models: 53

Sleath (1978) 53

Hallermeier (1982) 55

2.3.3 u^5 model: 56

Hanes and Bowen's unidirectional-flow model (1985) 56

2.3.4 u^6 models: 59

Madsen and Grant (1976) 59

Shibayama and Horikawa (1980) 61

2.3.5 Other models: 62

Einstein's unidirectional-flow model (1950) 63

Einstein's oscillatory-flow model (1972) 65

3. EXPERIMENT 68

3.1 Sites 70

3.2 Instruments 75

3.2.1 Fluid measurement 75

3.2.2 Sand dyeing 81

3.2.3 Sand injection 84

3.2.4 Sand sampling 87

3.3 Experimental methods 87

3.4 Data reduction 94

4. RESULTS 96

4.1 Waves 96

4.2 Currents 100

4.3 Tracer controls 110

4.3.1 Matching tracer and in-situ sand 111

4.3.2 Tracer recovery 115

4.4 Transport thickness 118

4.5 Transport 127

5. DISCUSSION 134

5.1 Bedload model performances 134

5.2 Recommendations for using bedload models 153

5.3 Dimensional analysis model 155

6. CONCLUSIONS 163

7. REFERENCES 167

8. APPENDICES 175

Appendix 1: Measured vs. predicted transport 175

Appendix 2: Transport thickness 185

Appendix 3: Measured fluid velocity 192

Appendix 4: Energy spectra 195

Appendix 5: Transport thickness correlations 201

Appendix 6: Measured transport 204

Appendix 7: Computed transport 206

LIST OF SYMBOLS

Symbols from the Roman alphabet:

a	wave amplitude
C	wave phase speed
C_n	wave group speed
c_D	drag coefficient
c_f	friction coefficient
C_M	Madsen and Grant friction factor
c_{rb}	wave reflection coefficient
D	median grain diameter
d_o	wave orbital diameter
E	wave energy per unit area
F	number of dyed grains per dyed gram of sand
f_1	Sleath friction factor
g	acceleration of gravity
h	water depth
H	wave height
H_p	uncorrected wave height
i	immersed-wt. sediment transport per unit width
I	immersed-weight sediment transport
k	wave number
K	wave power coefficient
L	wave length
m_b	mass of moving sediment per unit bed area
m_b'	excess mass of moving sediment per unit bed area, $m_b' = m_b (\rho_s - \rho)/\rho_s$

M	mass of injected dyed sand
$N(x,y,z,t)$	number of dyed grains per gram of sand
N_{max}	maximum concentration of dyed grains in any slice in a sand core
N_o	solids concentration (sand volume/total volume)
P	normal stress in sediment
r	radius of sand core sample
R	Reynold's number, uD/ν
R_s	streaming Reynold's number, ud_o/ν
S	Strouhal number, d_o/D
t	time
T	wave period; also tangential stress in sediment
$U(t)$	sand velocity in x-direction
$u(t)$	instantaneous fluid velocity in x-direction
u_t	threshold fluid velocity at which sand motion begins
u_m	maximum orbital velocity
$u_T(t)$	total instantaneous fluid velocity, $u_T=(u^2+v^2)0.5$
$V(t)$	sand velocity in y-direction
$v(t)$	instantaneous fluid velocity in y-direction
W	fall velocity of sand
x	onshore spatial coordinate
y	longshore spatial coordinate
z	vertical spatial coordinate
Z_o	sand transport thickness

Symbols from the Greek alphabet:

α	angle of wave approach to beach
β	beach slope
δ	boundary layer thickness
Δz	thickness of a sand core slice
ϵ_b	bedload efficiency
ζ	angle indicating direction of fluid velocity in degrees clockwise from offshore
γ_s	specific weight of sediment in a fluid, $\gamma_s=g(\rho_s-\rho)$
θ	Shields' number, $c_f\rho u^2/[(\rho_s-\rho)gD]$
θ_t	threshold Shields' number at which transport is initiated
θ'	modified Shields' number ($\theta'=\theta/c_f$)
μ	fluid viscosity
ν	kinematic fluid viscosity, μ/ρ
Π	the dependent variable in dimensional analysis
ξ	Einstein's sand grain "hiding factor"
ρ	fluid density
ρ_s	sand density
σ	wave frequency, $2\pi/T$
ϕ	angle of internal friction of sediment also a measure of sand size

Φ	dimensionless sand transport, $i\rho^{1/2}[(\rho_s-\rho)gD]^{-3/2}$
Ψ	Einstein's fluid stress, $1/\theta'$
ω	rate of energy supply from fluid per unit area
Ω	rate of energy fluid expends transporting bedload
$\langle\ \rangle$	denotes time-averaged quantity

LIST OF FIGURES

Figure		Page
1-1	Transport regimes in the nearshore	4
1-2	Transition ripples in a sand bed at rest	5
1-3	Bursts of sand and normal carpet flow	10
2-1	Stresses acting on bedload	45
3-1	Experiment sites	72
3-2	Beach profiles at Torrey Pines	73
3-3	Beach profiles at SIO	76
3-4	Fluid sensors	80
3-5	Sand injection devices	85
3-6	Sand core sampler	88
3-7	Experiment layout	90
4-1	Transport thickness	120
4-2	Horizontal tracer distribution	128
8-1	Meyer-Peter & Mueller and Kobayashi models	176
8-2	Yalin model	177
8-3	Bagnold model and Bailard & Inman model	178
8-4	Sleath model and Hallermeier [illegible]	179
8-5	Hanes & Bowen model	180
8-6	Madsen & Grant model and Shibayama & Horikawa model	181
8-7	Einstein model	182
8-8	Reynold's number model and Shields' number model	183
8-9	Streaming Reynold's number model	184

8-10 Energy spectra at Torrey Pines 196

8-11 Energy spectra at SIO 197

8-12 Velocity spectra at Torrey Pines 198

8-13 Crosshore velocity spectra at SIO 199

8-14 Longshore velocity spectra at SIO 200

LIST OF TABLES

Table		Page
2-1	Variables used in bedload models	36
3-1	Characteristics of previous tracer experiments	69
4-1	Experimental conditions	97
4-2	Current velocities	101
4-3	Comparison of crosshore moments from redundant current meters	105
4-4	Effect of error in fluid-velocity measurement on predicted transport from models	107-109
4-5	Sediment size-distribution moments	112
4-6	Tracer controls	116
4-7	Correlation of orbital diameter with transport thickness	126
4-8	Fluid velocity correlations with transport	131
5-1	Sediment parameters	135
5-2	Coefficients used in transport models	137
5-3	Performance of bedload models	141-143
5-4	Conclusions on transport model performances	147-148
5-5	Nondimensional ratios of fluid-sediment parameters	157
5-6	Reynold's and Shields' number correlations with sediment transport	158-159
8-1	Summary of transport thickness from red tracer	186
8-2	Summary of transport thickness from grn tracer	187
8-3	Transport thickness estimates:	

red tracer at Torrey Pines 188

8-4 Transport thickness estimates:

red tracer at SIO 189

8-5 Transport thickness estimates:

green tracer at Torrey Pines 190

8-6 Transport thickness estimates:

green tracer at SIO 191

8-7 Fluid-velocity moments and transport 193

8-8 Velocity moment correlations with <u> 194

8-9 Correlation of Z_o with parameters from

surface-corrected wave heights 201

8-10 Correlation of Z_o with u_m from

current-meter measurements 202

8-11 Correlation of Z_o with d_o and u_T from

current-meter measurements 203

8-12 Crosshore transport 204

8-13 Longshore transport 205

8-14 Crosshore transport predicted by u^3 models 207

8-15 Crosshore transport predicted by u^4

and u^5 models 208

8-16 Crosshore transport predicted by u^6

and u^n models 209

8-17 Longshore transport predicted by u^3 models 210

ACKNOWLEDGMENTS

The experiments described herein would not have been possible without the more than 35 years of experience with sand-tracer experiments accumulated by Professor Douglas Inman. Procedures and techniques for dyeing, sampling, and counting sand were devised by Dr. Inman in the 1950's. Analytical procedures and instrumentation were developed and improved on over the following decades.

Dr. Inman also attracted many qualified personnel to the laboratory who developed the expertise necessary to mount field experiments in the surf zone. In particular, for this study many scuba divers braved horrendous conditions to obtain sand samples, often at risk to their health: Bill Boyd, Mike Clifton, Phil D'Acri, Jim DeGraff, Mike Freilich, Dan Hanes, Paul Harvey, Russ Johnson, Bill O'Reilly, Joe Wasyl and most especially Walt Waldorf.

Bill Boyd and Farhad Rezvani maintained the instruments and data recording. Murray Hicks helped in the field work on several occasions. Melinda Squibb provided essential help with computer programs on numerous occasions. Mike Clark drafted several of the figures.

The tedious and thankless job of counting dyed sand grains was performed by Paul Harvey, Russ Johnson, Dave Richardson, Joe Wasyl, and Jim Zampol.

These experiments would not have been possible without the loan of several instruments from other projects by Bob Guza and Scott Jenkins.

Finally, frequent and valuable advice on all aspects of this project was provided by Bob Guza, Douglas Inman, Scott Jenkins, and Dave King.

This research was supported by the Sea Grant National Sediment Transport Study (Contract #R-CZ-N-4B) and the Office of Naval Research (Contract #N00014-75-C-0300).

VITA

Born November 19, 1956 - Peoria, Illinois

1978 B.S., Civil Engineering, University of Miami, Coral Gables, Florida

1978 B.S., Physics, University of Miami

1978 B.A., German, University of Miami

1980 M.S., Oceanography, Scripps Institution of Oceanography, University of California, San Diego

1978-1985 Research Assistant, Scripps Institution of Oceanography, University of California, San Diego

PUBLICATIONS

Inman, D.L., J.A. Zampol, T.E. White, D.M. Hanes, B.W. Waldorf, and K.A. Kastens, 1980, "Field measurements of sand motion in the surf zone," Proc. 17th Coastal Engr. Conf., Amer. Soc. Civil Engrs., p 1215-1234.

White, T.E., 1984, "Nearshore bedload transport of sand," EOS, Trans., Amer. Geophysical Union, v 65, n 45, p 956.

White, T.E., 1986, ".6 Sediment Transport Modes" and ".7 Sediment Sinks" in Southern California Coastal Processes Data Summary (by D.L. Inman, R.T. Guza, D.W. Skelly, and T.E. White), US Army Corps of Engrs., LA District, Los Angeles, CA, Ref. No. CCSTWS 86-1, 572 pp.

White, T.E. and D.L. Inman, 1987, "Application of tracer theory to NSTS experiments," Chapter 6B of the National Sediment Transport Study Monograph, R.J. Seymour, editor, Plenum Pub., New York.

White, T.E. and D.L. Inman, 1987, "Measuring longshore transport with tracers," Chapter 13 of the National Sediment Transport Study Monograph, R.J. Seymour, editor, Plenum Pub., New York.

FIELDS OF STUDY

Major Field: Oceanography

Studies in Physical Oceanography
Professors R.T. Guza, M.C. Hendershott, J.W. Miles, W.H. Munk, J.L. Reid, R.C.J. Somerville, and C.D. Winant

Studies in Biological Oceanography
Professor M.M. Mullin

Studies in Chemical Oceanography
Professor J. Gieskes

Studies in Geological Oceanography
Professors G. Arrhenius, J.R. Curray, and D.L. Inman

Studies in Nearshore Processes
Professors R.T. Guza and D.L. Inman

Studies in Time Series Analysis
Professor R.A. Haubrich

Studies in Applied Mathematics
Professor S. Rand

ABSTRACT OF THE DISSERTATION

Nearshore Sand Transport

by

Thomas Ellis White

Doctor of Philosophy in Oceanography

University of California, San Diego, 1987

Professor Douglas L. Inman, Chairman

Sand transport in the nearshore occurs under oscillatory waves and steady currents, on rippled or flat beds, and as bedload or suspended load. Sand transport as bedload on nearly flat beds in shallow water outside the breakers is the subject of this study.

The appropriate variables necessary for computation of sediment transport are grouped into a few dimensionless force ratios using the techniques of dimensional analysis, forming a sediment transport model. Other investigators have proposed various bedload models relating fluid velocity and other parameters to transport. Seventeen different bedload models are classified, described, reduced to the same set of notation, compared, and tested against measured transport.

Field experiments measuring fluid velocity and sand transport were performed seaward of the breaker region. Fluorescent sand tracer was used to measure both

sediment-transport velocity and thickness. Techniques for dyeing, injecting, and coring sand were developed and tested. A total of 30 tracer experiments were performed under differing wave and sediment conditions.

Redundant instruments are used to estimate measurement errors in fluid velocity moments and sand transport. Recovery rates and size distributions of tracer were used to judge experiment quality and were comparable to previous studies in the surf zone.

Transport thickness is well correlated with orbital diameter but not wave height or fluid velocity. Different powers of the fluid velocity are compared with sediment transport. The lower velocity moments perform much better than the higher moments. Even more important than which lower-order moment is used to predict sediment transport is the accurate measurement of fluid velocity, particularly the mean flow. Use of a threshold criterion is essential in predicting whether the sand transport is onshore or offshore. Results suggest that the appropriate power of fluid velocity necessary for computing sand transport may itself be a function of the flow intensity.

Determining functional dependence of transport on quantities other than fluid velocity (sand size, sand density, transverse fluid velocity, peak wave period) requires a larger range of conditions than were present in these experiments.

1. INTRODUCTION

It has long been known that waves and currents move sand on beaches. Even the casual observer sees sand motion on many different time and spatial scales. Sand is moved back and forth with each wave. Berms and bars form and disappear. On many beaches, including the California beaches in this study, sand moves offshore in the winter and returns to form a subaerial berm in the summer. Geologists have attempted to describe these different morphological forms of sand accumulation but have been thwarted by the complex mixture of motions on so many scales.

Development of sediment-transport relations began by suggesting that longshore transport is proportional to the longshore component of wave energy (Scripps Institution of Oceanography, 1947). The U. S. Army Corps of Engineers (Beach Erosion Board, 1950) has used such a formulation, changing only the numerical coefficient in the model over the years. Many studies (Watts, 1953; Inman et al, 1968; Komar and Inman, 1970; Inman et al, 1980; Dean et al, 1982; Kraus et al, 1982; White and Inman, 1987b) have been performed to test the now well-known relation of wave properties and total longshore transport:

$$I = K\, E\, Cn \sin \alpha \cos \alpha \qquad (1.1)$$

where the wave parameters are energy E, group velocity Cn, and angle of wave approach at the breakpoint α.

The transport, I, in Equation (1.1) is an average quantity in both time and space. Although this relation yields the correct transport on average, it is now known that when it is applied to specific beaches under specific wave conditions it must be modified. The coefficient of proportionality K is not a constant, but depends on variables such as beach steepness and wave period (White and Inman, 1987b).

Because relation (1.1) averages over many of the temporal and spatial scales of interest, emphasis must be placed on understanding the underlying physics if the mechanics is to be understood. Specifically, the fluid forcing and resultant sediment transport must be measured on small temporal and spatial scales that can then be integrated to obtain larger-scale phenomena. One approach is to measure properties on scales smaller than the scales on which the wave and sediment properties vary substantially. That is the method used in this study: measure waves, currents, and sand motion in natural field conditions on sufficiently small scales that basic physical transport relations may be tested.

1.1 Transport regimes

Sand may form different morphological shapes in response to different energy levels and types of forcing. Only progressive oscillatory waves will be considered here.

The nondimensional forcing is given by the ratio of fluid stress to the force of gravity acting on individual sand grains, the Shields' number (Shields, 1936):

$$\theta = \frac{c_f \rho u^2}{(\rho_s - \rho) g D} \qquad (1.2)$$

This parameter was originally developed for steady flow, but has been used to describe conditions in oscillatory flow as well (Dingler and Inman, 1976). They used the wave orbital velocity amplitude u_m. However, since we measured the instantaneous velocity u(t), we use θ with the instantaneous u(t) throughout this study. As the flow becomes more energetic, the Shields' number for the flow increases, and the bedform type changes. In the nearshore Shields' number increases as depth decreases, both because wave height increases and there is less attentuation between the surface and the sea bed. The changes in energy level and transport regime as waves approach the shoreline are illustrated in Figure (1-1). Far offshore the bed is either flat or has remnant ripples from prior storms. As the Shield's number increases past some threshold value, the sand grains form vortex ripples, typically with wavelengths of tens of centimeters. The wavelengths and heights of the ripples are variable and a function of both fluid velocities and grain size (Inman, 1957). As the waves shoal, bottom velocities increase, and transition ripples are formed (Figure 1-2). As the waves shoal further, the ripples are entirely destroyed. Sand

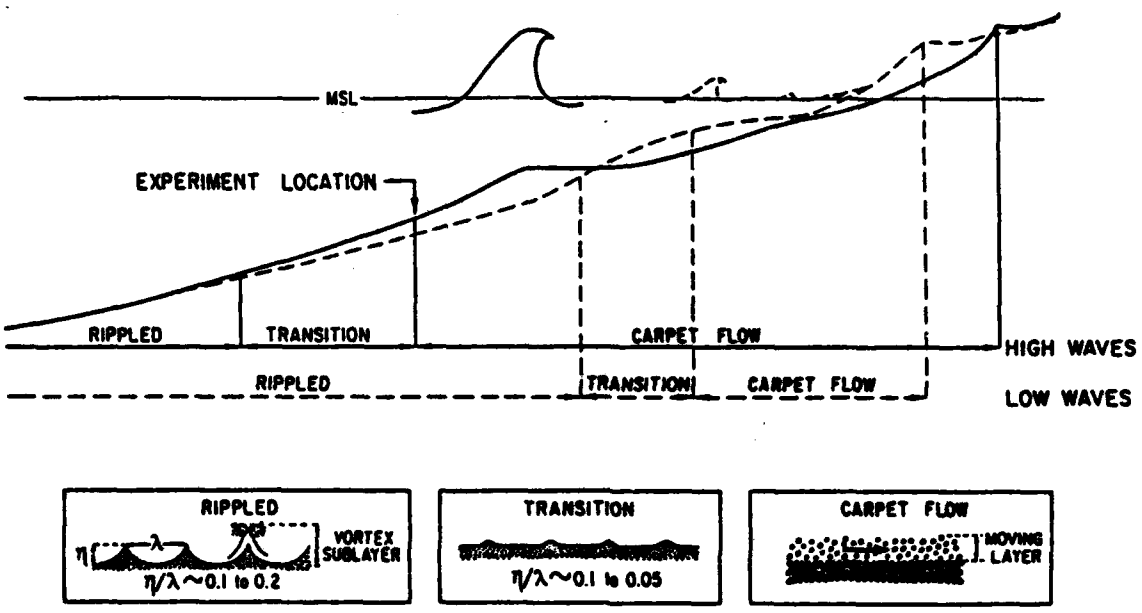

Figure 1-1. Transport regimes in the nearshore (from Inman, 1979). Experiments were performed at the boundary between transition flow and sheet flow.

Figure 1-2. Photograph of bed with transition ripples (from Inman et al, 1986). This type of topography was sometimes present during the experiments when the bed was not in motion.

then moves in what appear to be corrugated layers of densely packed granular-fluid. This type of transport has been referred to as "sheet flow" or "carpet flow." Large-scale bedforms with wavelengths of meters, such as dunes, anti-dunes, and bars, have also been observed under certain special conditions, but they were not observed during any of the experiments in this study. Their generation and behavior under oscillatory flow is poorly understood.

The experiments performed in this study were in the carpet flow regime. When the sediment was in motion (typically under long period swell) the sand bed moved as relatively flat carpet flow. However, once the wave crest passed and the sand settled back to the bed, the grains would typically reform into transition ripples. These experiments were performed outside the breakers where the sand moved as carpet flow and formed transition ripples at rest (Figure 1-1). Notice that the offshore location of this transport regime depends on the energy level of the waves.

Since the experiments took place in the carpet-flow regime, the quantitative description of this regime is important. Inman et al (1986) describe three different boundaries between types of flow: between no motion and the initial mobilization of sand grains (hereafter referred to as "threshold"), at the initiation of carpet flow, and

at the initiation of a very intense motion of the bed in flat sheets. The only one of these boundaries which we will use in computations is threshold. In this study we apply velocities in bedload models for all points in the time series during which sand is in motion (above threshold). Several investigators have formulated equations for the threshold Shields' number. We computed values from two different relations. The threshold velocities computed from the two methods differed by an average of 16%, but the predicted bedload transport differed by less than 1% once applied to various bedload equations (Section 5.1). Based on a transition-ripple study performed at the same beach as our experiments, Dingler and Inman (1976) expressed the threshold Shields' number necessary for initiation of transport as:

$$\theta_t = 0.065\ S^{0.6}\ R^{0.2} \qquad (1.3)$$

where $S = d_o/D$ is the Strouhal number and $R = \langle u \rangle D/\nu$ is the grain Reynold's number, and the coefficient 0.065 is between the values for the data sets of Bagnold (1946) and Dingler and Inman (1976). Seymour (1985) combined threshold Shields' numbers from three physically quite different relations and produced smooth curves joining the different relations. His curves were the second method used to compute threshold Shields' numbers for these experiments.

Henceforth it will be assumed that carpet flow is the type of transport measured in this study, since that is the transport regime observed during the times when the sand was in motion.

1.2 Transport kinematics

This study describes the modes of sediment transport from a dynamical approach, examining the relationships between the fluid forces and the resulting sand motion. Forces are averaged over many grain diameters and many wave cycles. Nevertheless, an understanding of the kinematics of transport, the details of the motion, is useful when examining the assumptions in the theoretical models and experimental methods to be described. Unfortunately, the details of the kinematics of carpet flow are not well known. Some kinematics inferred from visual observation of the flow are described below. However, complete description of the kinematics requires measurements of fluid and sediment flow within the boundary layer. For the preliminary results from such an investigation, the reader is referred to Inman et al (1986). The measurement of macroscopic flow parameters and test of macroscopic transport models in this dissertation do not require knowledge of the kinematic details.

The following is a description of the kinematics obtained from visual observations, which were part of this

study, and also appear in Inman et al (1986) in more detail. When waves of sufficiently long period and of sufficient energy occur over either a flat bed or the transition ripples of Figure (1-2), grains first begin to move at the onset criterion (Equation 1.3) followed by intense mobilization at spots spaced a few centimeters apart. The entire bed forms these cylinders of swirling sand and water of a few centimeters in height. The mobilization of the sand bed proceeds from these cylindrical spots to the entire bed after only a fraction of a second. The completely mobilized bed then appears to have a very uneven surface, which might be described as "tufts" and resembling a carpet. This type of flow is illustrated in the right-hand side of Figure (1-3). The mobilized sand is confined to within a few centimeters of the original at-rest bed level. If sufficient energy is present during acceleration, the bed may proceed during deceleration to what has been termed "bursting" in which the sand bursts above the carpet-flow level. Following bursting the grains are scattered over several ripple wavelengths, and the at-rest bed is essentially flat. In the absence of bursting, the mobilized grains move in an ordered orbit about 3-5 cm long which settles to the bed as transition ripples.

Inman et al (1986) suggest an analog between this visual sequence of granular-fluid events and the somewhat

Figure 1-3. Photograph of sand burst over remnant ripples (left) and normal carpet-flow within the boundary layer (right) [from Inman et al, 1986]. The burst is about 10-15 cm thick and the carpet-flow about 3 cm thick.

better understood problem of fluid flow in boundary layers. They detail the conditions and sequence of events during both carpet flow and bursting.

1.3 Bedload, suspended load, and total load

Conceptually, sand transport consists of two fundamentally different types of motion, bedload and suspended load. Bedload is a dense concentration of sediment mixed with interstitial fluid which moves along the bed within the boundary layer. Suspended load occurs as discrete sand grains moving in the fluid interior far from the bed. Bagnold (1954) determined the boundary between suspended and bedload to be at a sediment concentration of about 0.08 of total volume. The transport physics for the two modes are quite different, because of the greatly different sediment concentrations. In suspension, the individual grains have essentially no interaction with each other. On the other hand, bedload consists of such dense sediment concentrations that the grains continually collide with each other and move as an interacting body of sediment and fluid rather than as discrete particles (Bagnold, 1954; Hanes and Inman, 1985). The bedload measured in this study includes both the very densely packed "granular-fluid" material very close to the at-rest bed described by Bagnold (1954) and a projectile type of bedload motion usually referred to as "saltation."

In this study we have measured bedload transport and will test bedload models. Under the conditions in our experiments suspended load was not a significant transport mode. This assumption is supported by three observations which are described in detail below: (1) suspension was not observed by eye or camera, (2) suspension outside the surf zone has been shown by other investigators to be quite small compared to bedload (Fairchild, 1972), and (3) even if suspension were present, it would not be measured by the sand-tracer methods employed in this study.

On those rare occasions when suspension was visually observed, we purposely did not do an experiment. Significant suspension was observed to occur under two types of conditions, storms and large rip currents. Because of these imposed restrictions on experimental conditions, the transports measured here are not representative of the highest transport rates during storms or the lowest rates in a vortex ripple field. Rather than describe the entire range of transports outside the surf zone, our purpose was to measure bedload in carpet-flow conditions in order to test bedload models.

The most extensive measurements of suspended sediment transport outside the surf zone appear to be those of Fairchild (1972). He found concentrations by weight of suspended sediment several meters outside the surf zone to be about 0.00003 for half-meter mean wave heights. We can

convert this concentration to a transport rate and then compare it with transport rates measured in our experiments to determine the significance of the suspended component of transport. We first convert Fairchild's weight concentration of 0.00003 to a volume concentration of 0.000011 and then use the equation which converts volume concentrations to immersed-weight transport i (Crickmore and Lean, 1962b):

$$i = (\rho_s - \rho)\, g\, N\, U\, Z \qquad (1.4)$$

where N is the volume concentration of sediment, U the crosshore velocity of the sediment (and also of the fluid in the case of suspension), and Z the vertical distance over which the concentration was measured. Using Fairchild's concentration N over his Z=10 cm and the crosshore drift velocities in our transport experiments (0.3 to 8.5 cm/s) in Equation (1.4), we obtain a range of suspended transports of 0.05 to 1.5 dynes/(cm-s). The crosshore transports measured in our experiments ranged from 2.4 to 344.6 with a mean of 31.7 dynes/(cm-s). Under these assumptions, the suspended component is clearly a very small part of the measured transport.

Our final argument in excluding suspension from our experiments is the fact that even if significant suspension were present, it would not be measured by the methods used in our experiments. We injected dyed sand into the bed and monitored the motion of the tracer centroid with a grid of

core samples. Some argue that tracer grains may become suspended and then drop back to the bed prior to sampling of the bed, thus distorting the estimate of the tracer-centroid location. White and Inman (1987b) provide several arguments supporting the conclusion that devices which sample the sand bed will measure bedload and not suspended load. The most basic argument states that althought suspended concentrations are low, suspension velocities are about two orders of magnitude larger than bedload velocities. Thus suspended tracer grains will continuously move out of the sampling grid.

White and Inman (1987b) use the dimensions of their surf zone sampling grid to demonstrate that any tracer grain that spends more than 10% of its time in suspension will not be sampled in their grid of bed samples. The same calculations for the sampling grid in our experiments outside the surf zone show that grains which spend more than 7% of their time in suspension will move out of the grid before the first set of samples is taken. The cutoff percent for later sets of samples is even lower.

From the numbers presented above in the application of Equation (1.4) we conclude that in our experiments suspended transport was only about 1% of the bedload transport. In a case such as this it may then be argued that a measure of bedload is also a good measure of total transport, the sum of suspended and bedload transports.

Since we will be testing bedload models in this study, the question of whether our measurements are estimates of total load is moot. Nevertheless, there is some geological and engineering interest in the total crossshore transport rates which may be expected outside the surf zone. For those interested in such numbers, we submit that our measurements may be considered either bedload or total load, since the suspended component is so small.

2. THEORETICAL CONSIDERATIONS

2.1 Tracer theory

Monitoring the motion of dyed sand in order to determine the motion of in-situ sand has been a method used since the 1950's (Inman and Chamberlain, 1959). Such a method entails two basic assumptions: that the dyed sand behaves in the same manner as the natural sand and that the dyed sand's motion can be adequately monitored. Methods of evaluating these two assumptions will be detailed here. The extent to which our experiments fulfilled these two criterion will be examined in Section 4.

Sand transport will be expressed in terms of immersed weight of sand per unit width and unit time. The term "immersed" means that we will be using the effective weight, the dry weight of the sand minus its buoyancy in water. When we speak of crosshore transport, it will be motion across a unit width longshore. Longshore transport will be across a unit width crosshore. The determination of the two transport quantities, mass and velocity, can be accomplished by measuring two quantities known as transport velocity, U, and transport thickness, Z_o. The proper equation was first expressed by Crickmore and Lean (1962b):

$$\vec{i} = (\rho_s - \rho)\, g\, N_o\, \vec{U}\, Z_o \qquad (2.1)$$

where N_o is the volume concentration of sediment within the sand bed, equal to one minus the porosity. For typical wave-driven quartz beach sand it varies from about 0.50 to

0.65. Six sand samples from our experiments were examined for their solids concentration using a vacuum pump. N_o was found to be 0.60 with a standard deviation of 0.02.

2.1.1 Transport velocity

In principal the method of determining the sand's velocity is quite simple: the distance moved by the mass centroid of tracer is divided by the time between injection and sampling. Data consist of a number of discrete samples of the bed which yield measures of the tracer concentration at those points.

The manner in which these discrete concentrations are translated into sand velocities depends on the type of sampling grid. There are two basic types. The most common method has been referred to as "spatial integration method," "spatial grid," or "Lagrangian." It consists of a sampling grid spread over all three spatial coordinates but which is sampled at one point in time. Each of the discrete sample concentrations is first vertically integrated within the bed to obtain a set of concentrations $N(x,y,t')$ at each sampling time t'. The concentrations are then used to obtain the velocity in the x-direction (Crickmore and Lean, 1962a):

$$U(t') = \frac{\sum_{x,y} N(x,y,t') \frac{x}{t'}}{\sum_{x,y} N(x,y,t')} \qquad (2.2)$$

The velocities obtained are measures of the average sand velocity between the time of tracer injection (t = 0) and the time of sampling, t'.

When using Equation (2.2) care must be taken to justify the inherent assumptions of spatial uniformity. When computing the onshore (x-direction) velocity U(t'), it is assumed that transport is uniform in the longshore (y-direction) within the sampling grid. No topographical variations were observed within the 2 to 4.5 meter longshore extent of our grids, and we conclude that longshore uniformity is not a problem.

For grids used in previous tracer studies, the condition of spatial uniformity was often not met. Over the past 20 years, most tracer studies attempted to measure total longshore transport within the surf zone. Sand tracer was injected on a line across the surf zone. Sampling then occurred throughout the surf zone, both longshore and crossshore, at approximately one point in time. The longshore analog of Equation (2.2) was then applied:

$$V(t') = \frac{\sum_{x,y} N(x,y,t') \frac{y}{t'}}{\sum_{x,y} N(x,y,t')} \qquad (2.3)$$

In previous tracer studies (Komar, 1969; Inman et al, 1980; Kraus, Farinato, and Horikawa, 1981) it was either assumed that there was no variation in the crossshore (x-direction) or that such variation could be neglected. However, if

either V(t') or the crosshore sample spacing Δx were strongly functions of x, then the assumption of crosshore uniformity breaks down, and Equation (2.3) becomes invalid. In such a situation, the longshore transport velocity must first be computed at each crosshore location (White and Inman, 1987a).

Provided there is longshore uniformity within the sampling grid, Equation (2.2) provides a Lagrangian measure of the crosshore sand velocity. There is no need to assume crosshore uniformity within the grid in order to obtain this velocity. However, if this Lagrangian measure is to be combined or used in conjunction with other Eulerian quantities, then we must further assume crosshore uniformity within the grid. In fact, this is what has been done in our set of experiments, because the measures of waves and currents were obtained with Eulerian instruments (current meters and pressure sensors fixed at essentially one point in space). When we test bedload transport models, we will be using these Eulerian current measurements as inputs in the models and then compare the estimated transport with our Lagrangian sand transports. To justify this, we must assume spatial uniformity in the crosshore direction throughout the sampling grid. This is a much more restrictive assumption than the previously outlined one of longshore uniformity, for the simple reason that waves, currents, and topography are observed to vary

on smaller scales in the crosshore direction. Nevertheless, the crosshore extent of our sampling grid (6-8 meters) is still quite small compared to the scale on which significant crosshore variations in waves, currents, and topography occur. Care was taken to place the entire sampling grid outside the region of wave breaking. In no case were different topographical features ever observed at the two crosshore ends of the sampling grid.

The other type of possible tracer sampling grid is known as "time integration method," "temporal grid," or "Eulerian." In such a grid the sampling is spread in time but occurs at one crosshore location. Such grids were not attempted in this study because they require temporal uniformity during sampling. The requirement of temporal uniformity in an Eulerian grid was judged to be a much more difficult criterion to meet than the spatial uniformity requirement of a Lagrangian grid. The appropriate equations, assumptions, and limitations of Eulerian grids are detailed in White and Inman (1987a).

2.1.2 Transport thickness

A knowledge of the transport velocity is not sufficient to determine transport rates. The velocity must be multiplied by the mass of sediment in motion as indicated in Equation (2.1). This mass is the product of the thickness Z_o and the concentration of sediment N_o.

From conservation of sediment mass, we know that the product of concentration and thickness will yield the same value, regardless of whether the measurements are taken while sand is moving or at rest. In practice, it is far easier to measure both concentration and thickness at rest. The vertical concentration profiles of tracer within the sediment cores provide a record of the active sand layer. However, these vertical profiles must be made to yield a single objective estimate of the transport thickness. Various statistical estimators can be applied to the vertical concentration profile. The thickness estimates from all the core samples can then be averaged to yield a single estimate of average thickness during the experiment. We will now proceed to examine the various statistical estimators of this transport thickness. The reader may wish to refer to Figure (4-1) in the results chapter, which lists all of the following estimators and compares their behavior.

Estimates of this thickness have progressed from simply observing the depth of penetration of tracer within the core sample (King, 1951; Inman and Chamberlain, 1959; Komar, 1969) to objective semi-empirical estimators. Crickmore (1967) first applied an objective estimator of this thickness. His estimator gave realistic results only for vertical concentration profiles in which there is no increase of concentration with depth in the bed. After

modifying the concentrations in those horizontal slices of bed core samples, such that a given slice would have a concentration no smaller than the layer immediately below it (hereafter referred to as the "Crickmore profile"), the following estimator of transport thickness was applied:

$$Z_o = \frac{\sum_z N(z)\,\Delta z(z)}{N_{max}} \qquad (2.4)$$

where the summation is in the vertical, Δz is the vertical thickness of the horizontal slice, and N_{max} is the maximum tracer concentration in the core. Although Crickmore applied this method to transport in rivers, Gaughan (1978) later used this estimator in surf zone studies and found the desired result of relative uniformity of Z_o in time and space. The standard deviation of Z_o was equal to 42% of the mean in his fall/winter studies, 106% of the mean in his spring/summer studies, and 56% of the mean in our study (Figure 4-1). We confirmed Crickmore's observation that this equation yields realistic results only if applied to the "Crickmore profile." (When applied to the original profile, Equation (2.4) often yields values of Z_o far less than the observed location in z of the preponderance of tracer.) We also attempted a modification of Equation (2.4) by substituting the average concentration in place of the maximum concentration in the denominator, but found this often yielded values of Z_o far exceeding any penetration of tracer.

Observing the depth of maximum tracer penetration (King, 1951) overestimates Z_o. When a core tube is pressed into a sand bed, some tracer can be carried down the sides of the tube and later be counted at a greater depth than its in-situ depth. We believe that we have nearly eliminated this problem by removing the outer layer of core samples before determining tracer concentration. Sampling experiments have confirmed that more than 98% of the deeply penetrating tracer (>4 cm deep) has been removed from the cores by removing the outer 3 mm annulus. However, a few dyed sand grains are still present at greater than in-situ depths. If the maximum-penetration estimator of Z_o is used, these grains would completely determine Z_o. We therefore applied an estimator which equated Z_o to the maximum penetration of a concentration of 1.0 dyed grains per gram of sand (Inman et al, 1980), in an attempt to eliminate this problem. In analysis of our data, we have compared this estimator, a 0.5 grains/gram penetration estimator, and the maximum-penetration estimator.

Kraus, Farinato, and Horikawa (1981) applied an estimator which set Z_o equal to a depth of penetration of a certain percentage of the total amount of tracer found in the core. This selection was motivated by the observation that most of the tracer appears in the top few centimeters of the core. They plotted average Z_o from several cores versus the percent cutoff used to estimate it. The curve

was found to depart from linearity between 60 and 90% cutoffs. Their preferred estimator was the 80% cutoff. In order to observe and compare the behavior of this type of estimator with other methods, we computed 80 and 90% tracer cutoff estimates of Z_o.

Another objective estimate of Z_o was used by Inman et al (1980). This estimator was based on the fact that a completely uniform-with-depth distribution of tracer, which abruptly decays to zero at a certain depth, could be judged to have a transport thickness equal to that decay depth. The developed estimator yields perfect results for such a completely uniform vertical tracer distribution. This estimator is expressed as:

$$Z_o = 2 \frac{\sum_z N(z)\, z}{\sum_z N(z)} \qquad (2.5)$$

where the sum is taken vertically over the entire core, and z is the depth of the midpoint of each core slice. Equation (2.5) exhibits extremely aberrant behavior in the case of a "buried" profile. For example, consider the buried concentration profile which has the value zero to a depth z=d, N' between z=d and z=2d, and zero everywhere below. Equation (2.5) applied to such a profile yields Z_o = 4d, an obviously unrealistic answer. In order to solve this problem, we first changed the concentration profile to a "Crickmore profile" and then applied (2.5). Of course, with this method (2.5) will yield the same answer for both

uniform and buried profiles. For comparison, the experimental data were used to compute Z_o from (2.5) using both the original and "Crickmore" vertical concentration profiles.

2.1.3 Tracer recovery

One of the two basic assumptions in tracer methods, adequate monitoring of the tracer, may be tested by balancing the budget of tracer. If the sampling can account for most of the tracer, then the set of sand cores is considered to be a good sampling of the tracer distribution. The tracer in each core sample represents the concentration of tracer in a rectangular area surrounding the sample, the boundaries of the rectangle lying midway between sample points. This method of accounting for the amount of tracer recovered was first used by Inman and Chamberlain (1959) and has since been used in many tracer studies (Inman, Komar, and Bowen, 1968; Komar, 1969; Komar and Inman, 1970; Inman et al, 1980; Kraus et al, 1982; White and Inman, 1987a). However, some tracer studies are still performed without this check on the quality of the experiment (Russel, 1960; Rance, 1963; Ingle, 1966; Murray, 1967; Murray, 1969; Miller and Komar, 1979; Duane and James, 1980).

In our experiments we used a "spatial" or "Lagrangian" sampling grid, consisting of sample points

distributed along lines in both x (crossshore) and y (longshore) directions, sampled at one point in time. To determine the total mass, M, of tracer recovered in the sampling grid, we vertically sum the total number of tracer grains in each core sample. Then each N(x,y) is multiplied by the ratio of the representative rectangular area, $\Delta x \Delta y$, to the core area, πr^2:

$$M = \frac{1}{F \pi r^2} \sum_x \sum_y [\sum_z N(x,y,z)] \Delta x(x) \Delta y(y) \qquad (2.6)$$

where F is the number of dyed grains per unit mass in the tracer sand, r is the radius of the core tube, and N(x,y,z) is in units of grains. This mass M of tracer recovered is then compared to the amount injected to determine the fraction of tracer recovered.

The tracer recoveries for all our (Lagrangian) grids were computed and are listed in Section 4.3. Methods of estimating recoveries for Eulerian grids may be found in White and Inman (1987a).

2.: Dimensional analysis

A word of caution regarding dimensional analysis and all bedload models in this study is appropriate. All the variables considered are macroscopic quantities which ignore the detailed kinematics of the boundary layer. It may be that the most complete transport model must contain detailed physics relating macroscopic quantities to boundary-layer variations, which in turn relate to the

sediment transport. This study attempts to judge the relative effectiveness of various models which ignore the poorly understood boundary-layer mechanics. Future progress in understanding the kinematics may result in rejection of all macroscopic models used today.

The technique of dimensional analysis has several limitations. The appropriate number of dimensional variables necessary to describe a problem must be decided by other means. However, once the number of dimensional variables is selected, dimensional analysis determines the correct number of dimensionless variables to be formed from the original set of variables. Furthermore, there is no uniqueness in variable selection. Dimensional analysis will not suggest which variables to choose from the original list, nor will the resulting dimensionless variables be unique.

There are many different mathematical models of sediment transport with many different functional forms, but many investigators agree that the appropriate number of macroscopic variables describing transport is seven (i.e., Yalin, 1972; Dingler, 1974; Sleath, 1978). Yalin (1972) presents a series of arguments demonstrating that each of several additional variables can be expressed in terms of the seven variables he chose. However, the choice of seven variables from a list of fluid and sediment quantities is not unique. When developing and examining various models,

we will refer to Yalin's choice of seven variables. This will allow us to determine which transport models have too few variables (underdetermined) and which models have so many variables that there is redundancy (overdetermined). Underdetermined models may work well for the specific situation for which the model was designed but not apply well to more general situations. Overdetermined models may be impossible to truly test because functional variation in one variable may appear as variance in another related variable.

Dimensional analysis will lead to a transport relation consisting of dimensionless groupings of variables, which may in itself be considered a transport model. In fact, such a dimensionless model is very well suited to testing with empirical transport data, such as from this study. In addition to using dimensional analysis to compare other models, we will use our empirical data to test a model arrived at solely by means of dimensional analysis.

The basis of dimensional analysis is the Buckingham Pi Theorem, postulated in 1914. A complete proof may be found in Langhaar (1951). The two requirements for correct application of the theorem are that all the possible variables in the problem must be known and that one must not include other variables which are functions of those already listed. Application of the theorem results in a

set of independent dimensionless variables which completely determines the problem. The set obtained is not unique, but every other possible set of dimensionless variables is a product of powers of the variables obtained. The theorem is applied by stating the dependent variable, Π, as a function of N=n-d dimensionless variables, X_k, where n=the number of dimensional variables in the problem, and d=the number of physical dimensions in the problem:

$$\Pi = f(X_1, X_2, X_3, \ldots, X_N) \tag{2.7}$$

Note that in addition to forming dimensionless groups which are convenient to test, the theorem has the advantage of reducing the number of variables in the problem by d. This reduction in variables is accomplished by solving the N homogeneity equations, which provide that the dimensions of the original dimensional variables, a_k, add up in a way such that the X variables are dimensionless. The homogeneity equations are:

$$\begin{aligned} X_1 &= a_1^{\alpha_1} a_2^{\beta_1} a_3^{\gamma_1} \ldots a_n^{\delta_1} \\ X_2 &= a_1^{\alpha_2} a_2^{\beta_2} a_3^{\gamma_2} \ldots a_n^{\delta_2} \\ X_N &= a_1^{\alpha_N} a_2^{\beta_N} a_3^{\gamma_N} \ldots a_n^{\delta_N} \end{aligned} \tag{2.8}$$

The X's above are the resulting independent variables, whereas the dependent dimensionless variable has the form

$$\Pi = A\, X_1^{\alpha} X_2^{\beta} X_3^{\gamma} \ldots X_N^{\delta} \tag{2.9}$$

In the above analysis the a's are the postulated dimensional variables, the X's are the dimensionless variables obtained in the analysis, the subscripted Greek letters are the exponents obtained in the analysis, and the unsubscripted Greek exponents in Equation (2.9) are unknown exponents (to be determined from experimental data).

We now proceed to apply the above general analysis to the problem of sediment transport in oscillatory flow. Although the number of different variables for such a problem is potentially endless because many variables are functions of each other, it is generally recognized that there are seven independent dimensional variables for this problem (Yalin, 1972; Dingler, 1974; Sleath, 1978). The Buckingham Pi Theorem allows us to select which seven variables to use, as long as they are independent. The following selection of variables will result in a set of dimensionless variables which is well known and physically meaningful. The dimensional variables consist of static fluid parameters (ν, the kinematic viscosity, and ρ, the fluid density), static sediment parameters (D, the median grain diameter, and ρ_s, the sediment density), and dynamic flow parameters (u(t), the flow velocity, d_o, the wave orbital diameter, and g, the acceleration of gravity). For notational convenience, we will substitute for gravity the factor which converts solids volume to immersed weight, $\gamma_s = g(\rho_s - \rho)$. This is done because in sediment transport

mechanics, g always appears in conjunction with $(\rho_s-\rho)$. Finally, we select sediment transport, i, as the dependent variable.

Other variables could have been chosen, which the examination of other models illustrates. For example, the orbital diameter could easily be replaced by the wave period. Some models include the angle of internal friction in the sediment instead of grain size (Bagnold, 1963; Bailard and Inman, 1981). Bagnold's (1963) model also includes beach slope, a friction factor, and an "efficiency" factor instead of viscosity, sediment density, and orbital diameter. Yalin (1972, Section 3.5) examines this flexibility of choices in detail. In particular, he shows how gravity, friction factors, slope, and the flow depth may be interchanged for studies of unidirectional flow. However, the relation between beach slope and the other variables is not as well understood for oscillatory flow. Thus we choose not to select beach slope in our analysis. Many investigators choose to select only the peak velocity, u_m, and ignore temporal variation. Such a variable is not independent of the ones we have selected, since it is a simple function of u(t) and d_o for linear waves. We selected u(t) because it is more accurately obtained from our measurements.

The only macroscopic variable which is independent of the above selections, and which we deliberately choose

to ignore for the moment, is the transverse fluid velocity. The variable u selected above is the fluid velocity in the direction of transport (crosshore for our data set). But it has been suggested that the transverse velocity, v, may play a role in sediment transport by contributing to the effective bottom stress (Bailard and Inman, 1981; Kobayashi, 1982). In our data set v was generally not important, because the onshore grid orientation was set up to agree with the direction of wave approach and other contributions to longshore velocity were small. This is usually not true in the surf zone.

We now apply Equations (2.8) to the seven variables chosen. In our problem, the number of physical dimensions, d, is three. This is the case for most mechanical problems, since there are three basic dimensions of time, length, and mass (Hughes and Brighton, 1967; Yalin, 1972). Thus there are four equations in (2.8). That is, N (4) = n (7) - d (3). Applying these equations, and solving for the dimensionless variables X_k and their exponents, we obtain:

$$X_1 = \frac{u D}{\nu} \equiv R \text{ (grain Reynold's number)}$$

$$X_2 = \frac{\rho u^2}{\gamma_s D} \equiv \theta' \text{ (modified wave Shields' number)}$$

$$X_3 = \frac{d_\omega}{D} \equiv S \text{ (wave Strouhal number)} \qquad (2.10)$$

$$X_4 = \frac{\rho_m}{\rho} \quad \text{(specific mass)}$$

The dimensional transport, i, becomes nondimensionalized as:

$$\Pi = \frac{i\,\rho}{(\gamma_s\, D)^3} \equiv \Phi \qquad (2.11)$$

Subatituting (2.10) and (2.11) into (2.9), the transport equation can now be expressed as:

$$\Phi = \alpha_0\, R^{\alpha_1}\, \theta'^{\alpha_2}\, S^{\alpha_3}\, (\rho/\rho_s)^{\alpha_4} \qquad (2.12)$$

where the α's are unknown and to be determined empirically.

Yalin's (1972) arguments suggest that the above equation contains all the macroscopic variables necessary to describe sediment transport in oscillatory flow. In addition to comparing it with each of the transport models to be examined, we will test it empirically with the data obtained in this study.

2.3 Bedload models

Sand moves as bedload in a dense granular-fluid mixture along the bed. The reason that the bed is terred a granular-fluid is that bedload violates the basic assumption made in the development of fluid mechanics, the continuum hypothesis: "the macroscopic behaviour of fluids is the same as if they were perfectly continuous in structure" (Batchelor, 1967, p. 4). In practice Newton's laws of motion cannot be applied to individual particles and then integrated over the macroscopic region, because the medium is not continuous but consists of a complex mixture of sand and water of varying consistency. Some bedload models have been formulated which avoid the

continuum hypothesis by allowing the volume concentration of sediment to be an independent variable. These continuum theories (Goodman and Cowin, 1972; McTigue, 1979; Passman et al, 1980) postulate several constraints on the thermodynamic behavior of granular-fluid. Not surprisingly, these models all have several undetermined free parameters which make application and testing nearly impossible.

Another type of bedload model examines the particle interaction between grains of sand. The granular collisions transfer stress in a postulated manner, resulting in the transfer of force within the bed. Bagnold (1954) first measured the momentum transfer and verified the Coulomb yield relation between normal and tangential stresses. More recent models include the effect of fluctuating granular velocities on the stress (Ogawa et al, 1980; Ackerman and Shen, 1982; Savage and Jeffrey, 1981; Jenkins and Savage, 1983). These models have fewer free parameters than the continuum models but have yet to be tested. However, certain assumptions and conclusions of the models have been tested. Hanes and Inman (1985) verified the basic Coulomb yield criterion inherent in all such models and the quadratic stress/shear-rate relationship for different sediment concentrations.

A third type of bedload model may be termed "macroscopic dynamical models" or "integrated box models."

This is the type that will be examined in this study. They are dynamical because they relate the fluid forces to sediment transport, but they ignore the detailed kinematics. They are macroscopic in that they do not attempt to describe what happens on the level of the individual grain but consider only mean macroscopic quantities. Such models ignore the detailed physics and postulate relations between the macroscopic quantities of velocity, force, and stress of the fluid and sediment.

We will classify each of the macroscopic dynamical bedload models by the power of the fluid velocity in its transport relation. Each of the models to be examined can be put into a form stating that sediment transport, i, is proportional to some power of the measured fluid velocity, u.

There are also other quantities which appear in the models, listed in Table 2-1. Two models claim that the longshore current has some bearing on the crosshore transport. Many of the models recognize the need for a threshold fluid velocity, below which the sediment will not move. Three of the models contain beach slope and a measure of internal friction in the sediment, whereas most of the rest simply include grain size. All but two of the models contain an undetermined coefficient. Two of the models include the wave orbital diameter.

Table 2-1. Variables used in bedload models

Crosshore velocity moments:

u^3: Bagnold, Bailard & Inman, Kobayashi, Meyer-Peter & Mueller, Yalin
u^4: Hallermeier, Sleath
u^5: Hanes & Bowen
u^6: Madsen & Grant, Shibayama & Horikawa
Other moments: Einstein

Velocities:

u(t): All models
v(t): Bailard & Inman, Kobayashi
u_t: Bagnold, Bailard & Inman, Kobayashi, Madsen & Grant, Meyer-Peter & Mueller, Sleath, Yalin

Beach slope:

β: Bagnold, Bailard & Inman, Kobayashi

Grain size:

ϕ (internal angle of friction): Bagnold, Bailard & Inman, Kobayashi
D (median grain size): Einstein, Hallermeier, Hanes & Bowen, Kobayashi, Madsen & Grant, Shibayama & Horikawa, Sleath, Yalin

Coefficients:

c_f: Bagnold, Bailard & Inman, Hanes & Bowen, Kobayashi, Madsen & Grant, Meyer-Peter & Mueller, Shibayama & Horikawa
c_D (drag coefficient): Kobayashi, Madsen & Grant, Shibayama & Horikawa
ϵ_b (efficiency): Bagnold, Bailard & Inman
f_1 (friction & lift coefficient): Sleath

Density:

ρ: All models
ρ_s: Einstein, Hallermeier, Hanes & Bowen, Kobayashi, Madsen & Grant, Shibayama & Horikawa, Sleath, Yalin

Wave orbital diameter:

d_o: Hallermeier, Sleath

All of the following models will be tested with our oscillatory transport data. Some of the models were developed and intended only for unidirectional transport conditions, but we will apply them to oscillatory flow anyway. In the search for a good transport model, we do not wish to eliminate models simply because they were developed for unidirectional flow. We will describe the limitations of each model in terms of its application to our type of oscillatory flow. However, we do not suggest that the developers of unidirectional models in any way erred in deriving a model which we have extended beyond its originally intended use.

2.3.1 u^3 models

The following models all postulate that sediment transport is proportional to the third power of the fluid velocity. The first two models (Meyer-Peter and Mueller, 1948; Yalin, 1963) were developed for unidirectional flow. Nevertheless, we will be testing them with our oscillatory-flow transport data.

Meyer-Peter & Mueller's unidirectional-flow model (1948)

The Meyer-Peter and Mueller bedload equation is the oldest and simplest model we will examine. It is much more widely used in Europe than in this country, but since it is old and familiar, it is still used as a basis of comparison

when testing new models (Goud and Aubrey, 1985; Hanes and Bowen, 1985).

This model was developed in a series of laboratory flume tests on a sloping bed for unidirectional flow. The ranges of characteristics in the tests are:

Flow depth	1 cm < h < 120 cm	
Slope	0.023 < β < 1.15	(2.13)
Grain size	400 μ < D < 30000 μ	
Specific gravity	1.25 < ρ_s < 4.2	

The above condition which most restricts the use of their model is the lower limit on grain size. They had few data points for D < 2000 microns and no data for grains smaller than 400 μ, whereas most beach sand has a median grain size of about 200 μ. Bagnold (1974) suggests that important changes in the relative magnitudes of forces (lift and drag) occur for D > 1000μ. This model was never intended for use with small grain sizes or in oscillatory flow.

The transport equation in dimensionless form is:

$$\Phi = 8\,(\theta'-0.047)^{3/2} \qquad (2.14)$$

The number 0.047 serves as a threshold stress, necessary for the initiation of motion. The authors were apparently unaware of Shields' (1936) work expressing the threshold stress as a variable. Furthermore, for the large grain sizes used in Meyer-Peter and Mueller's experiments, threshold stress is roughly a constant. We will now change this value to a variable threshold stress, as expressed by

Shields. This adaptation extrapolates the model to include our beach-sand grain size. This is in keeping with most other modern authors who make the same adaptation when applying the model (Yalin, 1972; Goud and Aubrey, 1985). The dimensionless and dimensional versions of (2.14) then become:

$$\Phi = 8\,(\theta' - \theta'_t)^{3/2} \qquad (2.15)$$

$$i = 8\,\rho\,(u^2 - u_t^2)^{3/2}$$

Before (2.15) can be used in our tests of oscillatory transport, one more modification must be considered. Clearly if a time-varying velocity, u(t), is inserted in (2.15), transport will always be positive. This was not a problem with the original model, since it was used only in steady flow. Thus in testing (2.15) we will compute the transport for each time step, but then multiply the result by the sign of the velocity.

When transport equations from steady flow are applied to oscillatory flow, it is customary to include a friction factor, c_f, which in some manner accounts for the difference in the boundary layers between the two flows [Bagnold (1963), Bailard and Inman (1981), Kobayashi (1982), Sleath (1978), and Madsen and Grant (1976)]. Inserting a friction factor will result in absolute transport numbers which are much more realistic, but will make absolutely no difference in judging how well the model performs. All the transport numbers will be reduced by

about two orders of magnitude by including the friction factor, but all the numbers will be reduced in exactly the same proportion, since the same friction factor will be used in all experiments. Including a friction factor in (2.15) results in the following forms:

$$\phi = 8\,(\theta-\theta_t)^{3/2} \qquad (2.16)$$

$$i = 8\,\rho\,c_f^{3/2}\,(u^2-u_t^2)^{3/2}$$

This is the form that will be tested with our data.

The Meyer-Peter and Mueller model is underdetermined. By comparing (2.16) with our dimensionless transport model derived from dimensional analysis in Equation (2.12), we see that (2.16) has omitted three important parameters: Reynold's number, Strouhal number, and the ratio of the densities. Shields' number, θ, in (2.16) may be the most important parameter in sediment transport, but it is clearly not the only one. Omission of the Reynold's number in (2.16) means that this model will not perform well when viscous effects are important (i.e., small grain sizes, since $R = uD/\nu$). Omission of the Strouhal number will result in neglecting the possibility that accelerations as well as velocities are important. Omission of the density ratio will not be a problem as long as we restrict ourselves to one set of materials (i.e., quartz sand in water), but the equation may not be considered applicable when applied to materials with varying density differences.

Yalin's unidirectional-flow model (1963)

Yalin (1963, 1972) developed a transport equation based on evaluating the forces acting on an individual grain in order to determine when and how far it would move. This type of motion occurs above the granular-fluid region and is considerably less dense. It is an important part of bedload transport, but not the only part. The cumulative interaction of densely packed grains in a granular-fluid, first examined by Bagnold (1954), results in the grains moving in a manner which cannot be explained by simply summing up the forces on the individual grains. Nevertheless, many investigators have developed models based on motion of individual grains.

Yalin developed separate expressions for the total mass of sediment moving per unit area of bed and for the mean velocity of grain motion. The product of these two quantities is transport. The details of deriving these two quantities are quite complex (Yalin, 1972). The concepts and assumptions involved in deriving the velocity of transport are as follows. Both drag and lift forces on an individual spherical grain are considered. The vertical profile of horizontal fluid velocity near the bed is assumed to linearly decrease to zero at the bed. A threshold shear stress like that of Shields (1936) is applied. The resulting expression for the average transport velocity is:

$$U/u = c_1 [1 - \ln(1 + as)/(as)] \quad (2.17)$$

where c_1 is some unknown coefficient to be experimentally determined, and:

$$a = (\theta-\theta_t) / \theta_t \quad (2.18)$$

$$a = 2.45 \sqrt{\theta'_t} / (\rho_s/\rho)^{0.4}$$

As Yalin admits, with little theoretical justification he assigns the form for the mass in motion as:

$$m_b' = m_b \gamma_s = c_2 \gamma_s D s \quad (2.19)$$

where s is defined in (2.18). Combining (2.17) and (2.19) and doing some manipulation yields the dimensionless transport equation:

$$\Phi = 0.635 s \sqrt{\theta'} [1 - \ln(1 + as)/as] \quad (2.20)$$

where the coefficient 0.635 is the product of c_1 and c_2 which Yalin determined from some experimental laboratory data. Equations (2.18) and (2.20) can be transformed into dimensional quantities:

$$i = 0.635 \gamma_s D u (u^2-u_t^2) u_t^{-2} [1 - 0.41 \rho_s^{0.4} \rho^{-0.9} (\gamma s D)^{0.5} u_t (u^2-u_t^2)^{-1} \ln(1 + 2.45 \rho^{0.9} \rho_s^{-0.4} (\gamma_s D)^{-0.5} u_t^{-1} (u^2-u_t^2))] \quad (2.21)$$

Equation (2.21) is the one which we tested with our experimental data. Yalin considers the case of $u >> u_t$ for which (2.21) simplifies to:

$$i = 0.635 \gamma_s D u u_t^{-2} (u^2-u_t^2) \quad (2.22)$$

It can be seen from (2.22) that Yalin's model is a u^3 transport model in the limit of strong flow. An important point to notice in (2.22) is the fact that it is not

possible to omit the concept of threshold velocity from Yalin's model, even when flows are quite strong. Setting u_t to zero would cause (2.22) to approach infinity.

Now consider the limitations in applying Yalin's model to oscillatory flow. For oscillatory flow relation (2.20) is an underdetermined model. The variables omitted are viscosity and orbital diameter. Thus we would expect this model to be inaccurate in viscous flows (very small grains). The observed increase in transport with wave period would also be lacking from this formulation. We also must keep in mind the severe theoretical limitation of describing only individual grain motion and not the granular-fluid portion of bedload.

Bagnold model (1963)

The transport models that appeared before Bagnold (Meyer-Peter and Mueller, 1948; Einstein, 1950) were entirely empirical. Bagnold was the first to develop a transport model based on principles of physics. Since many authors (Bailard and Inman, 1981; Kobayashi, 1982) followed Bagnold's lead in deriving a bedload equation, we will examine Bagnold's logic in some detail.

Bagnold first used the concept of fluid shearing, in which the rate of energy dissipation per unit volume is the stress tensor times the deformation tensor (Batchelor, 1967). Analogously, for a granular-fluid (sand forced by

air or water), he expressed the fluid power expended in transporting bedload, per unit bed area, as the sediment stress times its velocity:

$$\Omega = T\ U \qquad (2.23)$$

A well-known property of sediment mechanics is called the Coulomb yield criterion. The tangential stress in the sediment, T, is equal to the normal stress, P, times the internal angle of friction:

$$T = P \tan\phi \qquad (2.24)$$

The angle ϕ is a somewhat easier property to measure than the internal stresses. Bagnold then considered the stress balance on a sloping bed, as in Figure (2-1). Applying simple trigonometry to the stresses and the angles of internal friction, ϕ, and beach slope, β, he obtained:

Stress from fluid:

$$T_f = P \tan\phi = m_b' g \cos\beta \tan\phi$$

Gravitational stress:

$$T_g = m_b' g \sin\beta$$

Total stress:

$$T_f - T_g = m_b' g (\cos\beta \tan\phi - \sin\beta)$$

$$= m_b' g \cos\beta (\tan\phi - \tan\beta) \qquad (2.25)$$

Combining (2.23) and (2.25) we have:

$$\Omega = T\ U = m_b' g \cos\beta\ U (\tan\phi - \tan\beta) \qquad (2.26)$$

Now the transport rate of sediment is defined as the sediment weight per unit area times the velocity with which it moves:

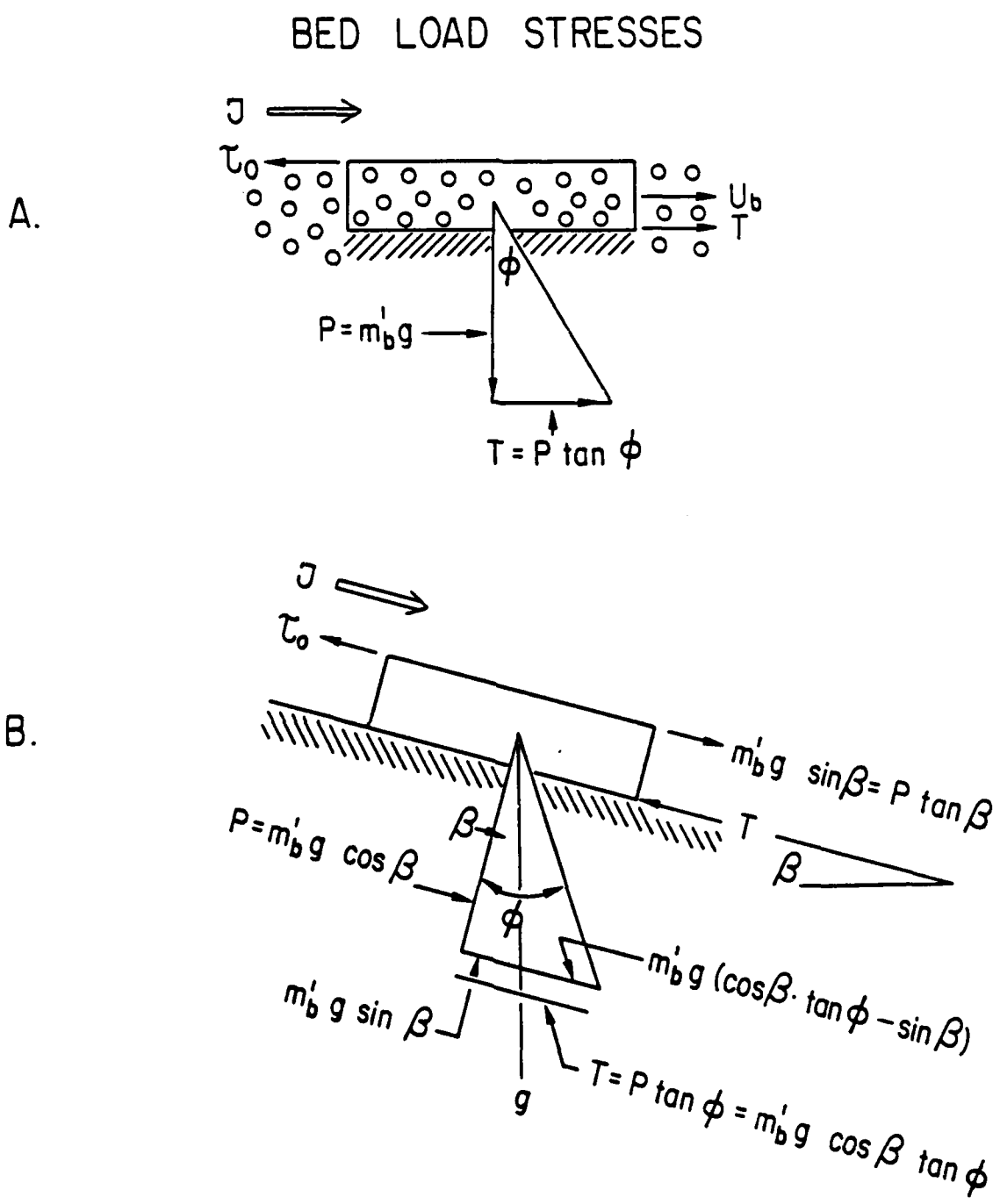

Figure 2-1. Forces acting on bedload (from Inman, 1979): (A) horizontal bed and (B) bed sloping at angle ß.

$$i = (\rho_b' g \cos\beta) U \qquad (2.27)$$

Combining (2.26) and (2.27):

$$\Omega = i (\tan\phi - \tan\beta) \qquad (2.28)$$

At this point Bagnold applied the concept of machine efficiency to a stream transporting sediment. The power expended by the fluid in transporting the sediment is some fraction of the total power available in the fluid:

$$\Omega = \epsilon_b \omega \qquad (2.29)$$

Equating (2.28) and (2.29) we arrive at the expression for sediment transport:

$$i = \frac{\epsilon_b \omega}{\tan\phi - \tan\beta} \qquad (2.30)$$

The total available fluid power is equal to the fluid stress times the velocity, $\omega = \tau u$. A quadratic stress law is then applied to obtain the fluid stress, so that:

$$\omega = \tau u = (\rho c_f u^2) u = \rho c_f u^3 \qquad (2.31)$$

Combining (2.30) and (2.31) we have Bagnold's transport model:

$$i = \frac{\epsilon_b \rho c_f u^3}{\tan\phi - \tan\beta} \qquad (2.32)$$

Equation (2.33) cannot be directly translated into a dimensionless form like (2.13), because it contains variables such as c_f, ϵ_b, ϕ, and β, which are related only in some unknown way to the variables used in our dimensional analysis. Variables such as fluid and sediment densities, grain size, viscosity, and orbital diameter which we used in deriving (2.13) may be functions of the

efficiency and friction factors or the angles in the denominator in (2.33). In considering the limitations of (2.33) we can only express the practical problem of attempting to evaluate two unknown coefficients. It is particularly unclear how the efficiency factor should be evaluated, since it does not appear in many other models. There is evidence for unidirectional flow which suggests that ε_b increases as the fluid power ω increases, until ε_b reaches a constant value of about one-third at some value of ω (Bagnold, 1966; Inman, 1979). We can only assume that the conditions determining the efficiency in (2.33) remain constant for our experiments.

Equation (2.33) was developed for unidirectional flow, but Bagnold (1963) made suggestions as to how it might be adapted to oscillatory flow. He suggests that the stress on the bottom may be proportional to the maximum orbital velocity u_m. Thus

$$\begin{aligned} i &= K' \omega u/u_m \\ &= K' (\rho c_f u_m^3) u/u_m \\ &= \frac{\varepsilon_b \rho c_f u u_m^2}{\tan\phi - \tan\beta} \end{aligned} \qquad (2.33)$$

which is the same as (2.32), except that uu_m^2 has replaced u^3.

Relation (2.33) was tested in the crosshore direction in the laboratory by Inman and Bowen (1962). It was reformulated into a longshore transport model by Inman and Bagnold (1963). Bailard (1981) points out several

models which incorporate this concept. Komar and Inman (1970) show that (2.33) is equivalent to the integrated longshore model of relation (1.1) under certain assumptions. We will test both the original unidirectional-flow model and the suggested u u_m^2 model with our oscillatory transport data.

Bailard and Inman model (1981)

The Bagnold transport relation (2.33) was derived for steady flow, but may be applied without modification to oscillatory flow. However, Bailard and Inman (1981) looked at all the assumptions in the derivation of Bagnold's model and made changes whenever differences between steady and oscillatory flow applied. The basic manner in which the fluid velocity enters into the derivation did not change. That is, instead of using a nonvarying fluid velocity as assumed in Bagnold's derivation, they used the mean value of the time-varying oscillatory fluid velocity. It was necessary to assume that the phase difference between the fluid velocity above the bed and the stress acting on the bed did not significantly affect this method of handling the velocity. Such an assumption is not necessarily justified, but there is no practical alternative. All authors developing such a model find it necessary to make such an assumption of small phase difference (Yalin, 1972; Madsen and Grant, 1976; Sleath, 1978; Kobayashi, 1982).

Two sets of laboratory experiments (Kalkanis, 1964; Sleath, 1970) suggest this phase difference to be somewhere between zero and $\pi/4$.

The one significant difference in the assumptions used by Bagnold (1963) and by Bailard and Inman (1981) was that Bailard and Inman did not assume the flow direction and the slope of the bed to be in the same direction, as had Bagnold. The two forces acting on the sand, fluid stress and gravity, are therefore not necessarily parallel. The Bailard and Inman model is thus a two-dimensional transport model. It yields transport equations for both the crosshore and longshore directions.

Once the small-phase assumption and stress bidirectionality have been addressed, the derivation of the Bailard and Inman transport equation is a matter of algebra. A detailed derivation may be found in the appendix of Bailard and Inman (1981). The transport equations for the crosshore and longshore directions are:

$$i_x = \frac{\rho_b \epsilon_f}{\tan\phi}\left[u_T^2 u - \frac{\tan\beta}{\tan\phi} u_T^3\right] \qquad (2.34)$$

$$i_y = \frac{\rho_b \epsilon_f}{\tan\phi} u_T^2 v \qquad (2.35)$$

where u_T is the total velocity, $(u^2+v^2)^{0.5}$. Note the similarity of these equations to Bagnold's Equation (2.33). The same coefficients and the same u^3 dependence appear. However, both components of velocity must now be taken into account. The reason for this is that Bailard and Inman

assumed the stress on the bed to be proportional to the total velocity, not just the velocity in the direction of transport. Furthermore, the simple difference (tanϕ - tanβ) in the denominator of (2.33) now appears in (2.34) as a difference between two terms involving the velocity as well. One consequence of this is to change the concept of supercritical flow, usually referred to as "turbidity currents." When the denominator in (2.33) becomes negative, the equation implies the sediment will move downslope due to gravity. The condition for initiation of a turbidity current becomes a more complicated function of the velocity in (2.34).

Just as with the Bagnold model, we cannot compare the Bailard and Inman equation with our dimensional analysis in (2.13). It is unclear what variation is allowed in the two coefficients of friction and efficiency. As with the Bagnold equation, we can only assume that these two coefficients do not vary greatly in the conditions present in our experiments.

There are two practical limitations of the Bailard and Inman model. The presence of an efficiency coefficient as in Bagnold's model makes it difficult to determine what numerical coefficient should be used when applying the model. Furthermore, when computing the two velocity terms in (2.34) it is noted that the resulting crosshore transport is a small difference between two large numbers.

The practical consequence of this is that (2.34) is much more sensitive to errors in measurement of the velocity or the bed slope than most other models. This restriction does not apply to the longshore equation (2.35) which contains only one term.

Kobayashi (1982)

Kobayashi (1982) derived both instantaneous and mean bedload equations. The mean equation is intended for use in situations where the time-series u(t) is not available and was derived with the assumption of sinusoidal waves. The mean equation will not be considered here, since we measured the fluid velocity directly.

In deriving the instantaneous bedload equation, Kobayashi made all of the same basic assumptions as Bailard and Inman (1981): quadratic stress, stress proportional to the total fluid velocity (not just the velocity in the direction of transport), insignificant phase difference between fluid velocity and sediment motion, and nonparallelism of beach slope and velocity. Thus it is subject to the same limitations and advantages of each of these assumptions.

Kobayashi derived his model by considering the drag, lift and gravitational forces on the "average" sand grain and integrating over the available mass sheared by the fluid stress. The resulting equations (21 and 22 in

his paper) are complicated functions of: beach slope, grain size, internal angle of friction, sand and fluid densities, drag and lift coefficients, the direction of fluid motion, Shields' yield criterion, gravity, fall velocity, and three empirical coefficients. He uses some laboratory data of Bagnold (1956) to suggest values for his coefficients. He includes a commonly used expression for fall velocity. With these additional assumptions, his equations can be translated into the set of variables we have been using as:

$$i_x = 1.65\, c_f\, u_t^{-1}\, ((1+0.1\tan\phi)\,\rho\,\gamma_s\, D\,(c_D\tan\phi)^{-1})\,(\cos\zeta\,(u_T^2-u_t^2)(u_T-0.7u_t) + \sin\beta\cot\phi\,[\cos^2\zeta\,(u_T^3-0.35\,u_t\,(u_T^2+u_t^2)) + 0.7\sin^2\zeta\,(1+0.1\tan\phi)\,u_t\,u_T^{-1}\,(u_T^2-u_t^2)(u_T-0.7u_t)])$$

(2.36)

$$i_y = 1.65\, c_f\, u_t^{-1}\, ((1+0.1\tan\phi)\,\rho\,\gamma_s\, D\,(c_D\tan\phi)^{-1})\,(\sin\zeta\,(u_T^2-u_t^2)(u_T-0.7u_t) + \sin\beta\cot\phi\cos\zeta\sin\zeta\,[u_T^3-0.35\,u_t\,(u_T+u_t) - 0.7(1+0.1\tan\phi)\,u_t\,u_T^{-1}\,(u_T^2-u_t^2)(u_T-0.7u_t)])$$

(2.37)

where ζ is the angle indicating direction of the fluid velocity in degrees clockwise of offshore. The two expressions for crosshore and longshore transport are quite complex, but an examination of the velocities reveals that the highest power of velocity in each term is three. Thus transport is proportional in some complicated manner to u^3.

Kobayashi's model is the only one we will examine which can be described as overdetermined. An overdetermined model contains more variables than are necessary to compute transport. Kobayashi includes variables which are clearly functions of each other, such

as grain size, internal angle of friction, and beach slope. Both friction and drag coefficients are included, whereas many authors consider these to be simply related to each other (Bagnold, 1963; Yalin, 1972; Sleath, 1984). This overdeterminedness will generally result in inaccuracy when the equation is applied to real data. Not only will the errors in measurement of each of these quantities be present, but measurement of each of these quantities requires considerably more effort than measurement of the fewer quantities required in other transport equations. Thus the principal disadvantage of Kobayashi's model is that it is too complicated, both theoretically and in its requirement of measuring more variables than are necessary.

2.3.2 u^4 models

Sleath (1978)

Sleath considered the various nondimensional parameters which describe sediment transport, just as we did in Section 2.2. He then proceeded to fit the experimental data from laboratory transport measurements to the various nondimensional parameters important in sediment transport. His conditions were restricted to flow in one direction under waves and did not include a sloping beach. The resulting equation which best fit his data can be expressed as:

$$i = \frac{17\,(2D/d_o)(\rho f_1/2)^{3/2}\, u\,(u^2-u_t^2)^{3/2}}{(\nu_m D)^{0.5}} \qquad (2.38)$$

where f_1 is a coefficient which includes both the friction coefficient c_f appearing in other models and a graphically determined empirical expression for a lift coefficient.

The data used to determine Equation (2.38) came from Sleath's series of experiments with small waves in which he counted individual grains of sand as they moved off the end of a flow channel. The transport rate was extremely small, about three orders of magnitude smaller than the rates present in our field experiments. Such low transports were necessary, since he was visually counting individual grains as they moved. His experiments were performed on a flat bed, but if the conditions of his experiments are used to obtain a Shields' number characteristic of the flow, then the type of flow predicted is well into the ripple transport regime. The only possible explanation for this discrepancy is verified by a statement made by Sleath concerning his experiments. His data were gathered very quickly after flow began. If flow continued, ripples appeared. Clearly he did not wait for conditions in his wave channel to equilibrate with the bed in order to achieve a steady state before beginning measurement. This places severe doubts on the applicability of his experiments to real transport conditions.

The limitations of Sleath's model may be summarized as follows. Viscous effects are excluded from his model.

(He did not find significant variation in transport with Reynold's number.) Only transport parallel to the fluid velocity is predicted. The effect of a sloping bed is excluded. As already described in detail, his supporting laboratory data are suspect because equilibrium conditions were not attained.

Hallermeier (1982)

Hallermeier used Sleath's transport equation (2.38) and calibrated it with more than 700 transport measurements from 20 different sources in the literature. However, all of these data were from laboratory experiments, many under conditions like those of Sleath (1978), in which transport was held at artificially low unequilibrated levels. We can thus expect Hallermeier's transport equation to yield very low values when used in field situations.

Before Hallermeier applied Sleath's equation (2.38), he made two significant changes in it. He removed the concept of a threshold velocity necessary for initiation of motion. Furthermore, he removed Sleath's coefficient f_1, which contained both a friction coefficient c_f and an empirical expression for a lift coefficient. Thus empirical variation in drag and lift forces were removed from Sleath's equation. Hallermeier's model contains no undetermined coefficient. He obtained a simple numerical coefficient which is the average value for all

the data he examined. In the units we have been using, Hallermeier's (1982) transport equation becomes:

$$i = \frac{(\rho/10)^{3/2}\ (2\ D/d_o)}{(\gamma_s\ D)^{0.5}}\ u^4 \qquad (2.39)$$

When we apply (2.39) we must multiply the computed transport by the sign of the fluid velocity at each time step, in order to obtain the correct transport direction. This procedure will be applied to all models which contain an even power of the fluid velocity.

Since Hallermeier used Sleath's model, the same limitations that were listed for Sleath's model apply to Equation (2.39): unrealistically low transport, exclusion of viscous effects, no provision for a sloping bed, and transport allowed in only one direction (parallel to the fluid flow). Since, Hallermeier has also removed Sleath's expression for lift force variations, the difference in performance between these two models will inform us how successfully Sleath modeled lift variation.

2.3.3 u^5 model:

Hanes and Bowen's unidirectional-flow model (1985)

Hanes and Bowen developed a bedload transport model from basic principals of physics in which the details of grain-to-grain interaction within the densely packed bed were considered. Many of the assumptions and first principles used in the model development were obtained from Bagnold's (1954) experiments which measured sheer and

strain in a rotating drum. Hanes and Bowen applied Bagnold's (1954) empirically derived relationship between grain shear and stress to a flat bed subject to an intense steady shear. In contrast to the data and assumptions of Sleath (1978) and Hallermeier (1982) which indicate transport orders of magnitude smaller than our field experiments, the conditions described by Hanes and Bowen indicate transport about two orders of magnitude larger than that of our experiments.

Hanes and Bowen derive relations for both velocity and thickness of transport from Bagnold's strain/shear equation. They obtain an expression which has several undetermined coefficients and also contains the Shields' number to the five-halves power, $\theta^{5/2}$ (their equation 18). We know that bedload consists of both grain-to-grain interactions in a densely packed granular-fluid and also saltation, grains moving as projectiles in a jumping motion. Thus Hanes and Bowen also derived a relation for bedload transport as saltation (their equation 31). Again they obtain an expression with several undetermined coefficients. The dependence on Shields' number is in this case much more complicated, since it appears in several locations in the relation. Under certain assumptions regarding the coefficients in the equation, the Shields' number dependence can again be approximated as the five-halves power.

The variation of coefficients in the transport equations was left for future investigators to determine with rigorous experiments. In order to provide a transport relation which could be tested now, Hanes and Bowen made many assumptions regarding the coefficients in their equations and determined that the sum of their granular-fluid and saltation equations could be approximated as:

$$\Phi = 3.5\ \theta^{5/2} \tag{2.40}$$

The resulting transport relation in dimensional variables becomes:

$$i = \frac{3.5\ \rho^2\ c_f^{5/2}}{\gamma_s\ D}\ u^5 \tag{2.41}$$

In adapting (2.41) to oscillatory flow, the limitations can be examined by comparison with the dimensional analysis of the necessary variables in Section 2.2. Equation (2.41) omits viscosity, wave orbital diameter, and the ratio of sediment and fluid densities. Thus it should not be expected to perform well for very small grain sizes (viscous flow), variable wave periods, and for materials of greatly different densities. The model was not developed for oscillatory flows. Beach slope is not expressly included, although its effect may appear in the various coefficients which have been eliminated in the simplified versions here.

2.3.4 u^6 models

Madsen and Grant (1976)

Madsen and Grant began their model derivation with an empirical expression obtained by Brown (1949) in a series of steady-flow laboratory sediment-trap experiments. Brown's empirical relation is:

$$i/(\gamma_s D W) = 40\ \theta'^3 \qquad (2.42)$$

in which the Shields' number uses a steady fluid velocity, u, and the sediment fall velocity appears as W. In order to adapt (2.42) to oscillatory flow, Madsen and Grant assumed the fluid velocity to be sinusoidal and averaged (2.42) over a half sine wave. Thus their shear stress could not have the usual u^2 dependence as in the models of Bagnold (1963), Bailard and Inman (1981), and Kobayashi (1982). Their modified shear stress was:

$$\tau = \rho\, c_f\, |u|\, u \qquad (2.43)$$

where |u| is the absolute value of u. This expression was necessary because a sine wave is symmetric and thus yields zero net transport. Madsen and Grant's transport relation derived from this half sine-wave assumption is:

$$i/(\gamma_s D W) = C_M\, \theta^3 \qquad (2.44)$$

They include C_M, a coefficient which includes the effects of threshold stress, and a friction factor in the Shields' number ($\theta = c_f\theta'$). Madsen and Grant chose not to include threshold stress in the way done in most models (by replacing θ with $\theta-\theta_t$). They include its effect in an

empirical coefficient for which they provide a table from laboratory data. For flows as intense as in the surf zone, C_M is constant at 12.5. However, for our experiments outside the surf zone it cannot be assumed constant. We now translate (2.44) into dimensional variables:

$$i = \frac{2\, C_M\, c_f^3\, \rho^{5/2}}{(\gamma_s\, D)^{3/2}\, (3\, c_D)^{0.5}}\, u^6 \qquad (2.45)$$

In order to obtain (2.45) an expression for the fall velocity W had to be included as:

$$W = [4\, \rho\, \gamma_s\, D/(3\, c_D)]^{0.5} \qquad (2.46)$$

Since (2.45) contains u to an even power, we must make the same modification that we made with the Meyer-Peter and Mueller model and the Hallermeier model: the transport evaluated at each time step in the integration must be multiplied by the sign of the velocity, so that the correct direction is predicted.

The limitations on Equation (2.45) may be examined by comparison with the complete set of variables obtained in the dimensional analysis of Section 2.2. Equation (2.45) omits viscosity, wave orbital diameter, and the ratio of sediment and fluid densities. Thus it should not be expected to perform well for very small grain sizes (viscous flow), variable wave periods, and for materials of greatly different densities. The model does not include beach slope explicitly, although it may be included in relation to the other variables present. Finally, keep in mind that the model was derived from the simple concept of

a half sine wave, whereas transport over an entire sine wave is zero.

Shibayama and Horikawa (1980)

Shibayama and Horikawa used Brown's (1949) transport relation (Equation 2.42) and followed Madsen and Grant's procedure and assumptions for shear stress and transport over a half sine wave. The only difference in their model from the Madsen and Grant model comes from the assumption that once a sand grain moves, it will continue to do so until the flow reverses direction, regardless of the flow velocity. Thus they obtain a different numerical coefficient for their model. The variable threshold coefficient C_M in Equations (2.44) and (2.45) becomes a simple constant. The dimensionless and dimensional analogs of the Madsen and Grant model are thus:

$$i/(\gamma_s D W) = 19\,\theta^3 \qquad (2.47)$$

$$i = \frac{38\,c_f^3\,\rho^{5/2}}{(\gamma_s D)^{3/2}\,(3c_D)^{0.5}}\,u^6 \qquad (2.48)$$

The same limitations that applied to the Madsen and Grant model also apply to (2.47) and (2.48) with the additional restriction that no yield criterion is applied. Equation (2.48) omits viscosity, wave orbital diameter, the ratio of sediment and fluid densities, and beach slope. It was derived from the simple concept of transport over a half sine wave. Finally, since it contains an even power of the fluid velocity, the transport must be multiplied by

the sign of the fluid velocity for each time step of integration.

2.3.5 Other models

In addition to the models we have already examined in which the transport is proportional to some power of the fluid velocity, it is also possible to model transport as a variable power of fluid velocity, $i \propto u^n$, in which n is itself a specified function of transport. The relation between i and u can be determined empirically, and the functional relation can be expressed graphically. This was the approach taken by Einstein (1950) in the development of a steady unidirectional transport model. Einstein's model was later adapted to oscillatory flow by Kalkanis (1964), Abou-Seida (1965), Einstein (1972), and Ackers and White (1973). The disadvantage of using such models is that the basic physics remains obscure. The transport relation is totally empirical. Nevertheless, such graphical expressions for transport can be applied in practice. In fact, Einstein's (1950) model is probably the most popular transport model for steady-flow conditions used in this country. We will test such models in order to examine the validity of the basic postulate that the power n increases as transport intensity increases.

The model of Ackers and White (1973) will not be tested here, since it adds little in the way of new physics

to Einstein's (1950) model. Ackers and White used both laboratory and field measurements of transport to develop empirical curves much like Einstein's, relating transport and fluid velocity. The numerical values obtained from Ackers and White's curves are different than those of Einstein's, but the basic trend remains: the power n increases with transport intensity. Ackers and White did include viscosity, which was ignored by Einstein, but such a change should only be noticeable for very small grain sizes.

Einstein's unidirectional-flow model (1950)

Einstein began his theoretical development with the description of saltation, projectile motion of individual grains. He ignored the intense transport which occurs beneath saltation, the grain-to-grain interaction of a densely packed granular-fluid. Thus he ignores a large portion of real bedload, just as was done in the development of Yalin's (1963) model, described earlier. By considering the forces acting on a single sand grain, Einstein eventually develops a very complicated integral expression containing seven undetermined parameters, which he is unable to evaluate. Nevertheless, the expression does contain Shields' number to the three-halves power, suggesting transport may be proportional to the third power of the fluid velocity. Einstein's relation for

nondimensional transport (Yalin, 1972, Chapter 5.5) may be expressed as:

$$\Phi = A\,\Theta'^{3/2} \int_{a-1}^{\infty} (1/\sigma\sqrt{2\pi}) \exp(-r^2/2\sigma^2)\, dr \qquad (2.49)$$

in which A contains five unknown coefficients, and a and σ are unknown. Since the seven undetermined parameters are unknown, and the integration cannot be performed, it is unclear what sort of dependence there is between fluid velocity and transport. Even though Shields' number appears to the three-halves power, there may be additional functional dependence on Shields' number in the remainder of the expression. The only practical information that Einstein could obtain from (2.49) was the fact that transport was in some way dependent on Shields' number:

$$\Phi = f(\Theta') \qquad (2.50)$$

Thus he proceeded to gather field data for steady flow and produced empirical curves relating Φ and Θ'. The slope of Einstein's curves show that the appropriate power of Shields' number varies from one at low intensity to three for intense transport. (Thus the power of the fluid velocity varies from two to six.)

When using Einstein's curves, several limitations need to be kept in mind. He developed his theory by considering only the saltation portion of bedload. Both his theory and his empirical curves were developed only for steady unidirectional flow. Furthermore, the only variables besides velocity that he takes into account are

γ_s and D (in ϕ) and Shields' number. Variations in density and viscosity are ignored.

We will test Einstein's (1950) empirical curves of relation (2.50) in order to examine his basic postulate that the power of u (to which transport is proportional) increases as the transport intensity increases. In fact, Bagnold (1986) provides some field verification of this postulate with unidirectional (river) data. We do not anticipate that the transport numbers we obtain from Einstein's (1950) model will even be the correct order of magnitude, since we will be applying his steady-flow curves to our oscillatory transport data. But the magnitude of the transport numbers will not be important. The variance of the transports computed from Einstein's curves will inform us as to the validity of his basic postulate.

Einstein's oscillatory-flow model (1972)

The oscillatory model of Einstein was developed from Einstein's original (1950) concept for steady flow by performing laboratory experiments in oscillatory flow. Kalkanis (1964) and Abou-Seida (1965) performed a series of experiments over an oscillating plate of sand. Transport was measured as it fell off the ends of the plate.

In their experiments it was only possible to examine transport occurring under a velocity field of a single frequency, rather than a mixed spectrum of flow as

in field conditions. Several of the theoretical procedures necessary in the application of the model require that waves of only one frequency be present. Einstein (1972) derives expressions for the velocity field within the boundary layer which require that the measured velocity outside the boundary layer and the wave phase both agree on the sign of the velocity at all times. In a mixed spectrum of waves this will not happen, even if all energy is collapsed into a single frequency. The resulting imaginary boundary-layer velocities make his model impossible to apply outside the laboratory.

The procedure for determining transport (Abou-Seida, 1965; Einstein, 1972) may be summarized as follows. The fluid velocity amplitude was determined using linear theory and the oscillating plate's period and amplitude. Then the fluid velocity within the turbulent boundary layer was computed at the distance 0.35 D from the bed using a very complicated expression for boundary-layer variation of velocity. This expression for the vertical variation of the horizontal velocity was an empirical adaptation of laminar boundary-layer theory in an attempt to simulate a turbulent boundary layer. Using the velocity from this expression, a Shields' number is computed. Then a "hiding factor" representing the effect of small grains "hiding" between the larger sand grains is computed using another empirical relation describing boundary-layer

behavior. The product of the Shields' number and the hiding factor then becomes yet another kind of Shields' number. The empirical curves obtained from the experiments of Kalkanis (1964) and Abou-Seida (1965) are then used to translate this Shields' number into a dimensionless transport. The number of assumptions made concerning the boundary layer makes the validity of Einstein's (1972) procedure quite dubious.

It is impossible to apply this procedure to a mixed spectrum of waves, even if collapsed into a single frequency. The model can only be applied in controlled laboratory conditions with a single frequency. Such laboratory experiments are currently underway (King and Seymour, 1984), in which the Einstein oscillatory flow model is one which will be tested. However, the basic postulate which makes Einstein's models unique (a variable exponent of u in the transport relation) is common to both Einstein's unidirectional and oscillatory models. In testing his unidirectional model we will be able to examine this basic postulate.

3. EXPERIMENT

Experiments with dyed sand as a tracer have been performed for more than 30 years. They quickly progressed from use as a visual estimator of transport thickness (King, 1951) to a full-fledged tracer experiment with estimates of transport velocities, thickness, and recovery (Inman and Chamberlain, 1959). A partial history of field tracer experiments and the characteristics of each is included here as Table 3-1. Most tracer experiments have been attempts to measure the total longshore transport in the surf zone, i.e., large-scale "global" (surf-zone scale) experiments. The list of global experiments in Table 3-1 is not complete, but some global experiments and their characteristics are listed for purposes of comparison. The type of experiment in which tracer is used to measure transport at essentially one point will be referred to as "point" experiments. All of the point experiments that we are aware of are listed in Table 3-1.

The experiments performed in this study are unique in that they use electromagnetic current meters to accurately measure the currents. The only other point experiment listed in the table in which such sensors were used was that of Miller and Komar (1969). However, they computed only sand diffusion estimates. For unknown reasons they did not report transport thickness, velocity, or tracer recovery.

Table 3-1. Characteristics of previous tracer experiments

	FORCING				EXPERIMENT LOCATION			COMPUTATION				TESTING	
	Drogues/Dye	Current Measurements — Waters	Wave Measurements — Visual	Wave Measurements — Sensors	Point Experiments	Offshore of Breakers	Sand Beach	Transport Thickness	Advection	Transport	Diffusion Estimates	Diffusion-Advection Models	Point Energetics Models
King, 1951			X			X		X					
Inman and Chamberlain, 1959	X			X	X	X	X	X	X				
Russell, 1960 and Rance, 1963									X		X	X	
Ingle, 1966	X		X		X	X	X						
Cricknore, 1967 (stream transport)		X						X	X	X			X
Murray, 1967				X	X	X	X						
Komar, 1969	X			X			X	X	X	X	X		
Gaughan, 1978					X		X	X					
Miller and Komar, 1969		X		X	X	X	X				X		
White, 1987		X		X	X	X	X	X	X	X	W	W	X

W: working on this now
X's indicate characteristics of a particular experiment.
Some surf-zone-wide experiments are not included.

Tracer experiments may be used to determine both total transport (advection or net velocity) and diffusion. The focus of our study is on total transport, but we plan to compute diffusion rates and test advection-diffusion models with both our data and that of Inman and Chamberlain (1959). Pizzuto (1987) developed a theoretical diffusion model, which was tested using the field data of Inman and Chamberlain (1959) and some laboratory diffusion data.

3.1 Sites

Several criteria were used in selecting experiment sites. Foremost was the requirement of sufficiently high waves to induce carpet-flow transport outside of the breakers. Any significant topographical variations must occur on larger spatial scales than the size of the sampling grid (6 m longshore by 8 m crossshore). The sand composition would need to be compatible with the sand dyeing techniques used. Shell fragments and dark heavy minerals did not dye as well as quartz, so the sand had to be principally quartz. The techniques used to count the dyed sand grains in the samples necessitated that the grains not be extremely fine. The counting procedures were much less reliable for grain sizes less than 75 microns. Finally, power access, data recording facilities, and access for scuba divers were considerations.

Several experiments were performed in 1980 in conjunction with wave-shoaling experiments for another study (Freilich, 1982). Both crossshore and longshore lines of electromagnetic current meters and pressure sensors were established at Torrey Pines beach for the wave-shoaling study. The crossshore line of instruments extended from 3 meters depth to 14 meters. Our sand-tracer experiments were performed near a current-meter station at 4.5 meters depth. For a complete listing of instruments, refer to Freilich's (1982) figure 2, in which our experiments occurred near C3.

Torrey Pines is a long straight beach with plane parallel contours about 5 km north of Scripps Institution of Oceanography (Figure 3-1). Offshore of the breakers the beach slope is about 1.5 degrees. Fathometer profiles of the offshore topography and rod-and-level profiles of the beach topography are drawn in Figure (3-2). Beach profiles were obtained with reference rods on frequent occasions between the fathometer profiles in Figure (3-2). All of the Torrey Pines sand-tracer experiments were performed near one fixed current meter, indicated on the fathometer profile. The median sand size at that location is about 200 microns. Shell content of the sand is nil, and dark heavy minerals compose about 10% of the sand. This site was chosen principally because data from the necessary current meters and pressure sensors were already being

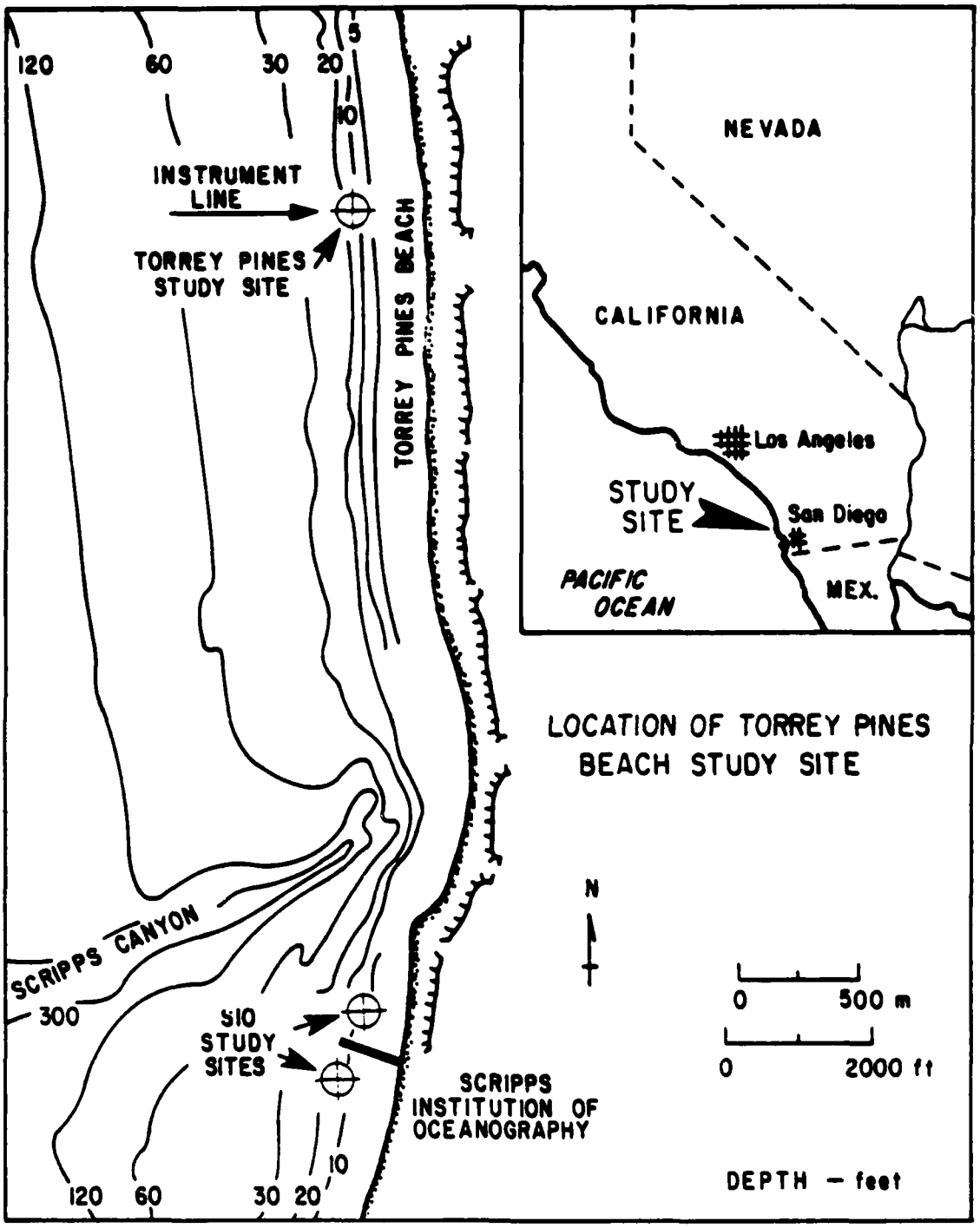

Figure 3-1. Experiment sites

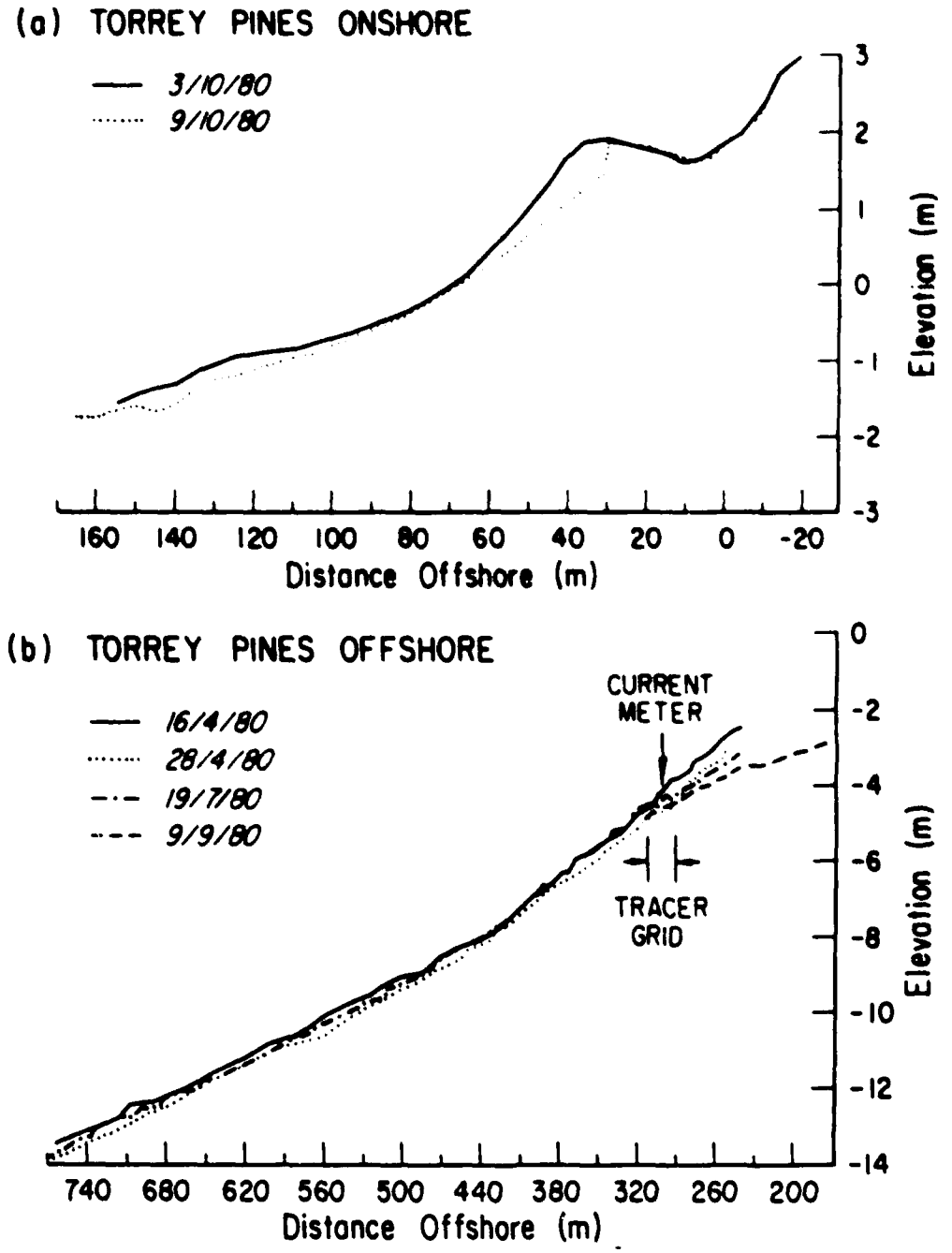

Figure 3-2. Beach profiles at Torrey Pines. The onshore portion of the profile was measured with rod-and-level. The offshore portion where the experiments took place was obtained with fathometer. (a) 20:1 vertical exaggeration (b) 30:1 vertical exaggeration

collected there for another experiment. Since the instruments were already in place, it was decided to attempt the sand-tracer experiments, even though some of the techniques had not yet been perfected.

Over the next couple years following the 1980 experiments at Torrey Pines, data were analyzed, and experimental techniques were improved. It was also decided to attempt experiments at another site in order to improve the generality of the data. All of the Torrey Pines experiments were performed under conditions in which the beach profile appeared to be in equilibrium. That is, the mean currents and the net sand transport were quite small in the crosshore. In order to obtain data for different wave conditions and hopefully to measure significant net transport, more experiments were performed near the Scripps Institution of Oceanography (SIO) pier in 1984 (Figure 3-1).

The 1984 experiments were performed approximately 100 meters from the pier. The experiments could not be located further from the pier because of the need to provide access by power and data cables to the instruments. Experimentation close to the pier was avoided, since bed features of long wavelengths occasionally occur in the wave shadow of the pier pilings (Inman, 1957). Not only were our experiments always performed well away from such topographical variations, but it was decided to experiment

on the side of the pier facing the oncoming waves. Both of these criteria of distance from the pier and choice of pier side insured avoidance of the pier-induced bed features. The topography for both the north and south sides of the pier is detailed in Figure (3-3). Additional reference-rod profiles were also obtained at the time of the experiments, and bottom slopes were calculated from them. The instruments used at the SIO site were mobile, as opposed to the fixed sensors at Torrey Pines, so the choice of both longshore and crossshore locations was made for each experiment, depending on wave conditions. The crossshore location of each experiment is listed separately in Figure (3-3). The beach slope at the experiment sites was about the same as the Torrey Pines experiments, about 1.5 degrees. Like Torrey Pines, the shell and heavy mineral content of the sand is small. However, at SIO the median grain size is smaller, about 180 microns. The specific sand and beach conditions for each experiment will be described in more detail in Section 5.1.

3.2 Instruments

3.2.1 Fluid measurement

Pressure sensors (strain-gauge type, Statham model PA 506-33) and electromagnetic current meters were used in all experiments. Other experiments have demonstrated that the pressure signal is quite linear and not subject to

AD-A185 083 NEARSHORE SAND TRANSPORT(U) CALIFORNIA UNIV SAN DIEGO 2/3
LA JOLLA T E WHITE 1987 N00014-75-C-0300

UNCLASSIFIED F/G 8/3 NL

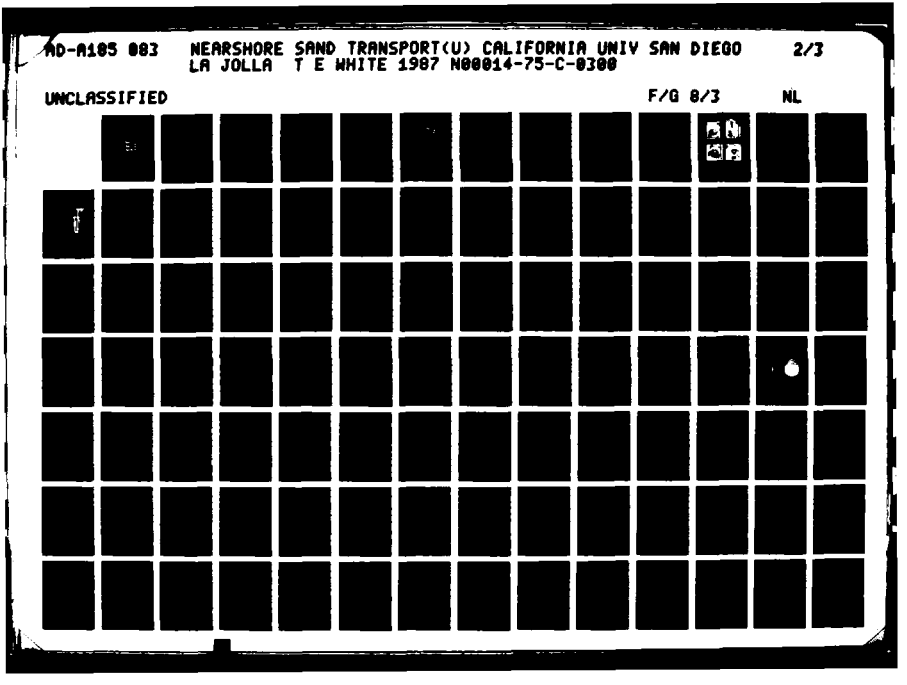

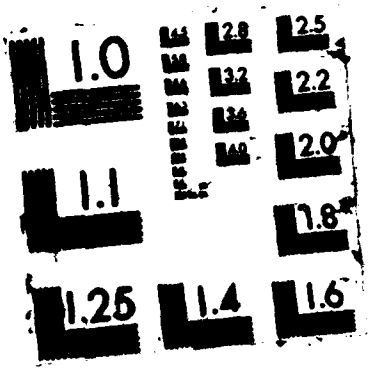
1.0
1.1
1.25
2.8
3.2
3.6
4.0
2.5
2.2
2.0
1.8
1.4
1.6

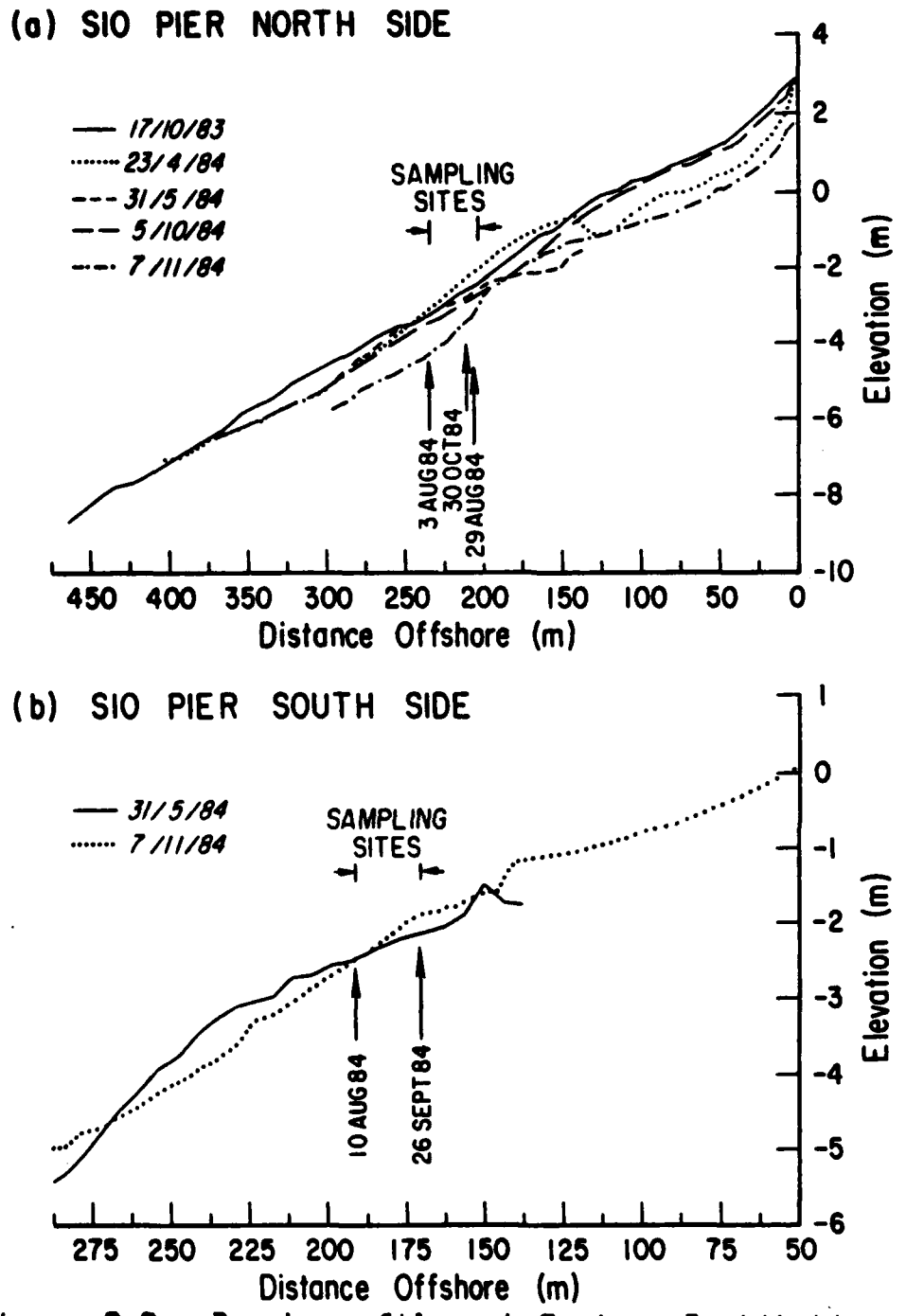

Figure 3-3. Beach profiles at Scripps Institution of Oceanography. Profiling and experiments took place about 100 meters north or south of the pier. Profiles are matched combinations of rod-and-level and fathometer profiling. Vertical exaggeration is 25:1.

drift with time. The pressure sensors were calibrated both before and after each year's experiments. Both gain and offset changed less than 3%.

Although data from pressure sensors can be used to compute fluid velocity with linear wave theory, such computations are not accurate enough for our requirements. Guza and Thornton (1980) found less than 20% error in pressure/velocity conversions for the depths in our experiments, but the bedload models we are testing require better accuracy. Furthermore, pressure sensors will not measure steady currents. The current meters (Marsh-McBirney #512 dual-axis spherical probes) were calibrated at the beginning and end of each year's experiments by towing them in a laboratory channel. The gains changed by less than 1%, and the offsets by less than 1 cm/s, except for one used only in the 30 October 1984 experiment which had an offset change of 3 cm/s. This is certainly not behavior that can be generally expected with such instruments. Calibrations in other experiments have been found to change considerably more than this. The reason that this did not occur here was that we required so few sensors, one or two current meters. Thus we could test many current meters and select the few that had the least noisy signal, typically the newest sensors.

There have been suggestions that there are fundamental flaws in the design of electromagnetic current

meters which prevent them from measuring velocity accurately when high levels of turbulence are present, or when significant levels of both steady and oscillatory flows are present (Aubrey and Trowbridge, 1985). However, when such sensors have been compared with other current meters of fundamentally different design (open-frame design), the excellent comparison of velocities suggests that there is no significant error due to design (Guza et al, 1986).

The sensors were deployed differently in the Torrey Pines and SIO experiments. At Torrey Pines, each instrument was located on a fixed pipe. There was one current meter seven meters longshore of the sand sampling grid. There were two pressure sensors located about 20 meters onshore and offshore of the current meter and sand sampling grid. Wave elevation spectra and mean depths were computed by linear interpolation between the two pressure sensors. Since only one current meter was used in the Torrey Pines experiments and its signal was noisier than the current meters used in the SIO experiments, we would expect less accuracy for the Torrey Pines fluid velocity measurements. Nevertheless, we will see that the sensor's measurement of very small crosshore mean velocities (generally less than 1 cm/s) agreed with the sand transport measurements of very small net crosshore transport. That

is, both the fluid and sediment measurements suggest near-equilibrium beach conditions.

A movable diver-deployed triangular frame (Figure 3-4) was used for sensor deployment in the 1984 experiments at SIO. As at Torrey Pines, the fluid velocity and sediment transport measurements were made at the same crosshore location. At Torrey Pines measurements were made at fixed locations, whereas at SIO both fluid and sediment sampling locations differed from day-to-day. At SIO the three legs of the sensor frame were screwed into the sand, and cables for data and power trailed off one of the legs back to the pier. The cables quickly scoured into the bottom. Sand sampling was always done on the side of the instrument frame away from the pier, in order to avoid any interference from the cables. One pressure sensor was deployed at the center of the frame, 22 cm above the sand bed.

Comparisons of measurements from two current meters (Figure 3-4) provided an estimate of the error in both the fluctuating and mean components of velocity. The current meters were far enough apart (1.2 m) to avoid electromagnetic interference. Experiments in the laboratory showed significant interference in the signals at 50 cm separation, barely noticeable noise at 75 cm, and no observerable interference at 100 cm separation.

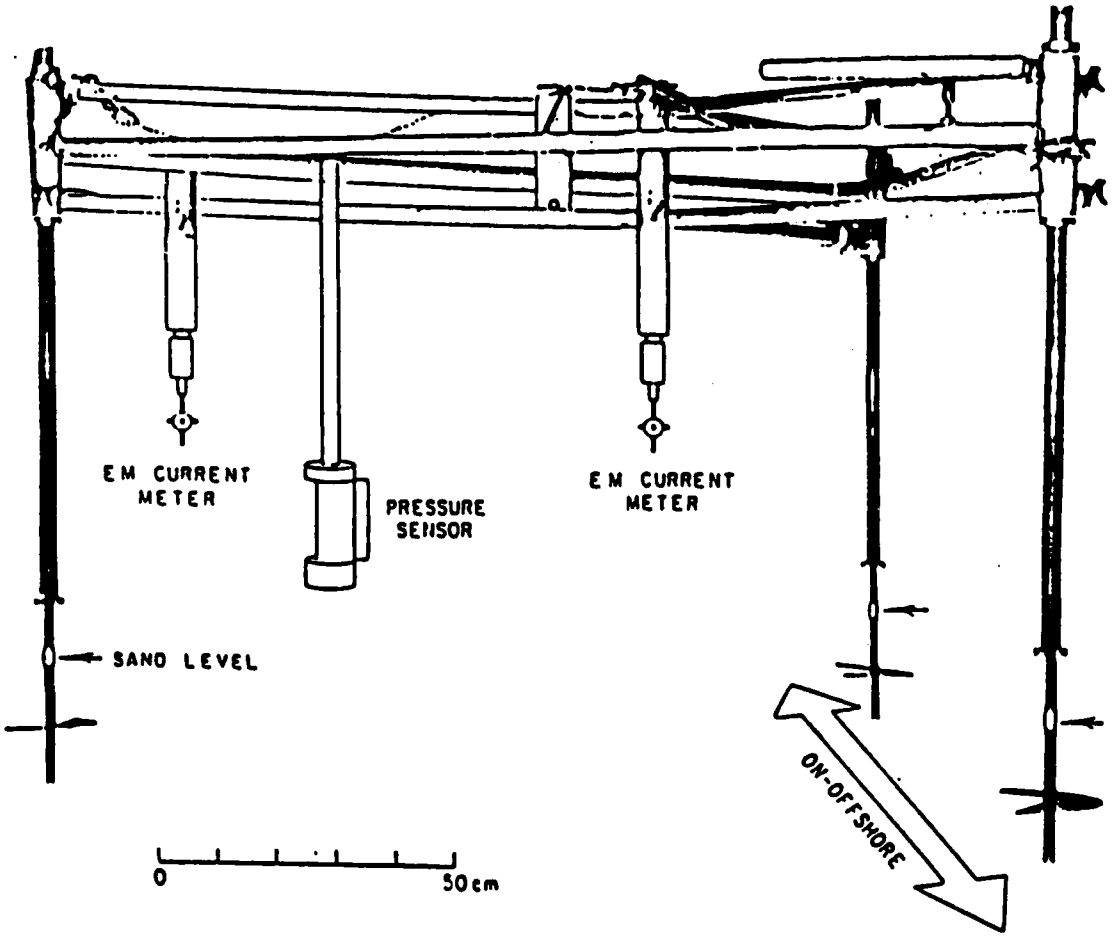

Figure 3-4. Frame and instruments used at the Scripps Institution of Oceanography experiments. Two current meters were mounted 1.2 meters apart and at the same height, along with one pressure sensor.

3.2.2 Sand tracing

Numerous studies have been performed with sand tracer in many countries. Soon after World War II there was interest in using irradiated sand tracers. Small quantities of quartz sand could be irradiated in nuclear reactors, injected into a sand bed, and then sampled in order to monitor the motion of the tracer centroid. Inman and Chamberlain (1959) used this technique successfully in an experiment similar to the ones we performed and at the same location near the SIO pier. However, more recent excessively stringent environmental policies have effectively prevented scientists from using radioactive sand tracers in this country. Long et al (1978) estimate exposure to someone swimming directly over the injection site for one hour or from ingestion of one irradiated grain to be about 2.5 millirems, an amount comparable to the exposure from a luminiscent watch over a year. The total average public exposure to all sources is about 200 mrem annually.

Because of environmental policies, studies performed by this laboratory after the 1950's used sand tagged with fluorescent dye by an outside company. Although the sand dyed by this company had good resistance to abrasion and visibility, it did have a few drawbacks. The formula was kept secret. Often the size distribution of the dyed sand varied somewhat from that originally

shipped. Finally, the entire process could take several days. Thus sand could not be obtained, dyed, and then reinjected into the ocean before size characteristics had changed. Therefore we decided to develop sand-dyeing techniques.

A good dyeing technique for sand should have several characteristics:

1. simple and low-cost formula,
2. the drying rate should be fast enough to allow rapid reintroduction into the ocean,
3. grain coatings should be of minimal thickness,
4. a wide selection of colors allows duplication of data or testing in the same area to be repeated,
5. colors should be both daylight visible and fluoresce under ultraviolet light for counting,
6. solubility in salt water should be low,
7. the dye should not abrade easily, and
8. the drying process should not cause the sand grains to clump together.

We tried several of the organic dyes and coating polymers suggested by Teleki (1966) but found them all to suffer from abrasion and solubility in water. The organic dyes did not bind well enough to the sand to stay on when exposed to surf zone abrasion or extended exposure to salt water. Yasso (1966) performed laboratory tests on many different types of dyes, including some of Teleki's. The

dyeing technique which we found worked best was one of those tested by Yasso. Three parts Day-Glo Acrylic Lacquer 202 Line (Switzer Bros., Inc.) are mixed with two parts Toluene solvent, combined with the sand, and then dried. The formulation is simple and relatively low cost. Yasso reported the drying time to be 11 minutes, but we found that complete drying took about 90 minutes. Yasso reported the coating thickness to be 38 microns, but variable, depending on techniques used. We found an average thickness of 3 microns. Ten Day-Glo colors are available, the largest selection either Yasso or we have found. We used both the "Rocket Red" and "Lightning Yellow," which were on either side in the light spectrum from the most visible color, orange. We used two colors simultaneously in order to duplicate all our data and provide error bars on our measurements. The dye is daylight visible and fluoresces under ultraviolet light. Yasso characterizes its visibility as "excellent" on a scale from "poor" to "excellent." We noticed no solubility in salt water, even after days of exposure. Yasso measured the abrasion percentage loss as 0.150% after rotation at 120 rpm for 18 hours. Finally, Yasso observed moderate clumping tendency of the drying grains, but he did not tumble the grains while they were drying as we did.

We dyed the sand in fine-weave cloth bags which were then immersed in the lacquer-solvent solution. After

stirring and prodding the bag for several minutes to insure complete coating, we dried the sand in a clothes dryer with moderate heat. The heat helped to bind the dye to the grains, and the tumbling prevented clumping of dyed grains. Dyed sand was ready to be used the day after the original sand was collected.

3.2.3 Sand injection

In previous tracer experiments (Komar and Inman, 1970; Inman et al, 1980; Kraus et al, 1982; White and Inman, 1987b) dyed sand was injected into the sand bed by swimmers opening a plastic bag of sand onto the bed. With such a technique, some of the dyed sand may be scattered throughout the water column but presumably falls quickly back to the bed. In the surf zone-wide experiments listed above, this procedure may have been acceptable, since plunging breakers can often stir up the dyed sand off the bed, just as occurs when injecting the sand with swimmers. But for our experiments outside the surf zone we used a more controlled means of sand injection.

A series of three sand-injection devices were built (Figure 3-5). The first was a simple metal cylinder with slots in the top for insertion of the diver's hands. A plastic bag of dyed sand was held in the device which was placed on the sand bed. The diver then opened the bag inside the cylinder. After waiting a minute to let the

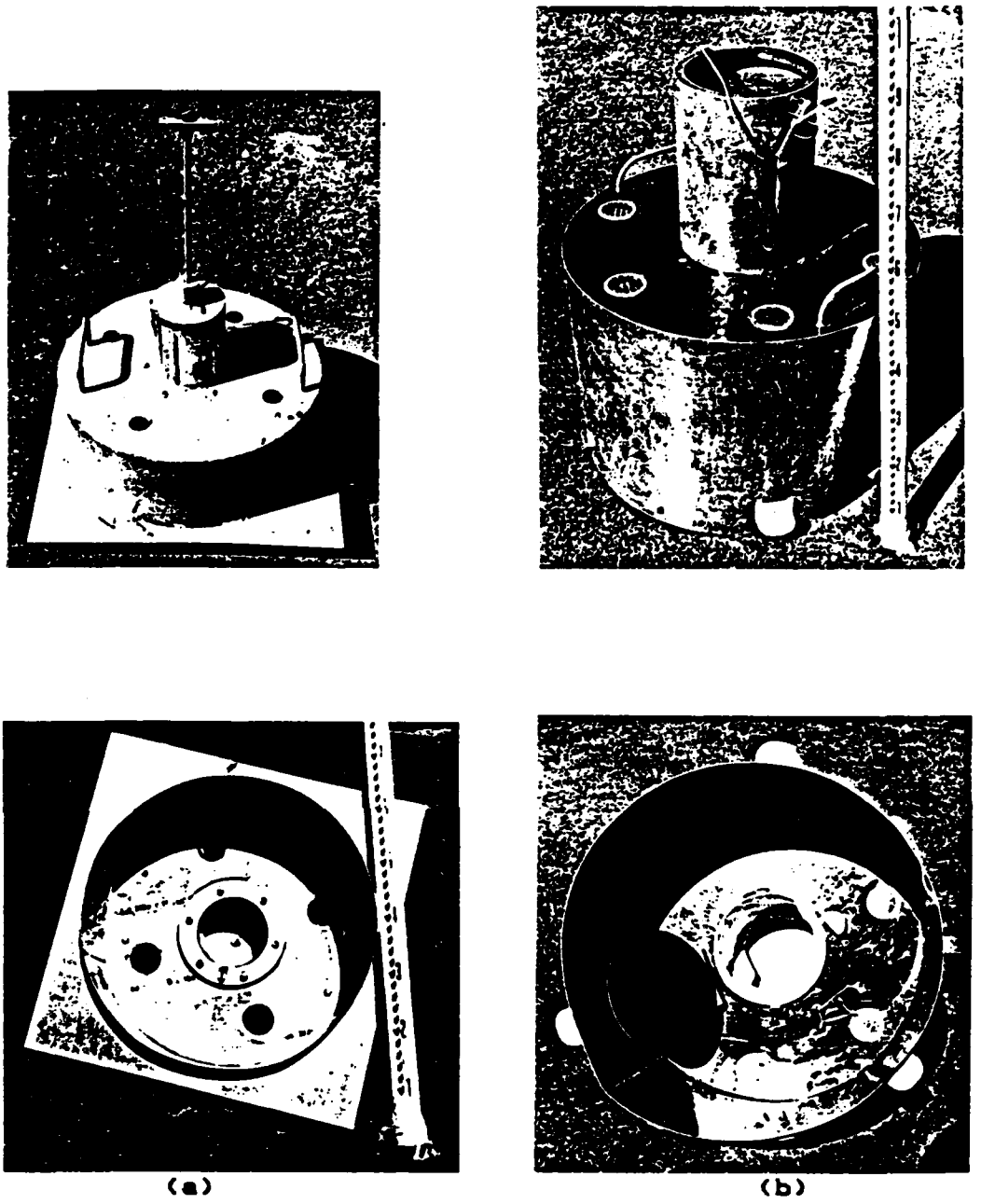

(a) (b)

Figure 3-5. Sand injection devices used in tracer experiments. (a) The model used at Torrey Pines with upper cylinder height = 16cm, diameter = 14cm; lower cylinder height = 20cm, diameter = 55cm. (b) The larger model used at SIO with upper cylinder height = 36cm, diameter = 25cm; lower cylinder height = 50cm, diameter = 70cm.

sand settle to the bed, the device and empty bag were removed. However, there was still some dyed sand which escaped through the hand slots.

Further designs consisted of two cylinders, a smaller one on top the other (Figure 3-5). At SIO a larger model ("b" in Figure 3-5) was used to decrease the tracer thickness. The wetted dyed sand was emptied into the top cylinder before entering the ocean. The top cylinder is closed on both ends. The device is then placed on the ocean bed, a lever is pulled, and a trap door in the bottom of the upper cylinder opens, releasing the dyed sand into the lower cylinder. Computation of fall velocities indicate that all the sand-sized grains will fall to the bed within one-half minute. The result is a 5-10 kg cylinder of dyed sand on the bed, about 0.5-1.0 cm in thickness. This was the thickness obtained in the third device shown in Figure (3-5). It was built to reduce the 2-3 cm thicknesses obtained in the second device (used in the Torrey Pines experiments). After waiting the half minute, the injection device is removed. This is not long enough for the injection device to cause scouring in the bed. Earlier trials indicated that three minutes are needed for scouring.

3.2.4 Sand sampling

The sand bed was sampled with diver-held coring devices (Figure 3-6) described in detail by Zampol and Waldorf (1987). The device consists of a long metal tube with a handle and valve at one end and a seat for a plastic core tube at the other end. The diver opens the valve at the top before sampling. This provides an open column throughout the length of the device, in order to relieve pressure caused by sand entering the core tube at the bottom. The diver presses the tube into the bed by pushing on the handle at the other end. Once the tube has been pressed into the bed several centimeters, the valve is closed, causing the constant pressure within the device to hold the sand in the tube. The device is then pulled from the bed, and the bottom of the tube is capped. The sand core obtained is 4 cm in diameter and 5 to 15 cm in length, depending on how far into the bed it was pushed.

3.3 Experimental methods

On each potential experiment day wave conditions were examined to determine whether conditions were optimum for a tracer experiment. The waves had to be sufficiently high to induce carpet-flow motion of the sand outside the breakers, but not so high as to make it impossible for scuba divers to work. Also good underwater visibility was necessary. Part of the experiment consisted of taking

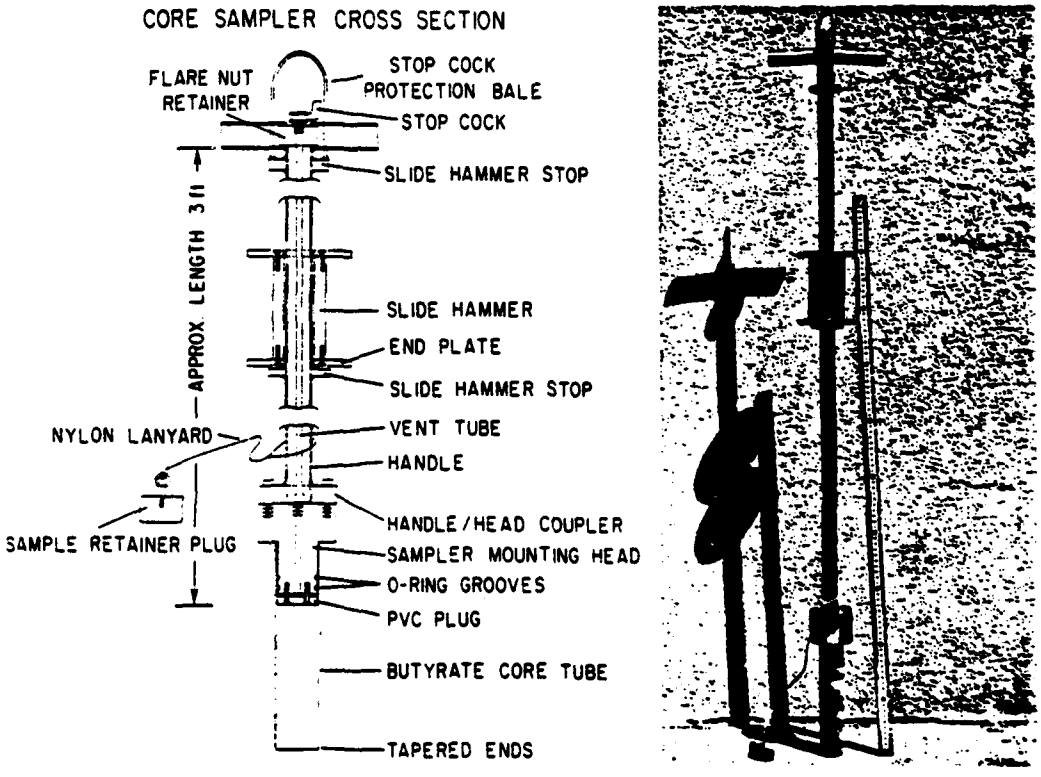

Figure 3-6. The sand bed coring device used in all experiments (from Zampol and Waldorf, 1987).

underwater photographs of the tracer on the sand bed, in order to have a check on the core-sample measurements of transport velocity. If the conditions of carpet-flow outside the breakers and good visibility were met, an experiment was attempted.

Experiments consisted of measurements of fluid quantities (pressure and velocity) and sediment quantities (velocity, transport thickness, grain size, and beach slope). At Torrey Pines the fluid pressure and velocities were measured from fixed instruments as described in Section 3.2.1. Several meters longshore of the current meter, metal pipes had been set in the sand. There were five pairs of pipes with ropes, establishing five crosshore lines. Flags attached to the ropes at half-meter intervals provided a sampling grid of known horizontal coordinates.

In the 1984 experiments at SIO the pressure sensor and two current meters were placed on a mobile metal frame (Figure 3-4) which was anchored in the sand bed. The grid for core sampling was established by flags attached to 1 mm diameter metal rods inserted in the sand bed at measured half-meter intervals (Figure 3-7). The metal rods were not observed to cause any scour in the bed. The fluid sensors and the core-sampling grid were at the same crosshore location.

In both the Torrey Pines and SIO experiments the same sequence of events was followed. Sensors were

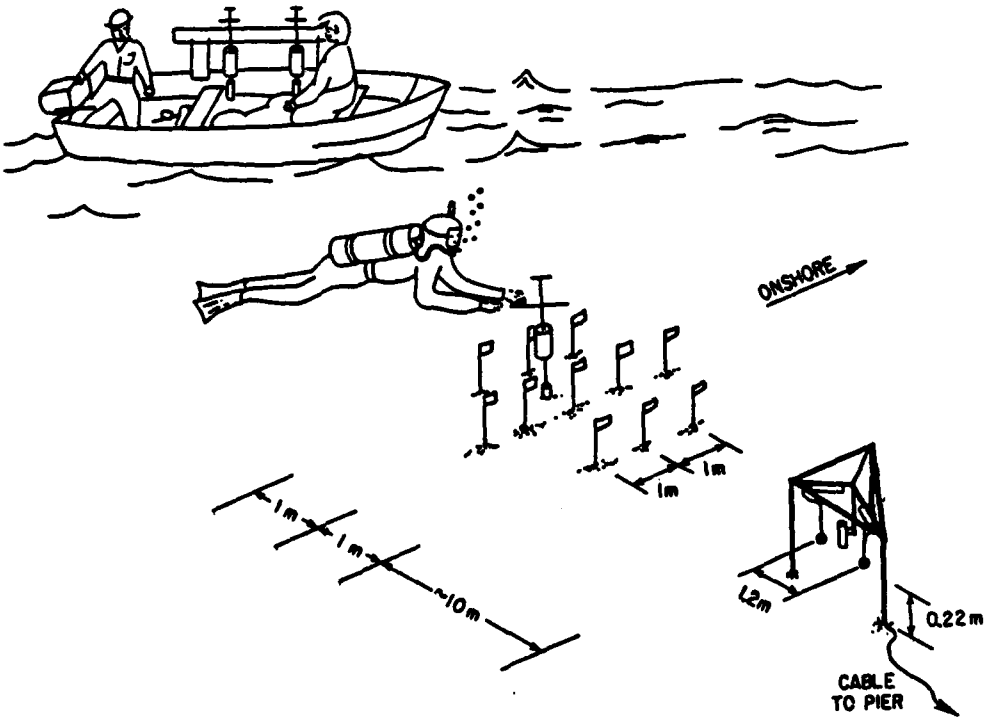

Figure 3-7. Experimental layout for the SIO experiments. The instrument frame and sampling grid were always longshore of each other. A cable led from the frame back to the pier.

connected, the grid of sampling locations was established, the sand-tracer injection device (Figure 3-5) was loaded with wetted dyed sand, and divers injected the tracer onto the bed. This injection was performed twice with different colors, at 1.5 m offshore of the grid center and at 1.5 m onshore of the center. This provided essentially two simultaneous tracer experiments. An experiment consisted of two to five grids of core samples, providing four to ten estimates of transport. (Two colors were used.) Throughout each experiment, the motion of the top layer of tracer could be seen. Before the next set of samples were taken, the locations for sampling would often be changed from the previous set, in order to monitor the tracer motion as completely as possible. This ability to change sample locations based on visual observation of the tracer motion is a major advantage of our experiments over experiments others have performed in the surf zone. It is not necessary to guess where most of the tracer is.

The determination of both fluid and sediment velocities required accurate knowledge of the compass orientation of both current meters and the sand sampling grid. Divers established compass orientations for both the instrument frame and the rangelines of flags in the sampling grid by sighting through an underwater compass along the frame and the line of flags. In the one experiment in which the orientations of the frame and line

of flags differed by more than one degree, the current-meter velocity records were later rotated to the same orthogonal lines as the sand grid.

In the Torrey Pines experiments both the sensor orientations and sand-sampling grid orientation were rigidly set before experiment. In both cases the orientations were recorded with an electronic compass (reading to tenths of a degree), which was rigidly attached to instrument mounting pipes or sand grid pipes during readings.

In conjunction with the tracer measurements, data were also obtained on sediment concentration N_0, sand size distributions, net erosion/accretion, and beach slope. In order to measure both beach slope and erosion, a grid of 2-meter long brass reference rods was permanently established in the sand bed on three 100 m long crosshore ranges. Fathometer surveys established a baseline beach profile. Then divers measure the distance between the top of the rod and the sand bed to provide a record of the level of sand accurate to 1 cm. Together with the fathometer profiles, these measurements provide a history of beach profiles at the site. Reference rods were measured during each experiment to provide slope and erosion estimates for each experiment. The beach slopes used in the bedload models were determined by measuring the slopes on the reference-rod profiles for each experiment

over the region marked "tracer grid" and "sampling sites" on Figures (3-2) and (3-3). Fortunately none of the experiments took place near a noticeable change in slope. Interpolations in time were made between profiles to coincide with tracer experiments.

Individual depth measurements from a fathometer record are very inaccurate. A study of fathometer and reference-rod methods by Inman and Ruanak (1956) showed accuracy of corrected fathometer surveys was ±15 cm and reference-rod accuracy was ±1.5 cm. However, over regions of slowly varying beach slope, random (wave-induced) error in fathometer records will average out over many sample points. Any offset error will effect depth measurements but not slope estimates. Only gain errors in the instrument and very long period (minutes) wavelike motions will effect the accuracy of beach slope measurements. These profiles are used to obtain estimates of beach slope, a quantity which appears in three of the bedload models described in Section 2.3. None of these models is very sensitive to beach-slope error. Sensitivity was estimated for the 23 June 1980 experiment by computing transport for the measured beach slope of 1.66 degrees, 1.76 degrees (6% slope error), and 2.16 degrees (30% slope error). The results indicate that error in computed transport is several times less than error in the beach slope. The (beach-slope error)/(transport error) ratio is about the

same for the two cases of 6% and 30% error in slope. The ratio is 20:1 for the Bagnold (crosshore) model, 8:1 for the Bailard and Inman crosshore model, no transport error in the Bailard and Inman longshore model since it has no beach-slope dependence, and 6:1 for the Kobayashi crosshore and longshore models.

Quite independently of the fathometer profiles, before-and-after reference-rod measurements also provide a record of net erosion or accretion during the tracer experiment. During some of the experiments erosion was measured at one end of the reference-rod grid and accretion at the other end. Sand-level changes suggest transport away from erosion sites and toward accretion sites. This holds true if the divergence of longshore transport is small, which is the case if the site is not near large topographical features such as headlands. This is another check on the transport directions obtained from the tracer experiment.

3.4 Data reduction

The pressure and velocity measurements were sampled at 16 Hz and recorded on analog tape. Occasional sharp spikes in the data, which were clearly instrument-related, were removed. Such spikes occurred once every several minutes in the current records and even more rarely in the pressure record.

The following sediment variables were measured: at-rest sediment concentration, sand size distribution of both dyed and in-situ sand, erosion/accretion, beach slope, sand velocity, and transport thickness. Methods for determining concentration, erosion, and beach slope have already been described. The sand size distributions were measured using standard sieving methods of dried sand.

The sand-transport velocity and thickness (needed in Equation 2.1) were obtained from the dyed-sand concentrations in each of the core samples. Each sand core was extruded using an extrusion device described in detail by Zampol and Waldorf (1987). During extrusion the device removed the outer 3 mm annulus which contains dyed sand pushed into the bed during coring. The resulting core had a 4.25 cm diameter. Vertical thicknesses of each horizontal slice were 0.25 cm for the top 4 cm of the core, 0.5 cm for 4-6 cm deep, and 1 cm for deeper slices. Each core slice was rinsed to remove salt, dried in an oven, and then spread on a counting grid. Under ultraviolet light, the number of dyed grains of each color in each core slice were visually counted and recorded, along with the total mass. These numbers yielded concentrations in numbers of dyed grains per unit mass. This vertical distribution of tracer was used in computing transport thickness, whereas the total tracer in each core was used in determining horizontal transport velocity.

4. RESULTS

4.1 Waves

The general wave and tidal conditions during each of the nine transport experiments are listed in Table 4-1. Tides during this period were determined from a gauge in continuous operation at the end of Scripps pier. The range in Table 4-1 is the total range of the tide during the four-hour experiment. One concern about the tides was that they would influence in some manner the direction of the crossshore sediment transport (onshore or offshore), as shown by Inman and Rusnak (1956). The experiments measured offshore sediment transport on two days (3 August 1984 and 29 August 1984) and onshore in the other days. For the experiments recording offshore transport, the tide was rising in one case and falling in the other. For the nine experiments listed in Table 4-1 there appears to be no correlation between tidal range or stage and the direction of transport. Of course tides must generally influence transport. Otherwise such morphological features as low-tide terraces and breaker bars would not be present. However, our experiments took place during a time period (about four hours) somewhat shorter than a tidal cycle and often on relatively flat portions of the tidal curve. Also there appears to be a seasonal pivot point in the beach profile just offshore of the depths at which we worked.

Table 4-1. Tides and waves

Date	Tide Range (cm)	Tide Stage	Depth h (cm)	Peak Period T (s)	Uncorrected Wave Height Hp (cm) Sig.	Mean
23Jun80	61	R	230	7.7	70	44
11Aug80	52	FR	260	22.7	39	42
12Sep80	21	RF	280	13.7	57	36
29Sep80	46	F	250	17.0	59	37
3Aug84	37	R	500	9.1	87	54
10Aug84	24	F	310	10.0	67	42
29Aug84	82	F	430	10.0	54	34
26Sep84	106	F	320	11.4	52	33
30Oct84	37	RF	430	6.7	47	29

Date	Surface-Corrected Wave Height H (cm) Sig.	Mean	Orbital Diameter d_o (cm) (Eq. 4.1)	Maximum Orbital Velocity u_m (cm/s) (Eq. 4.2)
23Jun80	91*	57*	141	58
11Aug80	42	26	182	25
12Sep80	75*	47*	191	44
29Sep80	75	47	251	46
3Aug84	113	71	139	48
10Aug84	83	52	145	46
29Aug84	69	43	101	32
26Sep84	72	45	141	39
30Oct84	61	38	58	27

*: Wavestaffs used to obtain surface wave heights.

Tidal Stage:
F=falling
R=rising
FR=falling, then rising
RF=rising, then falling

Aubrey (1979) documented a pivot point at 6 m depth at Torrey Pines Beach where our 1980 experiments took place.

The data from the near-bottom pressure sensors and surface-piercing wavestaffs were used to compute the following parameters: near-bottom pressure converted to wave height (Hp), surface-corrected wave height H, mean depth h, peak spectral period T, near-bottom orbital diameter d_o, and near-bottom maximum orbital velocity u_m. Of these quantities the only ones which are used in the tested bedload models are orbital diameter [in the Sleath (1978), Hallermeier (1980), and the dimensional-analysis models] and maximum orbital velocity [in one version of the Bagnold (1963) oscillatory-flow model]. Both quantities are also used in empirical correlations with transport thickness (Section 4.4).

The peak spectral period was obtained from the spectra of the pressure sensor and wavestaff data (Appendix 4). The mean depth $h=(p/\rho g)+z$ where p is the mean pressure signal and z the sensor height above the bed. The near-bottom wave height in units of cm (Hp) was not surface corrected. At SIO the sensor was at the experiment site, whereas at Torrey Pines some horizontal interpolation between sensors was required. The significant Hp were computed as four times the square root of the variance of the pressure signal divided by the conversion factor ρg. The mean Hp is the significant Hp divided by 1.6. The

upper cutoff frequency used in the summation of the variance was 0.4 Hz, except for 29 September 1980 for which the pressure data from another investigator's sensor were used. The spectra from that sensor had already been computed with a cutoff frequency of 0.25 Hz.

Pressure signals measured near the bed are damped as a function of frequency. The wave heights listed in the lower half of Table 4-1 were obtained by first surface-correcting the entire pressure spectra with the correction factor $\cosh[k(z+h)]/\cosh(kh)$. The same procedure that was used to obtain Hp was then applied to the surface-corrected data to obtain $H_{sig} = 4\,[(\text{pressure variance})^{0.5}]/\rho g$. These wave heights were then used to estimate orbital diameter and maximum orbital velocity near the bed. The orbital diameter is:

$$d_o = \frac{H_{mean}}{\sinh(kh)} \qquad (4.1)$$

where k is the wave number of the spectral peak. The maximum orbital velocity was computed from:

$$u_m = \pi\, d_o / T \qquad (4.2)$$

where T is the peak spectral period.

The spectral peak remained the same after surface-correcting for all experiments. In some of the Torrey Pines experiments wavestaffs were located closer to the experiment site than were pressure sensors. In these cases (indicated with an asterisk in Table 4-1), the wave heights were computed directly from the wavestaff variance

without surface-correcting, since wavestaffs are already located at the surface.

4.2 Currents

Several different first-order velocity moments were computed from the current meters and are listed in Table 4-2. The current meters at the same crosshore location as the tracer experiment were used to obtain moments corresponding to the time period covered by each tracer sampling grid. For example, the four rows of moments for the 23 June 1980 experiment were obtained by averaging the current velocities over the time ranges of tracer injection until the time of first tracer sampling, then tracer injection until the second sampling, etc.

The total velocity was computed as $u_T=\langle(u^2+v^2)^{0.5}\rangle$. The threshold velocity necessary to initiate sand motion was computed from the methods of Dingler and Inman (1976) and Seymour (1985) described in Section 1.1. There was an average 16% difference in the threshold velocity obtained from these two different methods. When applied to bedload equations, the resulting difference in transport was less than 1% for the two different methods of computing threshold velocity. Table 4-1 gives threshold values according to Inman (1979), our Equation (1.3).

In addition to computing the orbital diameter d_o and maximum orbital velocity u_m from the pressure data in

Table 4-2. Current Velocities

(Positive u is onshore, positive v to the north.)

Date	Mean Velocity (cm/s) u Onshore	v Longshore	Total Velocity u_T (cm/s)	Threshold Velocity u_t (cm/s) Eq.(1.3)	Seymour (1985)	Max. Orbital Velocity u_m (cm/s)	Orbital Dia. d_o (cm)
23Jun80	2.6	-1.6	26.6	35.7	34	64.9	159
	0.4	-1.6	26.0			63.0	154
	-0.3	0.9	24.8			60.1	147
	0.3	0.9	24.3			58.6	144
11Aug80	0.9	-3.1	13.3	36.5	20	30.8	233
	1.2	-3.8	13.7			31.0	224
	1.4	-3.6	13.6			30.8	223
	1.5	-3.4	13.6			31.0	224
	1.4	-3.4	13.7			31.2	225
	1.3	-3.6	13.8			31.4	227
12Sep80	-0.5	-3.1	11.6	33.7	36	26.8	117
	-0.7	-3.6	11.9			26.5	116
	-0.6	-3.9	12.1			26.8	117
	-0.5	-4.4	12.1			26.2	114
	-0.8	-4.6	12.0			26.2	114
	-0.9	-3.7	12.0			26.8	117
3Aug84	-8.3	-2.1	28.5	27.9	35	68.7	199
	-8.1	-2.6	27.7			66.5	193
10Aug84	10.5	9.2	27.7	27.4	36	63.4	202
	8.5	7.9	26.4			61.2	195
29Aug84	-8.5	-5.8	18.9	24.3	36	44.5	142
	-8.8	-4.9	19.0			45.1	144
	-8.5	-4.6	19.1			45.7	145
26Sep84	5.5	7.2	19.1	25.9	37	44.5	161
	4.7	7.8	20.1			46.9	170
	4.4	7.9	21.3			49.7	180
30Oct84	1.6	-0.0	16.4	19.8	31	38.8	83
	1.9	-1.0	16.8			39.3	84
	1.9	-1.5	17.2			40.1	86
	1.8	-1.8	17.4			40.4	86

$u_T = \langle (u^2+v^2)^{0.5} \rangle$

$u_m = 2\langle (\text{total variance}) \rangle^{0.5}$

$d_o = u_m T/\pi$

Table 4-1, we did so with the current-meter data in Table 4-2. Maximum orbital velocity u_m was estimated as two times the square root of the total velocity variance. This is an analogy with the method for computing significant wave height. The factor of two appears instead of the factor four in significant wave height, because wave height is a measure of trough-to-crest whereas u_m represents departure from the mean. The orbital diameter d_o was obtained from the u_m estimate using $d_o=u_mT/\pi$.

There is some question as to how well these measurements represent the currents near the sand bed. Some transformation of velocities takes place within the boundary layer. Sleath (1970) found that the boundary layer thickness for his laboratory experiments on oscillatory laminar flow over a flat stationary sand bed was:

$$\delta = a\,(2\nu/\sigma)^{0.5} \qquad (4.3)$$

where a is a dimensionless parameter between 1 and 10, varying as a function of the Reynold's number. Applying the 1-10 range in "a" to the peak frequencies in our experiments, Equation (4.3) suggests the boundary layer in our experiments ranged between 0.15 and 2.8 cm. Even though Sleath's boundary layer was laminar and ours turbulent, it is difficult to believe that this difference would increase the boundary layer thickness by more than

the order of magnitude necessary to place our current meters in the boundary layer.

One question we must address is whether there is sufficient vertical variation in the horizontal fluid velocities outside the boundary layer that it matters where we place the current meters. The available data suggest that there is little variation in horizontal velocities within the meter of fluid closest to the bed, but outside the boundary layer. Unfortunately, most of the work on this question has addressed velocity variation within the surf zone, and little work has been done just outside the breakers. Quantification of the phenomenon known as "undertow" has been the focus of several laboratory investigations within the surf zone (LeMehaute et al, 1968; Hansen and Svendsen, 1984; Svendsen, 1984) and two field studies (Inman and Quinn, 1952; Stive and Wind, 1986). The investigators found significant variation of the horizontal velocity field between the upper and lower parts of the water column in some cases (i.e., under breaking waves), but variation of the mean velocity within the bottom quarter of the water column was less than 10% (Stive and Wind, 1986, Figure 4). Presumably vertical variation of horizontal velocity outside the surf zone would be even less. This is now an active area of investigation (Doering and Bowen, in press).

The presence of more than one current meter allows estimation of measurement error. Comparisons of the current meter signals for the three SIO experiments in which both current meters were working are summarized in Table 4-3. The moments were computed both with and without a threshold criterion. The first through sixth moments predict the measured crosshore transport direction only 70% of the time, but correctly predict direction in all experiments when a threshold is applied. Accordingly, the moments listed in Table 4-3 were computed ignoring all velocities below threshold in the time series:

$$\langle u^n \rangle = \langle \mathrm{sgn}(u)\ |u|^n \rangle \qquad \text{for all } u_T > u_t$$

$$= 0 \qquad \text{for all } u_T < u_t \qquad (4.4)$$

where | | indicates absolute value, < > time averaging, and u_T is the total instantaneous velocity $u_T=(u^2+v^2)^{0.5}$. The percent difference is the difference between the two sensors divided by the average. There is less than 5% difference in the first, second, and third velocity moments. The difference in the higher moments is larger, rising to 20% for the sixth moment. Since measurement difference is also exponentiated, it is expected that the difference will increase with the higher moments. Somewhat surprisingly, the square root of velocity had the highest difference, 31%.

The moments used in the transport models tested cannot always be classified exactly as u^3, u^4, etc., since

Table 4-3. Comparison of Crosshore Moments from Redundant Current Meters

(Each of the eight experiments corresponds to the time during during which a tracer grid measured sand transport.)

Experiment	Sensor	Moment: $\langle u^n \rangle$ (Eq. 4.4) in $(cm/s)^n$						
	n =	0.5	1	2	3	4	5	6
				$x10^2$	$x10^3$	$x10^5$	$x10^7$	$x10^8$
10Aug84 #1	CM2	1.03	7.45	4.29	25.2	15.8	10.7	77.5
	CM3	.866	7.21	4.13	24.5	15.5	10.7	78.5
% Difference		17.3	3.3	3.8	2.8	1.9	0.0	-1.3
#2	CM2	-.612	6.14	3.62	21.7	14.0	9.75	74.2
	CM3	-.223	6.07	3.52	21.0	13.5	9.46	71.4
% Difference		93.2	1.2	2.8	3.3	3.6	3.0	3.9
29Aug84 #1	CM2	-.777	-6.37	-2.33	-9.15	-3.85	-1.73	-8.23
	CM3	-.799	-6.69	-2.34	-8.69	-3.43	-1.43	-6.27
% Difference		2.8	-4.9	-0.4	5.2	11.5	19.0	27.0
#2	CM2	-1.23	-6.44	-2.35	-9.13	-3.79	-1.67	-7.78
	CM3	-1.27	-6.65	-2.31	-8.52	-3.32	-1.36	-5.87
% Difference		-3.2	-3.2	1.7	6.9	13.2	20.5	28.0
#3	CM2	-.415	-6.28	-2.33	-9.18	-3.84	-1.69	-7.72
	CM3	-.548	-6.49	-2.29	-8.56	-3.36	-1.37	-5.78
% Difference		-27.6	-3.3	1.7	7.0	13.3	20.9	28.7
26Sep84 #1	CM2	.857	4.02	1.61	7.00	3.28	1.67	9.21
	CM3	.881	4.26	1.61	6.53	2.82	1.30	6.28
% Difference		-2.8	-5.8	0.0	7.0	15.1	24.9	37.8
#2	CM2	.0349	3.63	1.50	6.71	3.25	1.70	9.60
	CM3	.0808	3.95	1.55	6.60	3.03	1.50	7.92
% Difference		-79.3	-8.4	-3.3	1.7	7.0	12.5	19.2
#3	CM2	.515	3.59	1.56	7.35	3.78	2.10	12.6
	CM3	.650	3.85	1.60	7.21	3.55	1.89	10.9
% Difference		-23.2	-7.0	-2.5	1.9	6.3	10.5	14.5
Average of absolute values of % Dif. for the 8 experiments:		31.2	4.6	2.0	4.5	9.0	13.9	20.1
Standard deviation of the % Dif. for the 8 experiments:		33.2	2.2	1.3	2.2	4.6	8.4	12.0

the models are in some cases quite complicated functions of the fluid velocity. These moments were computed according to the model equations in Section 2.3. In some cases the models specify application of a threshold criterion by including the factor $u-u_t$ and specifying that values of $|u|<u_t$ are to be ignored (Meyer-Peter and Mueller, 1948; Yalin, 1963; Kobayashi, 1982; Sleath, 1978). For all the remaining models we computed the moments according to the model equation (which did not contain a threshold criterion) and also according to Equation (4.4). The latter method is listed in Table (4-4) as "with u_t."

The percent difference in the velocity moment required by each model (Table 4-4) is 5% or less for the Bagnold model and the Bailard and Inman model, about 10% for the other u^3 models, 10-15% for the u^4 and u^5 models, and about 20% for the u^6 models. The trend of increasing error with higher moment is the same as for the individual moments computed in Table 4-2, but some interesting differences appear between the models that are classified in the same moment category. For example, the Bagnold model and Bailard and Inman model contain somewhat less error than the other u^3 models, which contain very complicated functions of u.

Another source of measurement error examined was the sensitivity of transport calculations to measurement of the mean velocity. All transport models retain the mean

Table 4-4. Effect of Error in Fluid-Velocity Measurement on Predicted Transport from Models
(Computed transport in dynes/(cm-s) is listed for each sensor followed by % difference between the two.)

Part A: u^3 models

Experiment	Sensor	Computed Transport [dynes/(cm-s)]						
		Bailard & Inman		Bagnold		Meyer-Peter & Mueller	Yalin	Kobayashi
			with u_t		with u_t			
10Aug84 #1	CM2	60.4	57.2	68.6	65.0	80.7	451.9	11.8
	CM3	58.2	55.4	65.4	62.1	79.0	442.3	11.4
% Difference		3.7	3.2	4.8	4.5	2.1	2.2	3.9
#2	CM2	52.2	49.9	58.8	55.8	70.8	396.3	10.2
	CM3	50.4	48.6	56.7	54.0	68.7	385.0	10.3
% Difference		3.4	2.6	3.7	3.2	3.0	2.9	-0.3
29Aug84 #1	CM2	-27.6	-25.4	-25.6	-24.0	-21.3	-153.9	-4.9
	CM3	-27.1	-24.7	-24.0	-22.3	-18.3	-132.4	-4.4
% Difference		1.9	2.6	6.8	7.1	15.2	15.0	11.6
#2	CM2	-27.5	-25.2	-25.5	-23.7	-20.9	-151.1	-5.5
	CM3	-26.5	-24.0	-24.0	-22.1	-17.6	-127.1	-4.8
% Difference		3.8	4.7	6.3	6.9	17.4	17.3	13.8
#3	CM2	-27.4	-25.2	-25.4	-23.7	-21.5	-155.4	-6.0
	CM3	-26.3	-24.1	-23.8	-22.1	-18.1	-131.2	-5.1
% Difference		4.0	4.8	6.4	6.9	17.0	16.9	15.7
26Sep84 #1	CM2	18.6	17.5	20.6	19.2	17.2	98.7	2.4
	CM3	18.0	16.9	18.7	17.6	14.4	82.7	1.9
% Difference		3.6	3.3	9.7	9.0	17.9	17.6	22.8
#2	CM2	17.2	16.4	19.3	18.2	17.3	98.9	2.3
	CM3	17.6	16.9	18.8	17.9	15.8	90.7	1.9
% Difference		2.1	2.8	2.7	1.6	8.8	8.7	16.6
#3	CM2	18.2	17.7	20.7	19.9	20.3	116.4	2.9
	CM3	18.5	18.0	20.1	19.5	18.9	108.1	2.5
% Difference		1.6	2.0	2.8	2.0	7.5	7.4	13.9
Average of absolute values of % Dif. for the 8 experiments:		3.0	3.3	5.4	5.2	11.1	11.0	12.3
Standard deviation of the % Dif. for the 8 experiments:		0.9	0.9	2.2	2.6	6.1	6.1	6.7

Table 4-4. Effect of Error in Fluid-Velocity Measurement on Predicted Transport from Models
(Computed transport in dynes/(cm-s) is listed for each sensor followed by % difference between the two.)

Part B: u^4 and u^5 models
(Sleath and Hallermeier are u^4 models and Hanes & Bowen u^5)

Experiment	Sensor	Computed Transport [dynes/(cm-s)]				
		Sleath	Hallermeier with u_t		Hanes & Bowen with u_t	
10Aug84 #1	CM2	1.72	2.50	2.50	52.1	51.8
	CM3	1.71	2.42	2.37	51.2	50.9
% Difference		0.6	3.3	1.8	1.8	1.8
#2	CM2	1.54	2.19	2.15	47.3	47.0
	CM3	1.50	2.13	2.09	45.8	45.6
% Difference		2.6	2.8	2.8	3.1	3.1
29Aug84 #1	CM2	-0.27	-0.86	-0.83	-8.28	-8.17
	CM3	-0.22	-0.75	-0.73	-6.75	-6.65
% Difference		20.4	13.7	12.8	20.4	20.5
#2	CM2	-0.26	-0.84	-0.81	-7.98	-7.85
	CM3	-0.21	-0.74	-0.71	-6.53	-6.41
% Difference		21.3	12.7	13.2	20.0	20.2
#3	CM2	-0.27	-0.85	-0.82	-8.02	-7.91
	CM3	-0.22	-0.74	-0.72	-6.55	-6.44
% Difference		20.4	13.8	13.0	20.2	20.5
26Sep84 #1	CM2	0.24	0.52	0.50	9.08	8.96
	CM3	0.19	0.44	0.42	6.88	6.79
% Difference		23.3	16.7	17.4	27.6	27.6
#2	CM2	0.25	0.50	0.49	9.10	9.01
	CM3	0.22	0.47	0.46	7.98	7.92
% Difference		12.8	6.2	6.3	13.1	12.9
#3	CM2	0.31	0.58	0.57	11.15	11.08
	CM3	0.28	0.54	0.53	10.03	9.98
% Difference		10.2	7.1	7.3	10.6	10.5
Average of absolute values of % Dif. for the 8 experiments:		13.9	9.5	9.8	14.6	14.6
Standard deviation of the % Difference for the 8 experiments:		8.3	5.0	4.7	8.5	8.6

Table 4-4. Effect of Error in Fluid-Velocity Measurement on Predicted Transport from Models
(Computed transport in dynes/(cm-s) is listed for each sensor followed by % difference between the two.)

Part C: u^6 and u^n models
(Einstein is a variable u^n model)

Experiment	Sensor		Computed Transport [dynes/(cm-s)]					
			Madsen & Grant		Shibayama & Horikawa		Einstein's Φ (dimensionless)	
				with u_*		with u_*		with u_*
10Aug84	#1	CM2	73.9	73.5	112.3	112.1	1.63	0.0723
		CM3	73.5	73.2	111.7	111.5	1.70	0.0750
	% Difference		0.5	0.5	0.5	0.5	-4.2	-3.7
	#2	CM2	70.2	69.8	106.7	106.5	4.16	0.0856
		CM3	67.5	67.2	102.7	102.5	4.36	0.0881
	% Difference		3.8	3.8	3.8	3.8	-4.7	-2.9
29Aug84	#1	CM2	-7.57	-7.40	-11.51	-11.45	-2.79	-0.1362
		CM3	-5.69	-5.56	-8.65	-8.59	-2.77	-0.1357
	% Difference		28.4	28.4	28.4	28.5	0.72	0.37
	#2	CM2	-7.13	-6.97	-10.84	-10.77	-5.75	-0.1353
		CM3	-5.39	-5.27	-8.20	-8.13	-5.80	-0.1372
	% Difference		27.8	27.8	27.7	27.9	-0.87	-1.39
	#3	CM2	-7.04	-6.88	-10.71	-10.64	-9.30	-0.1365
		CM3	-5.28	-5.16	-8.03	-7.96	-9.39	-0.1385
	% Difference		28.6	28.6	28.6	28.8	0.96	1.45
26Sep84	#1	CM2	9.75	9.51	14.81	14.73	3.54	0.1748
		CM3	6.49	6.33	9.86	9.80	3.60	0.1749
	% Difference		40.2	40.2	40.1	40.2	-1.68	-0.057
	#2	CM2	10.00	9.76	15.20	15.14	7.86	0.1880
		CM3	8.23	8.03	12.50	12.46	7.74	0.1816
	% Difference		19.4	19.5	19.5	19.4	1.54	3.46
	#3	CM2	13.00	12.69	19.76	19.71	11.31	0.1812
		CM3	11.21	10.94	17.04	17.01	11.21	0.1769
	% Difference		14.8	14.8	14.8	14.7	0.89	2.40
Average of absolute values of % Dif. for the 8 experiments:			20.4	20.4	20.4	20.5	1.9	2.0
Standard deviations of the % Dif. for the 8 experiments:			12.6	12.6	12.6	12.7	1.5	1.3

velocity in their equations. To examine this sensitivity we altered the current-meter offsets for the two experiments in which we measured offshore sand transport with the tracer (3 August 1984 and 29 August 1984). When we reduced the measured offshore mean fluid velocities on both days by 5 cm/s the transport direction predicted with Equation (4.4) changed from offshore to onshore for both sets of experiments, even though the mean fluid velocity was still offshore (about 3 cm/s). Accurate measurement of the mean fluid velocity is very important when predicting transport direction.

4.3 Tracer controls

There are two important controls on tracer experiments which are used to test two basic assumptions: that the sand tracer behaves in the same manner as the natural sand and that the sand tracer is adequately monitored. The first assumption is tested by comparing the size distribution of the sand tracer with the size distribution of the natural sand present during the experiment. The assumption of adequate monitoring is tested by determining how much of the tracer has been accounted for in the sampling, known as "tracer recovery."

4.3.1 Matching tracer and in-situ sand

For each tracer experiment the size distributions were measured for the sand before it was dyed, the red dyed sand, the green dyed sand, and the in-situ natural sand present during the experiment. Statistical moments of all four of these distributions were computed for each experiment and are listed in Table 4-5.

Five different moments were computed from the size distributions: mean, median, disperaion, skewness, and kurtosis. The statistical moments use the data from each half-phi size interval in the size distribution. Detailed descriptions of each of these moments may be found in Inman (1952). The phi size measure used here can be converted to millimeters by:

$$mm = 2^{-\phi} \qquad (4.5)$$

A negative skewness (which is the case for most distributions in Table 4-5) indicates that the phi mean is numerically less than the phi median, and the distribution is skewed toward smaller phi (coarser grains). A normal distribution has a kurtosis of 0.65. A greater kurtosis indicates a greater spread, i.e., more sand in the tails of the distribution than for a normal distribution. This is generally the case in beach sand and is true of all samples in Table 4-5.

The higher moments of skewness and kurtosis are quite sensitive to methods and techniques of measurement.

Table 4-5. Sediment Size-Distribution Moments
(Median & mean are in phi units & microns, others in phi.)

Description	Date Sampled	Median		Mean		Dis-persion	Skew-ness	Kurtosis
		ø	μ	ø	μ	ø	ø	ø
Torrey Pines experiments (1980)								
250 meters offshore	15May80	3.09	117	3.08	118	0.51	-5.88	68.70
100 meters offshore	15May80	2.38	193	2.38	192	0.62	-0.55	8.72
Sand to dye	15May80	2.21	216	2.20	218	0.58	-0.42	8.06
Grn tracer	15May80	2.15	226	2.13	228	0.53	-0.31	6.49
Red tracer	15May80	1.98	253	1.95	258	0.55	-0.33	3.20
During exp.	23Jun80	2.00	250	1.92	264	0.65	-1.28	8.03
During exp.	11Aug80	2.20	218	2.12	229	0.73	-2.52	17.36
Sand to dye	18Aug80	1.95	258	1.93	262	0.68	-0.31	7.23
Grn tracer	18Aug80	1.12	459	1.17	445	0.69	0.14	3.74
Red tracer	18Aug80	1.40	380	1.40	380	0.64	0.21	3.21
During exp.	12Sep80	2.46	182	2.40	190	0.64	-1.68	10.66
During exp.	29Sep80	2.51	175	2.48	179	0.69	-1.21	9.82
Scripps Institution of Oceanography experiments (1984)								
Sand to dye	12Jul84	1.77	292	1.84	280	0.68	0.82	9.90
Grn tracer	12Jul84	1.91	266	1.93	263	0.50	-0.14	5.10
Red tracer	12Jul84	1.95	259	1.98	254	0.51	-0.10	4.73
During exp.	3Aug84	2.58	167	2.57	169	0.52	-0.43	3.79
Sand to dye	6Aug84	2.09	236	2.02	247	0.78	-2.97	19.86
Grn tracer	6Aug84	1.95	258	2.01	249	0.68	-0.12	12.19
Red tracer	6Aug84	1.93	262	1.94	262	0.64	-0.19	7.83
During exp.	10Aug84	2.31	201	2.16	224	0.97	-6.96	44.71
Sand to dye	13Aug84	2.24	212	2.24	211	0.64	-1.84	19.32
Grn tracer	13Aug84	2.15	225	2.12	230	0.69	-0.80	13.21
Red tracer	13Aug84	2.12	230	2.10	233	0.66	-0.97	11.48
During exp.	29Aug84	2.28	206	2.22	214	0.75	-1.40	8.98
Sand to dye	11Sep84	2.15	226	2.10	233	0.70	-3.11	23.40
Grn tracer	11Sep84	1.78	292	1.79	289	0.47	-0.14	8.94
Red tracer	11Sep84	1.74	299	1.76	295	0.56	-0.12	6.47
During exp.	26Sep84	2.45	183	2.36	195	0.78	-4.18	28.10
Sand to dye	26Sep84	2.31	201	2.26	209	0.72	-4.81	39.28
Grn tracer	26Sep84	1.94	261	1.95	259	0.57	-0.20	10.89
Red tracer	26Sep84	1.75	298	1.74	300	0.61	-1.38	12.03
During exp.	30Oct84	2.63	162	2.60	165	0.55	-1.18	7.76

White and Inman (1987b) found them to be more a function of computational method than of whether the sand was dyed or undyed. Median size and the dispersion of the natural and dyed sands should match as closely as possible. The skewness and kurtosis of the tracer are usually considered adequate if they are of the same sign as the natural sand.

In the Torrey Pines experiments the sand was sampled, taken to an outside company for dyeing, and then used in two tracer experiments. The mean, median, and dispersion measures for the 15 May 1980 undyed and dyed sands match well the in-situ sand for the 23 June 1980 and 11 August 1980 experiments. That is, the medians, means, and dispersions are close, and the skewness and kurtosis are of the correct sign. This is not the case for the tracer used in the September 1980 experiments. Apparently the company dyeing the sand lost some of the finer sand during the dyeing process, resulting in larger median dyed sand. Although the dispersion remained the same, the skewness switched sign. Thus the tracer distribution was skewed toward finer grains, but the increase in the median size indicates a shift of the entire distribution toward coarser grains. Tracer recovery results will show that this change of the tracer size distribution had a substantial effect on the September 1980 experiments, particularly the 29 September 1980 experiment, in which the

coarse dyed sand moved rapidly out of the sampling grid toward the breakers.

In the SIO experiments we dyed our own sand, and it can be seen from the statistics in Table 4-5 that this worked quite well in comparison to the September 1980 experiments. There was sometimes a lag of weeks between sand dyeing and experiment, but this was not because of the dyeing process. The time lag was caused by waiting for wave conditions and underwater visibility suitable for the experiment. As can be seen from Table 4-5, the mean and medians are somewhat coarser for the tracer sand than the in-situ, but dispersions all match quite well. The skewnesses and kurtosis are all of the correct sign. (The dyed sand used in the 3 August 1984 experiment had the correct sign of skewness, even though the original sand taken from the ocean did not.) The only consistent trend in the dyeing process is coarser tracer sand. The variation in dispersion, skewness, and kurtosis appears random.

In conclusion, the dyeing process worked relatively well for all but the two September 1980 experiments. The only consistent trend was for the tracer sand to be coarser than the in-situ sand (an average of 60μ coarser for all but the September 1980 experiments). The data from those experiments is suspect, and the next test of tracer

recovery is used to determine whether the tracer behaved adequately.

4.3.2 Tracer recovery

To determine whether the motion of the dyed sand has been adequately monitored by the core sampling, we computed (Table 4-6) the percent of injected tracer recovered in the sampling grid using the methods of Section 2.1.3. In tracer experiments a recovery rate between 70 and 100% is usually considered good, and rates between 50 and 70% are adequate (Inman et al, 1980; Kraus et al, 1982). If the recovery is less than 50%, the results are questionable, and recovery of less than 25% means that most of the tracer has moved out of the grid, and transport rates should not be used from such sampling. Most of these experiments had a good recovery rate, exceeding 70%, with a few in the 50-70% range. In some cases the computed recovery rate exceeded 100%, not unusual in tracer experiments. It indicates that each core sample does not always accurately represent the concentration in the surrounding area. Some core samples apparently had anomalously high concentrations.

Statistics for the measured recovery rates were computed. The 29 September 1980 experiments, which had very low recoveries and were therefore not used to test bedload models, were excluded from the statistics. The

Table 4-6. Tracer Controls

Experiment	Sampling Time (minutes)	Tracer Recovery (%) Green	Red	Transport Difference (%) (offshore)	(longshore)
23Jun80 #1	18.13	75.7	64.2	90	3
#2	39.75	45.2	41.4	-5	
#3	62.00	78.4	58.2	-15	-18
#4	131.11	83.7	74.9	-5	-100
11Aug80 #1	18.56	46.3	44.3	106	-30
#2	46.00	52.5	81.6	-589	-90
#3	72.77	58.0	78.2	-227	-300
#4	105.42	60.3	92.9	174	-13
#5	133.00	89.9	92.9	-197	-25
#6	160.19	173.8	198.1	-683	38
12Sep80 #1	25.13	73.4	14.5	795	1966
#2	55.46	91.1	29.6	80	-28
#3	87.00	64.6	35.9	242	-900
#4	131.65	55.9	51.5	-380	-1320
#5	180.65	119.5	42.1	68	75
#6	227.07	142.8	159.7	-29	-14
29Sep80 #1	19.50	12.1*	12.2*	-588	16
#2	36.59	13.1*	11.4*	-61	-99
#3	67.77	12.7*	15.7*	-358	-68
#4	110.00	20.9*	13.0*	-267	55
#5	137.17	18.8*	18.7*	154	-16
#6	168.43	12.6*	18.1*	-233	308
3Aug84 #1	66.33	82.3	64.6	27	-103
#2	141.33	72.6	78.7	-122	-81
10Aug84 #1	55.33	50.4	66.0	-76	-105
#2	120.00	30.0	40.5	-107	-53
29Aug84 #1	50.93	22.4	99.3	70	-114
#2	105.52	29.1	51.5	-20	-193
#3	167.33	27.2	69.0	-24	-16
26Sep84 #1	50.92	64.2	63.6	-83	-82
#2	100.60	94.2	93.5	-112	-80
#3	145.22	52.3	112.2	61	-90
30Oct84 #1	82.29	74.0	52.8	-59	
#2	135.50	94.5	141.2	-442	
#3	176.44	65.7	128.3	41	
#4	206.75	48.7	79.9	-78	

*: Not used to test bedload models.

remaining 60 recoveries had a mean recovery of 73.7% with a standard deviation of 36.2%. There was some tendency for recovery to increase in the later samplings. The correlation coefficient between time and recovery was 0.506. Presumably the tracer was dispersed more evenly at later times. That is, the spatial scale of significant change in tracer concentration may have increased in time relative to the sampling scale (distance between samples).

In the first two experiments, 23 June 1980 and 11 August 1980, the recovery was adequate to good. On 12 September 1980, the recovery of green tracer was good, but apparently the red tracer did not disperse adequately throughout the grid until the third or fourth sample set. The results for the 29 September 1980 experiment confirm the doubts based on the sand size distributions of Table 4-5. The tracer was too coarse and moved quickly out of the grid and toward the breakers. We did not use the 29 September 1980 data for any bedload-model testing, although there are still a sufficient number of dyed grains in each core sample to adequately compute transport thickness. All of the recovery rates for the 1984 experiments at SIO appear adequate to good, except for the green tracer on 29 August 1984. On this day, there was a strong offshore net transport rate. Since green tracer was injected 1.5 meters offshore of the grid center and the red tracer 1.5 meters

onshore, it is not surprising that considerable green tracer was lost.

Since we used two colors in each of our experiments, an additional test on the quality of each experiment is available. The transport differences, computed as [(green transport minus red transport)/red transport] x 100%, are listed in Table 4-6. It was hoped that these differences would correlate in some way with the tracer recovery rates, but there does not appear to be any obvious correlation. The lower differences for the 23 June 1980 experiment are due to the fact that the two colors were mixed together and injected simultaneously at the same location.

4.4 Transport thickness

The sand transport rate is proportional to the thickness times the velocity of transport (Equation 2.1). Each core sample contains a vertical distribution of tracer from which eight different estimates of transport thickness were computed by the methods of Section 2.1.2. Some of these estimators are known to be inaccurate but are included for purposes of comparison with other data sets. Daily averages of the mean thickness and the standard deviation are listed for each of the eight estimators in Appendix 2 as Tables 8-1 and 8-2. The complete list of

transport thicknesses obtained for each color in each grid on each day is in Appendix 2 (Tables 8-3 through 8-6).

The thickness values from each of the eight estimators for only one day's experiment are shown in Figure (4-1). Three of these estimators yield relatively large thicknesses. The maximum-penetration estimator is recognized as unrealistic, since it relies on the deepest penetration of any tracer, no matter how small a concentration. Since a few dyed grains can be pushed beneath the transport layer artificially by the sampling process, this estimator is rejected. As recognized by Inman et al (1980) the 0.5 and 1.0 grain/gram penetration estimators must also be rejected, since they yield thickness estimates which far exceed both subjective visual estimates of thickness and all other objective estimators now used (Kraus et al, 1982; White and Inman, 1987b).

The mean thicknesses from estimators A-D and G (Figure 4-1) agree with each other rather well. These estimators have been used recently (Kraus et al, 1982; White and Inman, 1987b). The disagreement between these five methods is small compared to the mean value obtained. However, there are some theoretical problems (Section 2.1.2) with the estimator $Z_o=2\Sigma Nz/\Sigma N$ (G in Figure 4-1) when used with the original vertical tracer profile. This estimator yields unrealistic results for "buried" concentration profiles, in which concentration is low near

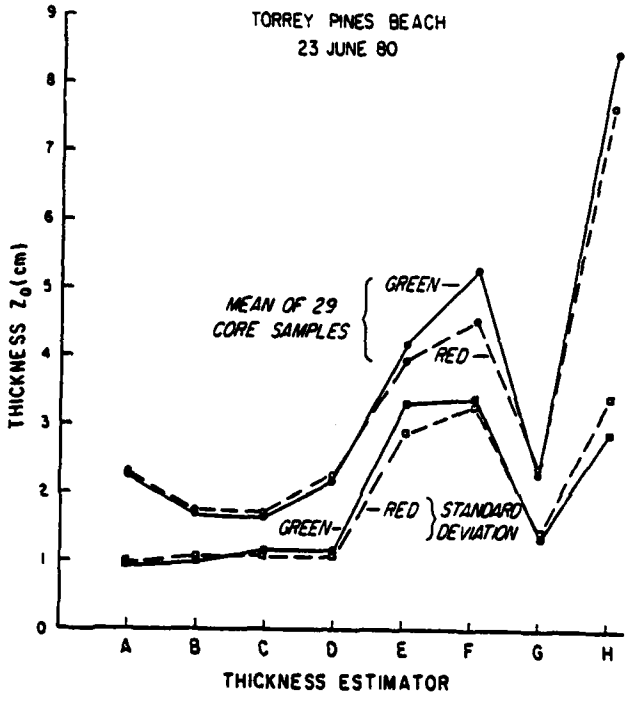

TRANSPORT THICKNESS ESTIMATOR:

CRICKMORE CONCENTRATION PROFILE

A. $Z_0 = \frac{2\Sigma N \cdot z}{\Sigma N}$

B. $Z_0 = \frac{\Sigma N \cdot \Delta z}{N_{max}}$

ORIGINAL CONCENTRATION PROFILE

C. PENETRATION OF 80% OF TRACER

D. PENETRATION OF 90% OF TRACER

E. 1.0 grains/gram PENETRATION OF TRACER

F. 0.5 grains/gram PENETRATION OF TRACER

G. $Z_0 = \frac{2\Sigma N \cdot z}{\Sigma N}$

H. MAXIMUM PENETRATION OF TRACER

Figure 4-1. Transport thickness estimates for 23 June 1980. The solid curves denote green tracer and the dashed curves red tracer. Both means and standard deviations for 29 core samples are plotted.

the top of the core sample but increases with depth. For this reason we recommend that this estimator (Inman et al, 1980) not be used. However, its behavior with the so-called "Crickmore profile" in which the negative concentration gradients within the core are eliminated, is quite reasonable (A in Figure 4-1). We conclude that any of the four estimators A-D (Figure 4-1) can be used to compute transport thickness. When we examine individual core samples, the Inman et al estimator with a Crickmore profile (A in Figure 4-1) seems to yield thickness estimates closer to what would be subjectively selected as the appropriate estimate. For this reason of agreement with subjective visual estimates of thickness, we will be using the Inman et al estimator with the Crickmore profile in further computations.

Note that for the four estimators we have selected as well-behaved, the standard deviations of the thickness estimates are about half of the means. This is in contrast to surf zone experiments in which the standard deviation ranges between one and two times the mean value (White and Inman, 1987b). Since the same methods and thickness estimators were used in experiments both inside and outside the surf zone, we conclude that there is two to four times less variation in transport thickness outside the surf zone than inside. In the surf zone waves sometimes penetrate through the water column and result in intense short-lived

vertical velocities throughout the water column and within the sand bed. This type of behavior contrasts sharply with fluid motion outside the surf zone, i.e., nearly horizontal velocities near the bed. Clearly more variance in the depth to which tracer is mixed should be expected under plunging breakers than in the less turbulent horizontal flows outside the surf zone.

Transport thickness must be related to the fluid motions above the sand bed. If a relationship could be found between fluid parameters and transport thickness, then it would not be necessary to measure the thickness with tracer methods. King (1951) first suggested that there might be a linear relationship between wave height and transport thickness. Sunamura and Kraus (1985) used the Kraus et al (1982) data from surf zone tracer studies to quantify this relationship. The best fit between wave height and transport thickness for their data set was:

$$Z_o = 0.027\ H_{sig} \quad \text{for } 60\text{ cm} < H_{sig} < 160\text{ cm} \qquad (4.5)$$

The coefficient in (4.5) decreased as H_{sig} rose above 1.5 meters. They did not attempt to use an additive constant in (4.5), nor did they report what level of correlation existed between wave height and transport thickness, simply that the data best fit Equation (4.5).

We correlated surface-corrected H_{sig} with Z_o and found an extremely low correlation coefficient (an average of 0.083 for the two tracer colors). The results for this

correlation are listed in Appendix 5 as Table 8-9. It appears that wave height is not a good predictor of transport thickness.

Sunamura and Kraus (1985) also examined the correlation between fluid velocity squared and transport thickness. There is some theoretical justification for selecting the second power of the fluid velocity (Hanes and Bowen, 1985), but no experimental data sets suggest such a selection. They found that the Kraus et al (1982) data set best fit the relation:

$$z_o = 81.4\ D\ (\theta-\theta_t) \qquad (4.6)$$

where $\theta=c_f\rho u_m^2/(\rho_s-\rho)gD$ and u_m was obtained from wavestaffs and surface-corrected pressure data at the breakpoint. For some reason they attempt to explain correlation between thickness and grain size, D, in (4.6), even though D appears in both the numerator and denominator and cancels out. Three artifical restrictions on (4.6) are apparent: arbitrary selection of the second power of fluid velocity, absence of any additive constant, and failure to quantify the level of correlation.

We removed these restrictions in attempting our correlation between fluid velocity and transport thickness. We attempted to follow the methods of Sunamura and Kraus (1985) in Equation (4.6) as closely as possible. Values of $D(\theta-\theta_t)$ were computed using u_m from the pressure-sensor data (Table 4-1), since this was the method of computing u_m

used by Sunamura and Kraus (1985). The correlation coefficient between Z_o and $D(\theta-\theta_t)$ was 0.047 (Table 8-9), an extremely low correlation. Apparently this is not a good predictor of transport thickness either.

We attempted a correlation between Z_o and the u_m's from both surface-corrected pressure data in Table 4-1 and the current measurements in Table 4-2. We considered the moments $u_m^{0.5}$, u_m, and u_m^2. The correlation coefficients for the different power of u_m fell in the range 0.32-0.36 for the surface-corrected u_m (Appendix Table 8-9) and -0.34 to -0.42 for the u_m's derived from current measurements (Appendix Table 8-10). Apparently this variable is not well correlated with Z_o either.

Another variable which we correlated with Z_o was the time-averaged total velocity u_T from the near-bottom current meters listed in Table 4-2. The velocity $\langle u_T \rangle = \langle (u^2+v^2)^{0.5} \rangle$ is a measure of bottom stress without regard to direction. The correlation coefficients in Appendix Table 8-11 for the moments $\langle u_T \rangle^{0.5}$, $\langle u_T \rangle$, and $\langle u_T \rangle^2$ ranged between -0.34 and -0.40, still rather low correlations.

Finally we correlated Z_o with the orbital diameter d_o. We considered the fact that d_o is a measure of how long the sand bed feels the velocity. That is, d_o is the product of u_m and the wave period (Equation 4.2). We used d_o from two different sources: the surface-corrected wave

heights in Table 4-1 and from the current-meter data in Table 4-2. The highest correlations were found using d_o from the surface-corrected wave heights in Table 4-1. The results for the seven moments $\langle d_o \rangle^n$ with n ranging from 0.5 to 6 are presented in Table 4-7. The correlation coefficients are somewhat higher than others we have performed (0.63 to 0.74) and are quite close for the different power of d_o. At 90% confidence the only moment which performs statistically less well than the others is $d_o^{0.5}$. An equation relating Z_o and d_o^n could be presented for any $n > 0.5$, but we will list here the dimensionally correct n=1 equation:

$$Z_o = 0.010\ d_o + 0.58\ cm \quad \text{for } 58\ cm < d_o < 251\ cm \qquad (4.7)$$

where d_o is computed from the surface-corrected wave heights and the peak spectral period (Table 4-1). The considerably lower current-meter derived d_o correlation coefficient of -0.22 is detailed in Appendix Table 8-11.

Equation (4.7) suggests a minimum value for Z_o. Inserting our smallest measured value of d_o=58 cm yields Z_o=1.16 cm. Physically this suggests that wave motions large enough to induce sand motion result in transport thicknesses of at least a centimeter. This should not be surprising, since sand requires a threshold stress to be applied before it moves and dynamic coefficients of friction are less than static coefficients. In fact, this is confirmed by all three data sets of Kraus et al (1982),

Table 4-7. Correlation of Orbital Diameter with Transport Thickness
(d_o from surface-corrected wave heights in Table 4-1.)

	Orbital Diameter Moment $\langle d_o \rangle^n$						
n =	0.5	1	2	3	4	5	6
	Part A: Red Tracer (295 samples)						
	(For Z_o, mean = 2.21 cm and st.dev. = 0.75 cm)						
Mean	12.51	162	2.94 x10^4	5.77 x10^6	12.0 x10^8	26.0 x10^{10}	58.4 x10^{12}
St.Dev.	2.36	56.3	1.82 x10^4	5.00 x10^6	13.2 x10^8	34.1 x10^{10}	87.4 x10^{12}
Slope, m	0.172	.00800	.281 x10^{-4}	.108 x10^{-6}	.0418 x10^{-8}	.0161 x10^{-10}	.00625 x10^{-12}
Intercept	0.08	0.94	1.41	1.62	1.75	1.83	1.88
Cor.Coef.	0.541	0.601	0.683	0.720	0.736	0.732	0.728
90% Confidence Limits:							
(lower)	0.504	0.564	0.646	0.683	0.699	0.695	0.691
(upper)	0.578	0.638	0.720	0.757	0.773	0.769	0.765
80% Confidence Limits:							
(lower)	0.517	0.577	0.659	0.696	0.712	0.708	0.704
(upper)	0.565	0.625	0.707	0.744	0.760	0.756	0.752
70% Confidence Limits:							
(lower)	0.526	0.586	0.668	0.705	0.721	0.717	0.713
(upper)	0.556	0.616	0.698	0.735	0.751	0.747	0.743
% Sig.	99.95	99.994	> 99.99999% for remaining moments.				
	Part B: Green Tracer (260 samples)						
	(For Z_o, mean = 2.28 cm and st.dev. = 0.96 cm)						
Mean	12.51	162	2.94 x10^4	5.77 x10^6	12.0 x10^8	26.0 x10^{10}	58.4 x10^{12}
St.Dev.	2.36	56.3	1.82 x10^4	5.00 x10^6	13.2 x10^8	34.1 x10^{10}	87.4 x10^{12}
Slope, m	0.290	0.0127	0.407 x10^{-4}	0.147 x10^{-6}	0.0544 x10^{-8}	0.0204 x10^{-10}	0.00772 x10^{-12}
Intercept	-1.35	0.22	1.08	1.42	1.62	1.74	1.82
Cor.Coef.	0.713	0.745	0.773	0.766	0.748	0.725	0.703
90% Confidence Limits:							
(lower)	0.676	0.708	0.736	0.729	0.711	0.688	0.666
(upper)	0.750	0.782	0.810	0.803	0.785	0.762	0.740
80% Confidence Limits:							
(lower)	0.689	0.721	0.749	0.742	0.724	0.701	0.679
(upper)	0.737	0.769	0.796	0.790	0.772	0.749	0.727
70% Confidence Limits:							
(lower)	0.698	0.730	0.758	0.751	0.733	0.710	0.688
(upper)	0.728	0.760	0.788	0.781	0.763	0.740	0.718
% Sig.	Greater than 99.99999% for all moments.						
Mean correlation coefficient for the two colors:							
	0.627	0.673	0.728	0.743	0.742	0.729	0.716

White and Inman (1987b), and our data from outside the surf zone. In all three studies thicknesses less than a centimeter are rare.

4.5 Transport

Sand transport is the product of transport thickness, transport velocity, and other parameters which did not vary during the experiments [Equation (2.1)]. The transport rates were determined from grids of samples which concentrated sampling along the crosshore line through the grid center. Examples of the resulting distributions of tracer for two different times during the 12 September 1980 experiment are illustrated in Figure (4-2). The transport velocity was obtained by determining the distance that the tracer centroid moved during the time between injection and sampling, using the computational methods detailed in Section 2.1.1. The resulting transport velocities, thicknesses, and transports are listed in Appendix 6 (Table 8-12 for the crosshore direction and Table 8-13 for the longshore direction). There were sometimes insufficient samples in the longshore direction to determine longshore velocities, particularly for the 30 October 1984 experiment grids, each of which consisted of just one crosshore line of samples.

Comparisons with the data of Kraus et al (1982) and White and Inman (1987b) show that the transport thicknesses

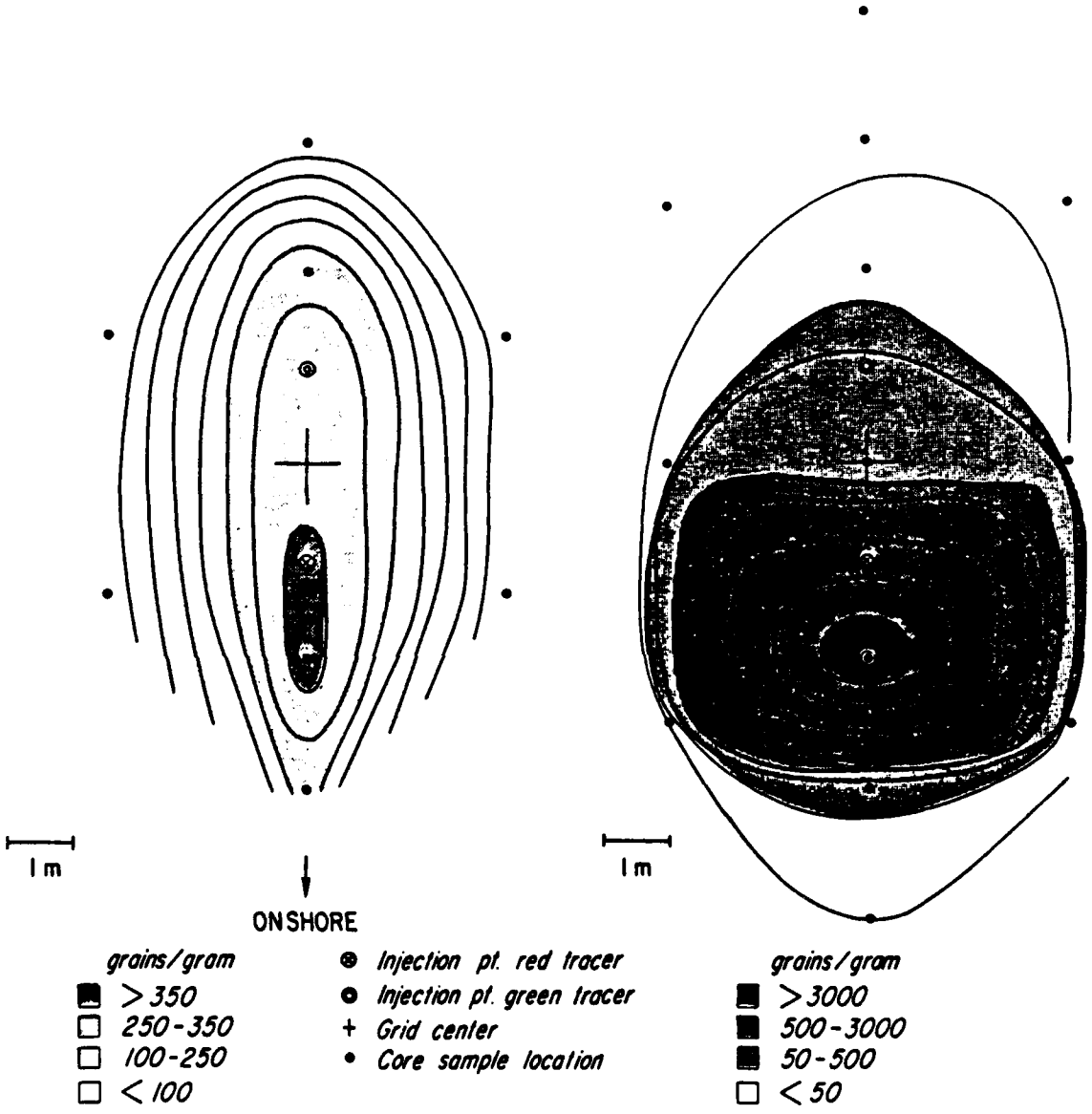

Figure 4-2. Horizontal tracer distribution of red tracer at two different times. The left figure is 25 minutes after injection and the right figure 86 minutes.

have about the same mean values both inside and outside the surf zone. But the longshore velocities (and transports) are about two orders of magnitude slower for transport outside the surf zone. Reliable crosshore transport rates in the surf zone have not been reported.

In all cases for which the transport difference between the two colors exceeded 100 dynes/(cm-s) (Table 8-12), there were low tracer recoveries for one or both colors (Table 4-6). Even after deleting these low-recovery grids, it is clear that the error in the transport velocity estimates far exceeds the error in transport thickness estimates. The thickness estimates vary by only about 5% between the two colors (Figure 4-1). The difference in estimates for transport velocity sometimes exceeds the average estimate (error greater than 100%). Perhaps the disagreement in tracer velocity between the two colors could be reduced by increasing the number of samples in the grid. Unfortunately, there are practical restraints on both the number of samples which can be obtained and counted. The more efficient counting methods possible with radioactive tracers (i.e., Inman and Chamberlain, 1959) would have allowed increased sampling and reduced error.

Correlations between various powers of fluid velocity and sediment transport were computed. The data show that the application of a threshold criterion to the fluid velocity is necessary. When a threshold was not

applied the resulting fluid velocity moments (first through sixth) predicted the correct direction of crosshore sand motion only 70% of the time. When a threshold criterion was applied, the fluid velocity moments (first through sixth) correctly predicted sand transport direction for all 30 experiments.

The correlations between each of the fluid-velocity moments and sand transport are listed in Table 4-8. Note that the appropriate power of the fluid velocity was applied prior to averaging in time. Averaging before exponentiating can yield quite different results. The slopes and intercepts in the table can be used to form a "model" for predicting sediment transport. However, cgs units must be used, since the resulting equation is not dimensionally correct. Using the slope m and the intercept b, we obtain for crosshore transport:

$$i_x = m \langle u^n \rangle + b \qquad (4.8)$$

where m, n, and b appear in Table 4-8. Part B of Table 4-8 shows correlations with dimensionless transport:

$$\Phi \equiv (\rho)^{0.5}\, i / [(\rho_s - \rho) g D]^{3/2} \qquad (4.9)$$

The correlation coefficients for either dimensional or dimensionless transport are about the same for all moments, which is not surprising because these fluid-velocity moments are strongly correlated with each other (Appendix Table 8-8). The one-half power of fluid velocity clearly has significantly less correlation with transport, even at

Table 4-8. Fluid Velocity Correlations with Transport (Fluid velocities are from Eq. 4.4 with a threshold.)

Part A. Correlation of Fluid Velocity with Dimensional Transport, i (Table 8-12)

	Velocity Moment $\langle u^n \rangle$						
n =	0.5*	1	2	3	4	5	6
Mean	5.93 $\times 10^{-4}$	3.02 $\times 10^{-2}$	13.1	1.21 $\times 10^{3}$	9.50 $\times 10^{4}$	7.05 $\times 10^{6}$	5.02 $\times 10^{8}$
St.Dev.	4.68 $\times 10^{-1}$	3.63	1.79 $\times 10^{2}$	1.03 $\times 10^{4}$	6.83 $\times 10^{5}$	5.05 $\times 10^{7}$	4.10 $\times 10^{9}$
Slope, m	49.9	7.76	1.60 $\times 10^{-1}$	2.76 $\times 10^{3}$	4.05 $\times 10^{5}$	5.29 $\times 10^{7}$	6.27 $\times 10^{9}$
Intercept	33.0	31.4	29.6	28.3	27.8	27.9	28.5
Cor.Coef.	0.532	0.642	0.656	0.650	0.631	0.609	0.586
90% Confidence Limits:							
(lower)	0.499	0.614	0.629	0.623	0.603	0.580	0.556
(upper)	0.563	0.667	0.681	0.675	0.657	0.636	0.615
80% Confidence Limits:							
(lower)	0.510	0.624	0.638	0.632	0.612	0.590	0.566
(upper)	0.553	0.659	0.672	0.666	0.648	0.627	0.605
70% Confidence Limits:							
(lower)	0.519	0.631	0.645	0.639	0.619	0.597	0.574
(upper)	0.545	0.652	0.666	0.660	0.642	0.620	0.598
% Sig.	99.796	99.992	99.998	99.998	99.988	99.976	99.952

Part B. Correlation of Fluid Velocity with Dimensionless Transport, Φ (Eq. 4.9)

Mean	5.93 $\times 10^{-4}$	3.02 $\times 10^{-2}$	13.1	1.21 $\times 10^{3}$	9.50 $\times 10^{4}$	7.05 $\times 10^{6}$	5.02 $\times 10^{8}$
St.Dev.	4.68 $\times 10^{-1}$	3.63	1.79 $\times 10^{2}$	1.03 $\times 10^{4}$	6.83 $\times 10^{5}$	5.05 $\times 10^{7}$	4.10 $\times 10^{9}$
Slope, m	.322	4.40 $\times 10^{-2}$	8.85 $\times 10^{-4}$	1.48 $\times 10^{-5}$	2.12 $\times 10^{-7}$	2.71 $\times 10^{-9}$	3.19 $\times 10^{-11}$
Intercept	0.177	0.176	0.165	0.159	0.157	0.158	0.161
Cor.Coef.	0.615	0.639	0.637	0.613	0.579	0.549	0.524
90% Confidence Limits:							
(lower)	0.586	0.612	0.609	0.584	0.549	0.517	0.490
(upper)	0.642	0.665	0.663	0.640	0.608	0.580	0.556
80% Confidence Limits:							
(lower)	0.596	0.622	0.619	0.594	0.559	0.528	0.502
(upper)	0.633	0.657	0.654	0.631	0.599	0.569	0.545
70% Confidence Limits:							
(lower)	0.604	0.628	0.626	0.601	0.567	0.537	0.510
(upper)	0.626	0.650	0.647	0.624	0.591	0.562	0.537
% Sig.	99.980	99.992	99.990	99.980	99.940	99.868	99.748

*: All n=0.5 moments predicted correct transport direction (onshore or offshore) 70% of the time, other moments 100%.

90% confidence. Furthermore, the correct prediction of transport direction is only 70% for this moment, even though a threshold criterion had been applied.

For correlations with dimensional transport i, we can only conclude at 90% confidence that $\langle u \rangle$, $\langle u^2 \rangle$, $\langle u^3 \rangle$ are better moments than $\langle u^6 \rangle$ for predicting transport. However, if we consider the correlations with dimensionless transport, more conclusions can be made. The moments $\langle u \rangle$ and $\langle u^2 \rangle$ are better predictors than $\langle u^4 \rangle$, $\langle u^5 \rangle$, or $\langle u^6 \rangle$. The moment $\langle u^3 \rangle$ is a better predictor than $\langle u^5 \rangle$ or $\langle u^6 \rangle$. As we shall see in Section 5, this behavior will be reflected in our tests of bedload models. Models which depend on the $\langle u^5 \rangle$ and $\langle u^6 \rangle$ moments to predict transport will not perform well.

Finally, we attempted to determine the appropriate combination of both crosshore and longshore fluid velocities which should be used to compute crosshore transport. Most models assume no crosshore fluid velocity in their derivations (i.e., normally incident waves). However, Bailard and Inman (1981) and Kobayashi (1982) suggest that the total stress acting on the bed depends on the total velocity vector, not just crosshore velocity. The moment suggested by Bailard and Inman (1981) is $\langle (u^2+v^2)u \rangle$. We computed correlations of various powers of this moment with dimensionless transport. In all cases, the correlations were almost identical to those in Part B

of the table, in which longshore velocity was ignored. However, the longshore velocities in our experiments were much smaller than the crosshore velocities. Perhaps experiments in which u and v are comparable in magnitude (i.e., in the surf zone) will be able to decide whether the longshore velocity should be included in models predicting crosshore transport (Equation 2.34) and vice versa (Equation 2.35).

5. DISCUSSION

5.1 Performances of bedload models

The 17 different bedload transport models detailed in Section 2.3 were tested using the measured fluid velocity as input and comparing the computed transport rates (Appendix 7) with the rates measured with sand tracer, averaged over both tracer colors (Appendix 6). Most of these models describe only crosshore transport, but two of the models also predict longshore transport (Bailard and Inman, 1981; Kobayashi, 1982). There were 30 crosshore tracer experiments with which to test the 17 models and 25 longshore transport measurements with which to test the two longshore models.

The principal input for the models was the measured crosshore fluid velocity. The longshore fluid velocity was also used in computing both crosshore and longshore transports from the Bailard and Inman (1981) and Kobayashi (1982) models. Several other parameters also appear in the models. The parameters beach slope β, median sand size D, internal angle of friction ϕ, and fall velocity W were computed for each day's experiments and are listed in Table 5-1. Beach slope and erosion were obtained from fathometer and reference-rod measurements described in Section 3.3, and median sand size was found with the sieving methods of Section 4.3.1. Many investigators (i.e., Bailard and Inman, 1981; Kobayashi, 1982) have assumed an approximate

Table 5-1. Sediment Parameters

Date	Beach Slope β	Median Sand Size D	Internal Angle of Friction ϕ	Fall Velocity W	Erosion Mean	Erosion St.Dev.
	(degrees)	(microns)	(degrees)	(cm/s)	(cm)	(cm)
23Jun80	1.66	250	33.8	3.3	2.2	5.3
11Aug80	1.26	218	32.2	2.9	0.2	1.3
12Sep80	1.43	182	30.3	2.0	1.4	1.8
29Sep80	1.37	190	30.7	2.1	0.4	4.2
3Aug84	1.15	177	30.0	1.9		
10Aug84	0.69	201	31.3	2.5	0.5	0.9
29Aug84	1.49	206	31.6	2.5		
26Sep84	1.32	183	30.4	2.0	0.1	1.2
30Oct84	1.72	162	29.3	1.6		

β from methods in Section 3.3

D from sieve analysis.

ϕ from Equation (5.1).

W from Equation (2.46)

Erosion was the average value from all reference rods during each day's experiments.

value of 32 degrees for the internal-friction angle ϕ, but it is known (Sleath, 1984) that this angle is slightly dependent on grain size. In a series of underwater measurements of the angle of repose of different sand sizes, Inman (1979) determined that the friction angle and the median grain size could be related by:

$$\phi = 28.8 + 20\ (D - 150) \qquad (5.1)$$

for the range $150 < D < 250$ microns, where D is in microns and ϕ in degrees. The resulting slight variation in ϕ for the experiments is listed in Table 5-1. The fall velocity was computed from Equation (2.46) using various static sediment parameters.

All of the models except Hallermeier (1982) and Yalin (1963) contain at least one undetermined coefficient. For a list of which coefficients appear in which models, refer to Table 2-1. The coefficients in the bedload models were either assumed to be constant for all experiments (c_f ϵ_b) or computed by the methods detailed by each author. thus the coefficients were in no way changed to fit the data. The coefficients used in each of the models were computed for each day's experiments and are listed in Table 5-2. The friction factor c_f is common to most transport models. It is meant to describe in some manner the intensity of transport. Since all our experiments describe relatively similar intensities of oscillatory carpet-flow, we used the same c_f for all our

Table 5-2. Coefficients used in Transport Models

Date	Friction Factor c_f	Sleath's Friction & Lift Factor f_1	Madsen & Grant Friction Factor C_M	Drag Coef. c_D	Bedload Efficiency ϵ_b	Einstein's Hiding Factor ξ
23Jun80	0.007	0.0182	12.5	8.0	0.21	1.2
11Aug80	0.007	0.0168	12.05	9.7	0.21	2.2
12Sep80	0.007	0.0175	12.5	11.0	0.21	1.8
29Sep80	0.007	0.0182	12.49	10.3	0.21	1.6
3Aug84	0.007	0.0161	12.5	11.0	0.21	2.2
10Aug84	0.007	0.0154	12.44	10.0	0.21	2.2
29Aug84	0.007	0.0112	12.21	10.0	0.21	3.4
26Sep84	0.007	0.0140	12.20	11.0	0.21	4.2
30Oct84	0.007	0.0091	12.29	12.0	0.21	6.8

c_f was the value found by Thornton (1970) and the average calculated from Bailard's (1981) values.

ϵ_b is the value found by Bailard (1981).

c_D is obtained from Sleath's (1984) Figure 3.1.

f_1, C_M, and ξ were obtained from figures in Sleath (1978), Madsen and Grant (1976), and Abou-Seida (1965), respectively.

experiments. Therefore, in testing the bedload models, it makes absolutely no difference what value we choose for c_f, so long as it is constant. The variance in the model predictions will be compared with variance in the transport measurements, and the application of a constant coefficient can make no difference in the correlation. Nevertheless, in order to obtain realistic numbers for the predicted transport, we compared different studies in which c_f has been measured in order to determine a reasonable value. Bailard (1981) estimated a value for c_f in surf zone carpet-flow conditions. The only field data in Bailard's (1981) analysis with grain sizes similar to our experiments were Komar's (1969) Silver Strand experiments. Bailard (1981) solved for c_f values in a longshore current model (Oatendorf and Madsen, 1979), using Komar's (1969) measurements of longshore currents. We averaged Bailard's (1981) values of c_f for the Silver Strand beach (the only beach with grain sizes similar to ours) to obtain a mean c_f=0.007. Thornton (1970) tested his longshore current model with field data from one California beach and also found a c_f value of 0.007. In view of this agreement, we selected the same value for our experiments. The coefficient f_1 of Sleath (1978) includes both the friction factor c_f and an attempt to describe the lift forces on individual grains. He includes a figure in his study for determining f_1.

The factor C_M of Madsen and Grant (1976) is an attempt to include threshold velocity in the model as a coefficient rather than by subtracting a value from the fluid velocity, as is done by most modelers. For surf zone conditions, C_M has the constant value of 12.5, but for our less energetic experiments, we computed C_M from the empirical table provided by Madsen and Grant (1976). The drag coefficient c_D was computed using Sleath's (1984) Figure 3.1 which connects different theories for drag coefficient computation.

The bedload efficiency ϵ_b used in both the Bagnold (1963) and Bailard and Inman (1981) models was obtained from a series of model tests using field data. Bailard (1981) obtained a bedload efficiency of 0.21 with least-squares methods by comparing the Bailard and Inman (1981) model predictions with measured surf zone transport rates. Just as with the friction coefficient c_f, choice of a bedload efficiency will not effect the tests of the transport models, since it is assumed not to vary between experiments.

The final coefficient in Table 5-2 is Einstein's "hiding factor" which attempts to account for the fact that some grains "hide" beneath other grains in the boundary layer. It was computed according to the methods of Abou-Seida (1965) and should be used in testing Einstein's

(1972) oscillatory flow model, but will not be used here in our test of his steady flow model (Einstein, 1950).

The transports computed by each of the 17 models for each of the 30 experiments are listed in the Appendix as Tables 8-14 through 8-17. A simple linear correlation was performed between these transports and the transports measured with sand tracer (Table 5-3).

The slope m in Table 5-3 is a measure of the accuracy of the coefficients in the model. A slope of one would indicate an exact fit between the model coefficients and the mean magnitude of transport in the experiments. Very large slopes for the Sleath (1978) and Hallermeier (1982) models indicate that the coefficients in their transport models seriously underpredict transport. This was expected, since their models were calibrated with laboratory experiments performed under extremely mild flow conditions. The very small slopes of the Einstein (1950) models were expected in this attempt to directly translate steady-flow models to oscillatory flow. The real surprise in the slope results was the closeness to a slope of one for the Bagnold (1963), Bailard and Inman (1981), and Hanes and Bowen (1985) models. Considering the degree of uncertainty in arriving at appropriate values for the friction coefficient and the bedload efficiency, it is remarkable that these coefficients produced results within 1 to 3% of the correct transports, as measured by sand

Table 5-3. Performance of Bedload Models

Part A: u^3 Models

	Model						
	Meyer-Peter & Mueller (1948)	Bagnold (1963)	Bagnold (1963) with u_t	Yalin (1963)	Bailard & Inman (1981)	Bailard & Inman (1981) with u_t	Kobayashi (1982)
Mean Transport	4.25	3.06	2.88	20.36	0.27	0.77	-0.49
St. Deviation	32.48	27.37	26.54	167.01	26.40	25.63	6.58
Slope, m	0.836	1.013	1.004	0.167	1.024	1.064	3.817
Intercept, b	28.11	28.56	26.01	34.93	31.38	30.84	33.52
Cor.Coef., r	0.629	0.643	0.618	0.647	0.627	0.632	0.583
90% Confidence Limits:							
(lower)	0.601	0.616	0.590	0.620	0.599	0.604	0.553
(upper)	0.656	0.668	0.645	0.672	0.655	0.658	0.612
80% Confidence Limits:							
(lower)	0.611	0.625	0.599	0.629	0.608	0.614	0.563
(upper)	0.647	0.660	0.636	0.664	0.645	0.650	0.602
70% Confidence Limits:							
(lower)	0.618	0.632	0.607	0.636	0.616	0.621	0.572
(upper)	0.640	0.654	0.629	0.658	0.638	0.643	0.594
% Sig.	99.988	99.992	99.982	99.999	99.986	99.99	99.948
% Cor. Dir.	96.7	86.7	100	96.7	83.3	100	70.0

Part B: u^4 and u^5 Models

	Model				
	Sleath (1978)	Hellermeier (1982)	Hellermeier (1982) with u_t	Hanes & Bowen (1985)	Hanes & Bowen (1985) with u_t
Mean Transport	0.11	0.13	0.13	2.35	2.48
St. Deviation	0.68	0.93	0.92	24.47	24.74
Slope, m	38.97	30.21	30.57	1.028	1.035
Intercept, b	27.51	27.69	27.64	29.25	29.10
Cor. Coef., r	0.616	0.651	0.651	0.583	0.594
90% Confidence Limits:					
(lower)	0.588	0.624	0.624	0.555	0.566
(upper)	0.643	0.676	0.676	0.611	0.622
80% Confidence Limits:					
(lower)	0.597	0.633	0.633	0.565	0.576
(upper)	0.635	0.668	0.668	0.601	0.612
70% Confidence Limits:					
(lower)	0.605	0.640	0.640	0.572	0.583
(upper)	0.627	0.662	0.662	0.594	0.605
% Significance	99.982	99.999	99.999	99.948	99.962
% Correct Dir.	96.7	100	100	100	100

Table 5-3. Performance of Bedload Models

Part C: u^6 and u^n Models

	Model					
	Madsen & Grant (1976)		Shibayama & Horikawa (1980)		Einstein (1950)	
		with u_t		with u_t		with u_t
Mean Trans.	2.74	2.76	4.16	4.13	216.8	622.10
St. Dev.	40.07	40.01	60.90	60.87	952.0	8540.0
Slope, m	0.6060	0.6051	0.3987	0.3989	0.0164	0.00332
Intercept	30.00	29.99	30.00	30.01	28.00	29.59
Cor. Coef.	0.563	0.561	0.563	0.563	0.362	0.658
90% Confidence Limits:						
(lower)	0.535	0.533	0.535	0.535	0.334	0.630
(upper)	0.591	0.589	0.591	0.591	0.390	0.686
80% Confidence Limits:						
(lower)	0.545	0.543	0.545	0.545	0.344	0.640
(upper)	0.581	0.579	0.581	0.581	0.380	0.676
70% Confidence Limits:						
(lower)	0.552	0.550	0.552	0.552	0.351	0.647
(upper)	0.574	0.572	0.574	0.574	0.373	0.669
% Sig.	99.906	99.902	99.906	99.906	95.104	99.999
% Cor.Dir.	93.3	93.3	93.3	93.3	80.0	100

Part D: Longshore Transport Models

	Model		
	Bailard & Inman (1981)		Kobayashi (1982)
		with u_t	
Mean Transport	-0.017	0.304	0.269
Standard Deviation	6.14	4.10	4.53
Slope, m	0.3855	0.1059	0.9086
Intercept, b	-8.81	-9.30	-9.06
Cor. Coef., r	0.077	0.014	0.135
90% Confidence Limits:			
(lower)	0.022	-0.041	0.081
(upper)	0.131	0.069	0.189
80% Confidence Limits:			
(lower)	0.041	-0.022	0.099
(upper)	0.113	0.050	0.170
70% Confidence Limits:			
(lower)	0.055	-0.008	0.113
(upper)	0.099	0.036	0.157
% Significance	28.2	5.0	47.4
% Correct Direction	80.0	68.0	88.0

Table 5-3. Performance of Bedload Models

Part E: Bagnold's (1963) u u_m^2 Oscillatory Model

	--No threshold applied--		--Threshold applied--	
	Method of computing u_m (described below)			
	#1	#2	#1	#2
Mean i	1.491	0.280	0.697	-0.371
St. Dev.	11.15	40.17	10.41	32.37
Slope, m	2.193	0.639	2.662	0.830
Intercept	28.39	31.48	29.81	31.97
Cor.Coef.	0.567	0.595	0.643	0.623
90% Confidence Limits:				
(lower)	0.522	0.550	0.598	0.578
(upper)	0.612	0.640	0.688	0.668
80% Confidence Limits:				
(lower)	0.537	0.565	0.613	0.593
(upper)	0.597	0.625	0.673	0.653
70% Confidence Limits:				
(lower)	0.552	0.580	0.628	0.608
(upper)	0.582	0.610	0.658	0.638
% Sig.	99.92	99.96	99.992	99.986
% Cor Dir	76.7	76.7	100	100

Source #1: Surface-corrected wave heights (Table 4-1)
Source #2: 2 times (total velocity variance from current meter)$^{0.5}$ (Table 4-2)

tracer. We can only conclude that Bailard (1981) did a very good job of solving for the best value of these coefficients with field data.

The significance of the intercept between the mean predicted transport and the mean measured transport appears to be related to the measured transport, since it is approximately constant for all models. Disagreement in the transport values between the two different colors of tracer was interpreted as initial offset in transport. That is, there may have been an initial artifical transport of tracer, induced by the 1 cm high bump in the bottom topography caused by the tracer placement. This interpretation appears to be confirmed with the transport model tests. The intercept is remarkably constant for the different transport model predictions. Since the models are quite different from each other, we must conclude that the intercept is related to some offset in the tracer data. We again emphasize that this will have no effect in judging either the performance of the models' functional form (which uses transport variance) or in judging the adequacy of the model coefficients (which was measured by the slope of the correlations). This error in measurement presumably caused by initial motion has been separated as an intercept in the correlations.

The percent significance listed in Table 5-3 is a test of the null hypothesis. That is, the percent listed

is the amount of confidence we have that the model is in some way correlated with measured transport.

There are two values in the table which tell us how well each model performed. The "% correct direction" is an indication of the percent of experiments for which the model predicted the correct sign for the transport, i.e., onshore or offshore. Clearly this is of great importance. One very clear result is that the application of a threshold criterion (for initiation of sediment motion) is often necessary to obtain the correct direction of transport (i.e., the Bagnold (1963) and Bailard and Inman (1981) models). In the correlation tests of Section 4.5 (performed directly between powers of fluid velocity and the measured transport), we determined that application of a threshold criterion was necessary to obtain the correct transport direction in all experiments, regardless of which moment was being tested. In the case of individual transport models, this was also often true.

The parameter in Table 5-3 which describes the ability of each model to correctly predict transport is the correlation coefficient. It matches the variance in the measured transports with the variance in the model predictions. In general, the correlation decreases as the power of the fluid velocity increases. That is, the models which use high powers of fluid velocity such as u^5 or u^6 perform poorly compared to models using u^3 or u^4. By

comparing the correlation coefficients we can determine which models perform better than others. However, we are working with a limited number of empirical data points. This means that differences in correlation coefficients between the models may not be statistically significant. In order to make statistically significant conclusions regarding relative model performances, we must consider confidence limits on the correlation coefficients.

The 90%, 80%, and 70% confidence intervals are listed in Table 5-3. If the confidence intervals for two models do not overlap, then it is possible to conclude that one model performed better than the other. These conclusions are presented as 90% and 80% confidences in Table 5-4. Each of the models is listed in the table along both the left and the top of each central box. Inside the box is a matrix of all possible combinations of any two models. Whenever a conclusion regarding the relative performance of two models is possible, an arrow is placed in the matrix pointing to the better model. The asterisks indicate which models predicted transport direction correctly 100% of the time, which is also of importance in judging model performance. At 80% confidence, additional conclusions are available and are indicated by double-lined arrows in the 80% confidence matrix in the lower half of the table.

Table 5-4. Conclusions on Transport Model Performances

Part A. Conclusions at 90% Confidence

KEY: Arrow points to the better model.
*: Model predicts correct transport direction for all experiments.
th: threshold criterion applied

	Meyer-Peter & Mueller 1948	Bagnold 1963	*Bagnold 1963 (th)	Yalin 1963	Bailard & Inman 1981	*Bailard & Inman 1981 (th)	Kobayashi 1982	Sleath 1978	*Hallermeier 1982	*Hanes & Bowen 1985	*Hanes & Bowen 1985 (th)	Madsen & Grant 1976	Madsen & Grant 1976 (th)	Shibayama & Horikawa 1980	Einstein 1950	*Einstein 1950 (th)
Meyer-Peter & Mueller 1948												←	←	←	←	
Bagnold 1963							←			←		←	←	←	←	
*Bagnold 1963 (th)													←		←	
Yalin 1963							←			←		←	←	←	←	
Bailard & Inman 1981												←	←	←	←	
*Bailard & Inman 1981 (th)												←	←	←	←	
Kobayashi 1982		→		→					→						←	→
Sleath 1978															←	
*Hallermeier 1982							←			←	←	←	←	←	←	
*Hanes & Bowen 1985		→		→					→						←	→
*Hanes & Bowen 1985 (th)									→						←	→
Madsen & Grant 1976	→	→		→	→	→			→						←	→
Madsen & Grant 1976 (th)	→	→	→	→	→	→			→						←	→
Shibayama & Horikawa 1980	→	→		→	→	→			→						←	→
Einstein 1950	→	→	→	→	→	→	→	→	→	→	→	→	→	→		→
*Einstein 1950 (th)							←			←	←	←	←	←	←	

Table 5-4. Conclusions on Transport Model Performances

Part B. Conclusions at 80% Confidence

KEY: Arrow points to the better model.
*: Model predicts correct transport direction for all experiments.
th: threshold criterion applied

	Meyer-Peter & Mueller 1948	Bagnold 1963	*Bagnold 1963 (th)	Yalin 1963	Bailard & Inman 1981	*Bailard & Inman 1981 (th)	Kobayashi 1982	Sleath 1978	*Hallermeier 1982	*Hanes & Bowen 1985	*Hanes & Bowen 1985 (th)	Madsen & Grant 1976	Madsen & Grant 1976 (th)	Shibayama & Horikawa 1980	Einstein 1950	*Einstein 1950 (th)
Meyer-Peter & Mueller 1948							←			←		←	←	←	←	
Bagnold 1963							←			←	←	←	←	←	←	
*Bagnold 1963 (th)												←	←	←	←	→
Yalin 1963							←			←	←	←	←	←	←	
Bailard & Inman 1981							←			←		←	←	←	←	
*Bailard & Inman 1981 (th)							←			←	←	←	←	←	←	
Kobayashi 1982	→	→		→	→	→			→						←	→
Sleath 1978												←	←	←	←	→
*Hallermeier 1982							←			←	←	←	←	←	←	
*Hanes & Bowen [illegible]	→	→		→	→	→			→						←	→
*Hanes & Bowen 1985 (th)		→		→		→			→						←	→
Madsen & Grant 1976	→	→	→	→	→	→		→	→						←	→
Madsen & Grant 1976 (th)	→	→	→	→	→	→		→	→						←	→
Shibayama & Horikawa 1980	→	→	→	→	→	→		→	→						←	→
Einstein 1950	→	→	→	→	→	→	→	→	→	→	→	→	→	→		→
*Einstein 1950 (th)			←				←	←		←	←	←	←	←	←	

The conclusions made in Table 5-4 inform us as to which models work best. Since we know what assumptions and what transport physics are present in each of the models, it is also possible to make some conclusions regarding the basic assumptions in each of the models. In general, we can conclude that lower moments of the fluid velocity (u^3 and u^4) work better than higher moments.

We can conclude that overdetermining the transport physics by including more variables than are necessary to describe transport (Kobayashi, 1982) can have detrimental effects on model performance. Kobayashi's model is extremely complicated and contains many variables. Its performance was quite poor compared to other u^3 models and was the poorest of all the models in predicting the correct direction of transport.

A conclusion regarding the relative importance of the two u^4 models (Sleath, 1978; Hallermeier, 1982) becomes available only at 79% confidence. Hallermeier's model performs better than Sleath's at that level of confidence. But the difference in functional form between those two models is the inclusion of a measure of lift forces in Sleath's formulation. With 79% confidence we can say that either Sleath erred in the manner in which he included lift forces, or they are not a very important part of transport physics. The Sleath and Hallermeier models are the only models tested which contain the wave orbital diameter as

one of the variables. The Hellermeier model performs better than any of the u^5 or u^6 models, but it is unclear whether this is due to a difference in the power of u used or due to the inclusion of the orbital diameter in the transport equation.

Since the Hanes and Bowen (1985) model is the only one which includes details of the physics within the moving bed, it was hoped that it would perform well. At 80% confidence, most of the u^3 and u^4 models performed better. One explanation for poor performance of this model is that it was intended to describe very intense unidirectional flows and may not be applicable to the relatively low transports occurring in the nearshore. Another possible explanation is the fact that many assumptions regarding the behavior of the many coefficients in their model were made by Hanes and Bowen (1985) in order to obtain a simple numerical approximation of the transport coefficient for their model. The various parameters in their model which they reduced to one simple number may be variables which are not yet well understood.

The poor performance of the u^6 models is clear even at 90% confidence. These models are empirically based on laboratory experiments. Unless reasonable theoretical justifications and experimental verification can be obtained for these models, they should be rejected.

The behavior of the Einstein (1950) model, tested both with and without a threshold criterion, is quite interesting. Without a threshold criterion it is clearly the worst model examined. Yet with a threshold it has the highest correlation of all the models tested. Why should there be this wide disparity in behavior? The final formulation of the Einstein model is unique in only one way. It allows a variable power of u in its transport relation. As the intensity of transport increases, the appropriate power of u increases. Such variability in the exponent would tend to exaggerate the effect of a threshold criterion, since the velocities lower than threshold which have been removed were also subject to variable exponentiation in the original model. Furthermore, the significant correlation obtained with the threshold Einstein model tells us that it is quite possible that Einstein's postulate of increasing power of u with increasing transport may be correct. Nevertheless, this postulate is by no means proven with our data, since Einstein's model does not perform significantly better than most u^3 models at 90% confidence (Table 5-4).

Bagnold (1963) suggested replacing the u^3 moment in his model with $u\ u_m^2$, if it were applied to oscillatory flow. He postulated that the bottom stress might be proportional to the maximum orbital velocity squared, u_m^2, rather than the oscillatory velocity squared. We compared

both formulations in our model tests. In Part A of Table 5-3 the u^3 moment is used, whereas in Part E the $u\,u_m^2$ moment is used. The moment u_m was computed using both methods of Tables 4-1 and 4-2. Comparing the methods for the case in which no threshold criterion was used, we conclude at 90% confidence that uu_m^2 performed less well than u^3 for the case of pressure-sensor derived u_m and at the same level of statistical performance for the case of current-meter derived u_m. For the cases in which threshold criteria were applied, no statistically significant difference in performance was observed between the two moments at 90% confidence. For our data set the choice between u^2 and u_m^2 for the bottom stress apparently makes no statistical difference.

In addition to the correlations presented in Tables 5-3 and 5-4, we also plotted the 30 predictions of computed versus measured transport for each model (Appendix 1). The dashed line in each figure is a line of slope one and thus a measure of the model coefficient performance. However, we caution against attempts to visually conclude how well each model performs, since the functional form of each model can be judged only by correlating the variance in measured and predicted transports.

The longshore bedload transport was computed from the Bailard and Inman (1981) and Kobayashi (1982) models using 25 experiments. The correlations with measured

longshore transport appear in Table 5-3, Part D. The longshore transport models all performed quite poorly. The transport direction was often incorrect (north or south). The correlation coefficients for the models were all less than 0.2, indicating very little correlation with measured transport. However, the tracer sampling grids were designed to measure crosshore, not longshore transport. There were considerably more sample points in the crosshore than the longshore direction. The low correlations in Table 5-3 for the longshore transport models may indicate that longshore sampling was inadequate rather than poor model performance. This is confirmed by the finding that the Bailard and Inman (1981) crosshore transport model is one of the better models. The mechanics and assumptions used in the derivation of the crosshore and longshore models was exactly the same. Physically it would make no sense for the crosshore model to perform well and the longshore model to perform poorly.

5.2 Recommendations for using bedload models

Based on the information in Tables 5-3 and 5-4 we make the following recommendations for application of each model in oscillatory sheet-flow/carpet-flow conditions.

Meyer-Peter and Mueller (1948), Equation (2.16): Change the model coefficient from 8 to 6.7, and use c_f=0.007.

Yalin (1963), Equation (2.21): Change the model coefficient from 0.635 to 0.106.

Bagnold (1963), Equation (2.32), and Bailard and Inman (1981), Equation (2.34): Apply a threshold criterion (Equation 4.4); use c_f=0.007 and Bailard's (1981) estimate of ϵ_b=0.21.

Kobayashi (1982), Equation (2.36): This is not recommended for use due to poor prediction of transport direction. If used, change the model coefficient from 1.65 to 6.30, and use c_f=0.007.

Sleath (1978), Equation (2.38): Change the model coefficient from 47 to 1832, replace f_1 with c_f, and use c_f=0.007.

Hallermeier (1982), Equation (2.39): Change the model coefficient from $(10)^{1.5}$=31.6 to 955.

Hanes and Bowen (1985), Equation (2.41): The use of this very simplified version of their model is not recommended for use due to poor correlation with measured transport. If used, no change in the model coefficient is necessary. Use c_f=0.007.

Madsen and Grant (1976), Equation (2.45), and Shibayama and Horikawa (1980), Equation (2.48): Do not use. Correlations with measured transport are extremely poor. If used, apply the threshold condition of Equation (4.4) rather than Madsen and Grant's inclusion of threshold in a variable coefficient. Change Madsen and Grant's

coefficient of 2 C_M=25 to 15 and Shibayama and Horikawa's coefficient of 38 to 15. Use c_f=0.007.

Einstein (1950), Equation (2.50) and his empirical curves: Do not use without first applying a threshold criterion (Equation 4.4). Multiply computed transports by 0.0033, or apply a friction coefficient such as c_f=0.007.

5.3 Dimensional-analysis model

In Section 2.2 we derived a transport model by determining each of the variables necessary to describe sediment transport, applying dimensional analysis techniques, and arriving at an expression for transport. This expression was placed in a form which gathered the variables into well-known nondimensional ratios of fluid-sediment parameters. The model is repeated here:

$$\Phi = \alpha_0 R^{\alpha 1} \theta'^{\alpha 2} S^{\alpha 3} (\rho/\rho_s)^{\alpha 4} \qquad (5.2)$$

in which the α's are all undetermined. The transport Φ and each of the three variables is nondimensional. The Reynold's number R is a ratio of inertial to viscous forces. The Shields' number θ' is a ratio of drag and gravitational forces. Many transport models contain only the Shields' number as their predictor of transport (Hanes and Bowen, 1985; Madsen and Grant, 1976; Shibayama and Horikawa, 1980). The Strouhal number S is the ratio of drag to inertial forces. Both R and S contain inertial forces. If they are multiplied together, we would obtain a

third type of dimensionless force ratio, the ratio of drag to viscous forces, known as the "streaming" Reynold's number, R_s. The ratio (ρ/ρ_s), "specific mass," is a measure of the relative inertias of the sediment and fluid components and does not vary in our experiments. Therefore we will be unable to determine any variation of transport with specific mass in our data.

The values of various nondimensional force ratios were computed for each of our experiments using threshold criteria (Equation 4.4) and are listed in Table 5-5. Recall that the fluid measurements for 29 September 1980 were lost. Thus R, R_s, and θ could not be computed for that day, and we did not use the transport data from that experiment to test models. The Irribaren number is a parameter which many investigators have found to be important in surf zone studies (i.e., White and Inman, 1987b). It is a measure of the amount of energy reflected from the beach face. Since it is more applicable to surf zone studies nearer the beach face, we will not use it in conjunction with our measurements outside the surf zone.

In order to determine the values of the exponents in Equation (5.2), we computed correlations between measured nondimensional transport and various powers of each of the three nondimensional force ratios R, R_s, and θ'. The results are presented in Table 5-6. In each case the best correlation was obtained for the power which

Table 5-5. Nondimensional Ratios of Fluid-Sediment Parameters

Experiment	Reynold's Number	Streaming Reynold's Number	Strouhal Number	Modified Shields' Number	Irribaren Number
	R	R_s	S	θ'	c_{rb}
23 Jun 80	2.43	23300	9600	2.19	0.026
11 Aug 80	0.210	3580	17064	0.157	0.235
12 Sep 80	0.199	3320	16703	0.179	0.120
29 Sep 80			21105		0.111
3 Aug 84	-11.43	-115000	10056	14.15	0.018
10 Aug 84	11.17	85500	7662	11.53	0.010
29 Aug 84	-11.97	-65100	5437	7.28	0.053
26 Sep 84	6.19	50700	8197	5.60	0.072
30 Oct 84	0.879	3960	4506	1.01	0.042

Definitions:

$$R = \frac{\langle u \rangle D}{\nu}$$

$$R_s = \frac{\langle u \rangle d_o}{\nu}$$

$$S = \frac{d_o}{D}$$

$$\theta' = \frac{\rho \langle u^2 \rangle}{\gamma_s D}$$

$$c_{rb} = \frac{2g \tan^2 \beta}{H \sigma^2}$$

A threshold has been applied to $\langle u \rangle$ in computing R, R_s, and θ':

$\langle u \rangle = \langle u \rangle$ for all $u_T > u_t$

$= 0$ for all $u_T < u_t$

Table 5-6. Reynold's and Shields' Numbers Correlation with Transport (A threshold has been applied.)

Part A. Reynold's Number, R, Correlation with Dimensionless Transport Φ

	Moment $\langle R^n \rangle$					
n =	1	2	3	4	5	6
Mean	0.126	32.1	2.94 x10^3	2.35 x10^5	1.80 x10^7	1.36 x10^9
St. Dev.	6.45	320.	1.86 x10^4	1.24 x10^6	9.24 x10^7	7.48 x10^9
Slope, m	0.0249	5.00 x10^{-4}	8.22 x10^{-6}	1.15 x10^{-7}	1.46 x10^{-9}	1.72 x10^{-11}
Intercept	0.174	0.161	0.153	0.150	0.151	0.153
Cor. Coef.	0.644	0.641	0.612	0.573	0.540	0.515
90% Confidence Limits:						
(lower)	0.617	0.613	0.583	0.542	0.507	0.481
(upper)	0.670	0.666	0.639	0.603	0.571	0.548
80% Confidence Limits:						
(lower)	0.626	0.623	0.593	0.553	0.519	0.493
(upper)	0.661	0.658	0.630	0.593	0.561	0.537
70% Confidence Limits:						
(lower)	0.633	0.630	0.600	0.561	0.527	0.502
(upper)	0.655	0.651	0.623	0.586	0.553	0.529
% Sig.	99.992	99.992	99.978	99.930	99.832	99.380

Part B. Streaming Reynold's Number R_s Correlation with Dimensionless Transport Φ

	Moment $\langle R_s^n \rangle$					
n =	1	2	3	4	5	6
Mean	3.47 x10^3	3.45 x10^5	2.70 x10^7	2.03 x10^9	1.50 x10^{11}	1.10 x10^{13}
St.Dev.	4.99 x10^4	2.66 x10^6	1.63 x10^8	1.13 x10^{10}	8.58 x10^{11}	7.04 x10^{13}
Slope, m	3.18 x10-6	5.77 x10^{-8}	8.88 x10^{-10}	1.20 x10^{-11}	1.50 x10^{-13}	1.75 x10^{-15}
Intercept	0.166	0.157	0.153	0.152	0.154	0.158
Cor.Coef.	0.636	0.616	0.581	0.544	0.515	0.495
90% Confidence Limits:						
(lower)	0.608	0.587	0.550	0.511	0.481	0.459
(upper)	0.662	0.643	0.610	0.575	0.547	0.528
80% Confidence Limits:						
(lower)	0.618	0.597	0.561	0.522	0.493	0.472
(upper)	0.653	0.634	0.600	0.564	0.536	0.516
70% Confidence Limits:						
(lower)	0.625	0.604	0.568	0.530	0.501	0.480
(upper)	0.647	0.627	0.593	0.556	0.528	0.508
% Sig.	99.990	99.980	99.944	99.848	99.692	99.504

Table 5-6. Reynold's and Shields' Numbers Correlation with Transport (A threshold has been applied.)

Part C. Modified Shields' Number θ' Correlation with Dimensionless Transport Φ

	Moment $\langle \theta'^n \rangle$					
n =	1	2	3	4	5	6
Mean	9.83 $\times 10^{-2}$	8.89 $\times 10^{1}$	6.27 $\times 10^{4}$	2.34 $\times 10^{8}$	5.14 $\times 10^{12}$	8.22 $\times 10^{16}$
St. Dev.	7.85 $\times 10^{-1}$	2.15 $\times 10^{3}$	7.78 $\times 10^{6}$	3.56 $\times 10^{10}$	2.02 $\times 10^{14}$	1.40 $\times 10^{18}$
Slope, m	2.10 $\times 10^{-1}$	7.09 $\times 10^{-5}$	1.80 $\times 10^{-8}$	3.68 $\times 10^{-12}$	6.13 $\times 10^{-16}$	8.36 $\times 10^{-20}$
Intercept	0.197	0.183	0.178	0.178	0.180	0.184
Cor. Coef.	0.659	0.610	0.560	0.525	0.498	0.470
90% Confidence Limits:						
(lower)	0.633	0.581	0.528	0.492	0.463	0.435
(upper)	0.684	0.638	0.590	0.557	0.531	0.505
80% Confidence Limits:						
(lower)	0.642	0.591	0.539	0.503	0.475	0.447
(upper)	0.676	0.628	0.580	0.546	0.520	0.493
70% Confidence Limits:						
(lower)	0.649	0.598	0.547	0.512	0.484	0.456
(upper)	0.670	0.622	0.573	0.538	0.512	0.485
% Sig.	99.998	99.976	99.900	99.756	99.548	99.196

contains the first power of the fluid velocity. Smaller fractional powers of each parameter were also attempted, but just as we found in Section 4.2, correlations were quite poor. Furthermore, the predicted direction of crossshore transport was often incorrect when fractional powers of u were used.

By examining the confidence intervals of the correlations, we can conclude with 69% confidence that the first power of the streaming Reynold's number R_s is better than other powers of R_s, with 89% confidence that the half power of θ' is better than other powers of θ', and with 75% confidence that the correct power of the Reynold's number must be either one or two. We can further conclude with 70% confidence that the Shields' number is a better predictor than streaming Reynold's number. Values of the wave orbital diameter needed to compute the Strouhal number S did not vary significantly during the course of each day's experiments. Thus there were only eight data points for any correlation between Strouhal number and transport. This is an insufficient number to obtain correlations with sufficiently narrow confidence intervals to enable conclusions regarding the appropriate power of S in Equation (5.2).

Each of the three variables in Table 5-6 may be used alone as a predictor of sediment transport. The appropriate transport equations are:

$$\Phi = 0.210 \langle \theta'^{1/2} \rangle + 0.197 \qquad (5.3)$$

$$\Phi = 0.0249 \langle R \rangle + 0.174 \qquad (5.4)$$

$$\Phi = 3.18 \times 10^{-6} \langle R_s \rangle + 0.166 \qquad (5.5)$$

Just as with correlations of the transport models in Section 5.1, we caution that the intercepts in Equations (5.3), (5.4), and (5.5) may be due to errors in tracer measurements. Plots of measured versus predicted transport for the three variables in Equations (5.3), (5.4), and (5.5) are included in Appendix 1.

We have determined the appropriate powers of R, R_s, and θ for transport prediction, if each of these variables alone were to be used as a predictor. But when they are combined as in Equation (5.2) there are intercorrelations among these three variables. When their product in Equation (5.2), $RS\sqrt{\theta}$, is correlated with transport, the intercorrelations may result in less correlation with transport Φ. In fact, the correlation for such a model was found to be 0.582, somewhat less than for one of the variables alone. We need to perform a multiple linear regression on our set of variables, in which the variables are all varied at the same time in order to determine the best possible combination for predicting transport. We performed multiple regressions on these variables, and it was discovered that combinations of the variables could not be found which had statistically significant higher correlations with transport than R, R_s, or θ alone. The

reason for this is that we have a statistically large number of measures of only two parameters, transport and fluid velocity. Nondimensional parameters such as R, R_s, or θ contain fluid velocity and various other variables for which we have at most eight estimates during the experiments. Parameters such as orbital diameter, grain size, fluid viscosity, and sediment density did not vary significantly enough to produce a statistically large amount of variation. Any attempt to correlate combinations of these parameters with transport simply emphasizes the fact that our only statistically significant independent variable is fluid velocity.

We present the model in Equation (5.2) to future investigators. It contains all the macroscopic variables necessary to determine sediment transport and separates the different types of physical forces into nondimensional parameters. In order to properly test it, sufficient variation must occur in some of the dimensional variables. Any one data set is unlikely to contain such variation. Perhaps after a sufficient number of investigators have performed transport experiments in sufficiently different conditions, we can determine the appropriate functional form for each of the independent variables.

6. CONCLUSIONS

The set of 30 experiments, which included measurements of fluid velocity, bedload thickness, and bedload velocity, allows several conclusions to be reached based on linear correlations between the different variables. Correlations between both computed quantities (from bedload models) and measured variables enable us to make conclusions about the behavior of transport thickness, transport velocity, friction factors, transport efficiencies, threshold criteria, appropriate functional forms of bedload models, relative importance of different physical forces, required accuracy in measurements, and the relative performance of different bedload transport models. Specific recommendations for the use of each bedload model are listed in Section 5.2.

1. The thickness of the bedload does not correlate well with wave height or fluid velocity, as has been suggested by others (Sunamura and Kraus, 1985). But the transport thickness is very well correlated with orbital diameter.

2. The application of a threshold criterion to the fluid velocity is essential in determining the correct direction of sediment transport (onshore or offshore). But the different threshold theories tend to agree well enough that in practice, it does not matter which of the threshold theories is used.

3. Lower powers of the fluid velocity predict sediment transport better than higher moments. With 90% confidence, we conclude that $\langle u \rangle$ and $\langle u^2 \rangle$ moments are better predictors than $\langle u^4 \rangle$, $\langle u^5 \rangle$, or $\langle u^6 \rangle$. Also at 90% confidence, $\langle u^3 \rangle$ predicts better than $\langle u^5 \rangle$ or $\langle u^6 \rangle$.

4. Fractional powers of u such as $\langle u^{0.5} \rangle$ performed significantly poorer than any other moment tested. At 90% confidence it performs more poorly than $\langle u^n \rangle$ with n=1 to 5. Furthermore, it predicts the correct direction of transport for only 70% of the experiments, whereas $\langle u^n \rangle$ for all n=1 to 6 always predicts the correct direction.

5. Accurate measurement of fluid velocity, particularly the mean which is included in all transport models, is critically important in determining transport direction. In fact, it is much more important than the choice between lower-order moments (u^3 and u^4 transport models).

6. The performance of u^3 as a transport predictor was compared with the same-order moments of uu_m^2 (Bagnold, 1963) and $u(u^2+v^2)$ (Bailard and Inman, 1981). No statistically significant difference in performance was observed. In the case of $u(u^2+v^2)$ this was due to the very small values of v in our data.

7. The combination of Bailard's (1981) estimate of bedload efficiency e_b=0.21 with c_f=0.007 [based on both Thornton's (1970) and Komar's (1969) longshore current

measurements were in remarkably good agreement with the measurements in this experiment (1-3% error).

8. Including more variables in transport models than are necessary (Kobayashi, 1982) results in significant deterioration in model performance, in addition to increased experimental effort and theoretical complication.

9. With 79% confidence we conclude that either lift forces are not important compared to drag forces in transport calculations, or lift force description was performed improperly (Sleath, 1978).

10. With 80% confidence we conclude that the Hanes and Bowen (1985) model performed significantly less well than several other models. This may be due to insufficient knowledge of their many model parameters, inapplicability to our data of the very intense type of transport described by them, or different flow regimes.

11. With 90% confidence we conclude that the u^6 transport models (Madsen and Grant, 1976; Shibayama and Horikawa, 1980) performed significantly poorer than most other models. These empirical transport models should not be used, unless significant experimental and theoretical verification are obtained.

12. It is possible that n in $i \propto \langle u^n \rangle$ is a variable and not a constant. Allowing n to vary (Einstein, 1950) produced high correlations, although not statistically more significant than u^3 models. The possibility that n

increases in a specified manner as i increases should be considered by modelers.

13. Reynold's number, streaming Reynold's number, and particularly Shields' number are each significant predictors of transport.

14. More experiments under widely varying conditions are necessary to determine transport's dependence on fluid viscosity ν, specific mass ρ_s/ρ, wave orbital diameter d_o, and grain size D. Such experiments would also allow determination of the proper combination of nondimensional force ratios, such as Reynold's, Shields' and Strouhal numbers, in predicting transport.

7. REFERENCES

Abou-Seida, M.M., 1965, "Bed load function due to wave action," Univ. of Calif., Berkeley, Hydraulic Engr. Lab., Inst. of Engr. Res., Tech. Rep. HEL-2-11, 78 pp.

Ackerman, N.L. and H. Shen, 1982, "Stresses in rapidly sheared fluid-solid mixtures," J. Engr. Mechanics Div., Amer. Soc. Civil Engrs., v 108, n 1, p 95-113.

Ackers, P. and W.R. White, 1973, "Sediment transport: new approach and analysis," Proc. ASCE J. Hydr. Div., v 99, n HY11, p 2041-2060.

Aubrey, D.G., 1979, "Seasonal patterns of onshore/offshore sediment movement," J. Geophys. Res., v 84, n C10, p 6347-6354.

Aubrey, D.G. and J.H. Trowbridge, 1985, "Kinematic and dynamic estimates from electromagnetic current meter data," J. Geophys. Res., v 90, n C5, p 9137-9146.

Bagnold, R.A., 1946, "Motion of waves in shallow water; interaction between waves and sand bottoms," Proc. Roy. Soc. (London), Series A, v 187, p 1-18.

Bagnold, R.A., 1954, "Experiments on a gravity-free dispersion of large solid spheres in a Newtonian fluid under shear," Proc. Roy. Soc. (London), Series A, v 225, p 49-63.

Bagnold, R.A., 1956, "The flow of cohesionless grains in fluids," Proc. Roy. Soc. (London), Series A, v 249, n 964, p 235-297.

Bagnold, R.A., 1963, "Beach and nearshore processes: mechanics of marine sedimentation," Ch. 21 of The Sea, v 3, M.N. Hill, ed., Wiley, New York, p 507-528.

Bagnold, R.A., 1966, "An approach to the sediment transport problem from general physics," U.S. Geol. Sur., Prof. Paper 422-I, 37 pp.

Bagnold, R.A., 1974, "Fluid forces on a body in shear-flow; experimental use of 'stationary flow,'" Proc. Roy. Soc. (London), Series A, v 340, p 147-171.

Bagnold, R.A., 1986, "Transport of solids by natural water flow: evidence for a worldwide correlation," Proc. Roy. Soc. (London), Series A, v 405, p 369-374.

Bailard, J.A., 1981, "An energetics total load sediment transport model for a plane sloping beach," J. Geophys. Res., v 86, n C11, p 10938-10954.

Bailard, J.A. and D.L. Inman, 1981, "An energetics bedload model for a plane sloping beach: local transport," J. Geophys. Res., v 86, n C3, p 2035-2043.

Batchelor, G.K., 1967, An Introduction to Fluid Dynamics, Cambridge Univ. Press, Cambridge, 615 pp.

Beach Erosion Board, 1950, "Munch-Peterson's littoral drift formula," U.S. Army Corps of Engineers, Beach Erosion Board Bulletin, v 4, p 1-31.

Brown, C.B., 1949, "Sediment transportation," Ch. XII, Sections A-C, in Engr. Hydraulics, Proc. 4th Hydraulics Conf., Iowa Inst. of Hydraulic Res., H. Rouse, ed., Wiley, New York, p 769-804.

Crickmore, M.J., 1967, "Measurement of sand transport in rivers with special reference to tracer methods," Sedimentology, v 8, p 175-228.

Crickmore, M.J. and G.H. Lean, 1962a, "The measurement of sand transport by means of radioactive tracers," Proc. Roy. Soc. (London), Series A, v 266, p 402-421.

Crickmore, M.J. and G.H. Lean, 1962b, "The measurement of sand transport by the time-integration method with radioactive tracers," Proc. Roy. Soc. (London), Series A, v 270, p 27-47.

Dean, R.G., E.P. Berek, C.G. Gable, and R.J. Seymour, 1982, "Longshore transport determined by an efficient trap," Proc. 18th Coastal Engr. Conf., Amer. Soc. Civil Engrs., p 954-968.

Dingler, J.R., 1974, "Wave-formed ripples in nearshore sands," University of California, Ph.D. dissertation, 136 pp.

Dingler, J.R. and D.L. Inman, 1976, "Wave-formed ripples in nearshore sands," Proc. 15th Coastal Engr. Conf., Amer. Soc. Civil Engrs., p 2109-2126.

Doering, J.C. and A.J. Bowen, in press, "Skewness in the nearshore zone: a comparison of estimates from Marsh-McBirney current meters and 'colocated' pressure sensors," J. Geophys. Res.

Duane, D.B. and W.R. James, 1980, "Littoral transport in the surf zone elucidated by an Eulerian tracer experiment," J. Sed. Petrol., v 50, n 3, p 929-942.

Einstein, H.A., 1950, "The bed-load function for sediment transport in open channel flows," U.S. Dept. of Agriculture, SCS, Tech. Bulletin No. 1025.

Einstein, H.A., 1972, "A basic description of sediment transport on beaches," Waves on Beaches and Resulting Sediment Transport, R.E. Meyer, ed., Academic Press, New York, p 53-93.

Fairchild, J.C., 1972, "Longshore transport of suspended sediment," Proc. 13th Coastal Engr. Conf., Amer. Soc. Civil Engrs., p 1069-1088.

Freilich, M.H., 1982, "Resonance effects on shoaling surface gravity waves," Univ. of Calif., Ph.D. dissertation, 113 pp.

Gaughan, M.K., 1978, "Depth of disturbance of sand in surf zones," Proc. 16th Coastal Engr. Conf., Amer. Soc. Civil Engrs., p 1513-1530.

Goodman, M.A. and S.C. Cowin, 1972, "A continuum theory for granular material," Archives for Rational Mechanics and Analysis, v 44, p 249-266.

Goud, M.R. and D.G. Aubrey, 1985, "Theoretical and observational estimates of nearshore bedload transport rates," Marine Geology, v 64, p 91-111.

Guza, R.T., M.C. Clifton, and F. Rezvani, 1986, "Intercomparisons of electromagnetic current meters in the nearshore," EOS, Trans., Amer. Geophys. Union, v 67, n 44, p 1025.

Guza, R.T. and E.B. Thornton, 1980, "Local and shoaled comparisons of sea surface elevations, pressures, and velocities," J. Geophys. Res., v 85, n C3, p 1524-1530.

Hallermeier, R.J., 1982, "Oscillatory bedload transport: Data review and simple formulation," Cont. Shelf Res., v 1, n 2, p 159-190.

Hanes, D.M. and A.J. Bowen, 1985, "A granular-fluid model for steady intense bed-load transport," J. Geophys. Res., v 90, n C5, p 9149-9158.

Hanes, D.M. and D.L. Inman, 1985, "Observations of rapidly flowing granular-fluid materials," J. Fluid Mech., v 150, p 357-380.

Hansen, J.B. and I.A. Svendsen, 1984, "A theoretical and experimental study of undertow," Proc. 19th Coastal Engr. Conf., Amer. Soc. Civil Engrs., New York, p 2246-2262.

Hughes, W.F. and J.A. Brighton, 1967, "Fluid dynamics," Schaum's Outline Series, McGraw-Hill, New York, 265 pp.

Ingle, J.C., Jr., 1966, "The movement of beach sand," Developments in Sedimentology, v 5, 221 pp.

Inman, D.L., 1952, "Measures for describing the size distribution of sediments," J. Sed. Petrol., v 22, n 3, pp 125-145.

Inman, D.L., 1957, "Wave-generated ripples in nearshore sands," U.S. Army Corps of Engineers, Beach Erosion Board Tech. Memo. No. 100, 65 pp.

Inman, D.L., 1979, "Physics of sediment transport," Class Syllabus, Univ. of Calif., Scripps Inst. Ocean., 250 pp.

Inman, D.L. and R.A. Bagnold, 1963, "Beach and nearshore processes: littoral processes," Ch. 21 of The Sea, v 3, M.N. Hill, ed., Wiley, New York, p 529-553.

Inman, D.L. and A.J. Bowen, 1962, "Flume experiments on sand transport by waves and currents," Proc. 8th Coastal Engr. Conf., Amer. Soc. Civil Engrs., p. 137-150.

Inman, D.L. and T.K. Chamberlain, 1959, "Tracing beach sand movement with irradiated quartz," J. Geophys. Res., v 64, p 41-47.

Inman, D.L., R.T. Guza, C.D. Winant, and R.E. Flick, 1981, "Fluid-sediment interactions on beaches and shelves," University of California, SIO Reference Series 81-27, 86 pp.

Inman, D.L., S.A. Jenkins, D.M. Hicks, and H.K. Kim, 1986, "Oscillatory bursting over beds of fine sand," University of California, SIO Reference Series 86-13, 46 pp.

Inman, D.L, P.D. Komar, and A.J. Bowen, 1968, "Longshore transport of sand," Proc. 11th Coastal Engr. Conf., Amer. Soc. Civil Engrs., p 298-306.

Inman, D.L. and W.H. Quinn, 1952, "Currents in the surf zone," Proc. 2nd Coastal Engr. Conf., Amer. Soc. Civil Engrs., p. 24-36.

Inman, D.L. and G.A. Rusnak, 1956, "Changes in sand level on the beach and shelf at La Jolla, California," Beach Erosion Board, U.S. Army Corps of Engrs., Tech. Memo. No. 82, 64 pp.

Inman, D.L., J.A. Zampol, T.E. White, D.M. Hanes, B.W. Waldorf, and K.A. Kastens, 1980, "Field measurements of sand motion in the surf zone," Proc. 17th Coastal Engr. Conf., Amer. Soc. Civil Engrs., p 1215-1234.

Jenkins, J.T. and S.B. Savage, 1983, "A theory for the rapid flow of identical, smooth, nearly elastic spherical particles," J. Fluid Mech., v 130, p 187-202.

Kalkanis, G., 1964, "Transportation of bed material due to wave action," U.S. Army Corps of Engrs., CERC Tech. Memo. No. 2, 38 pp.

King, C.A.M., 1951, "Depth of disturbance of sand on sea beaches by waves," J. Sed. Petrol., v 21, p 131-140.

King, D.B., Jr., and R.J. Seymour, 1984, "A new oscillatory flow tunnel for use in sediment transport experiments," Proc. 19th Coastal Engr. Conf., Amer. Soc. Civil Engrs., p 1559-1570.

Kobayashi, N., 1982, "Sediment transport on a gentle slope due to waves," J. Waterway, Port, Coastal and Ocean Div., Amer. Soc. Civil Engrs., v 108, n WW3, p 254-271.

Komar, P.D., 1969, "The longshore transport of sand on beaches," Ph.D. thesis, University of California, San Diego, 143 pp.

Komar, P.D. and D.L. Inman, 1970, "Longshore sand transport on beaches," J. Geophys. Res., v 75, n 30, p 5914-5927.

Kraus, N.C., R.S. Farinato, and K. Horikawa, 1981, "Field experiments on longshore sand transport in the surf zone," Coastal Engr. in Japan, v 24, p 171-194.

Kraus, N.C., M. Isobe, H. Igarashi, T.O. Sasaki, and K. Horikawa, 1982, "Field experiments on longshore sand transport in the surf zone," Proc. 18th Coastal Engr. Conf., Amer. Soc. Civil Engrs., p 969-988.

Langhaar, H.L., 1951, Dimensional Analysis and Theory of Models, Wiley, New York, 166 pp.

AD-A185 083 NEARSHORE SAND TRANSPORT(U) CALIFORNIA UNIV SAN DIEGO 3/3
LA JOLLA T E WHITE 1987 N00014-75-C-0300

UNCLASSIFIED F/G 8/3 NL

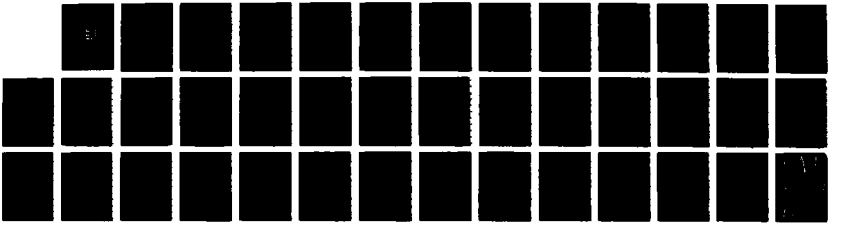

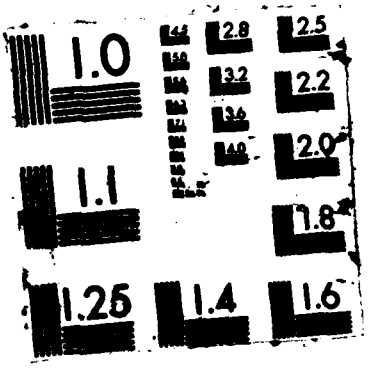
1.0
2.8
2.5
3.2
2.2
3.6
2.0
4.0
1.1
1.8
1.25
1.4
1.6

LeMehaute, B., D. Divoky, and A. Lin, 1968, "Shallow water waves: a comparison of theories and experiments," Proc. 11th Coastal Engr. Conf., Amer. Soc. Civil Engrs., New York, p 96-107.

Long, B., N. Kulkarni, and G. Joice, 1978, "Radioisotopes as sediment tracers: risks involved and proposed guidelines for use," Bedford Inst. of Oceanography, Report Series BI-R-78-3, 38 pp.

Madsen, O.S. and W.D. Grant, 1976, "Sediment transport in the coastal environment," Ralph M. Parson Lab. for Water Res. and Hydrodynamics, Dept. Civil Engr., MIT, Report No. 209, 105 pp.

McTigue, D.F., 1979, "A nonlinear continuum model for flowing granular materials," Ph.D. dissertation, Stanford University.

Meyer-Peter, E. and R. Mueller, 1948, "Formulas for bed-load transport," Proc. 2nd IAHR Congress, Stockholm.

Miller, M.C. and P.D. Komar, 1979, "Measurements of sand spreading rates under near-bottom wave orbital motions," J. of Geol., v 87, n 6, p 593-608.

Murray, S.P., 1967, "Control of grain dispersion by particle size and wave state," J. of Geol., v 75, n 5, p 612-634.

Murray, S.P., 1968, "Simulation of horizontal turbulent diffusion of particles under waves," Proc. 11th Coastal Engr. Conf., Amer. Soc. Civil Engrs., p 446-466.

Ogawa, S., A. Umemura, and N. Oshima, 1980, "On the equations of fully fluidzied granular materials," J. Appl. Math. Physics (ZAMP), v 31, p 483-493.

Ostendorf, D.W. and O.S. Madsen, 1979, "An analysis of longshore currents and associated sediment transport in the surfzone," Ralph M. Parsons Lab., Rep. 241, Dept. Civil Engr., MIT, Cambridge, Mass.

Passman, S.L., J.W. Nunziato, P.B. Bailey, and J.P. Thomas, Jr., 1980, "Shearing flows of granular materials," J. of Engr. Mechanics Div., Amer. Soc. Civil Engrs., v 106, n EM4, p 773-783.

Pizzuto, J.E., 1987, "Dispersion of dyed sand tracers in an oscillatory flow field," J. Geophys. Res., v 92, n C2, p 1923-1933.

Rance, P.J., 1963, "The determination of quantities of sediment transport in oscillatory motion by consideration of the dispersion of tracer-sediment," I.A.H.R. Congress, p 181-188.

Russell, R.C.H., 1960, "The use of fluorescent tracers for the measurement of littoral drift," Proc. 7th Coastal Engr. Conf., Amer. Soc. Civil Engrs., p 418-444.

Savage, S.B. and D.J. Jeffrey, 1981, "The stress tensor in a granular flow at high shear rates," J. Fluid Mech., v 110, p 255-272.

Scripps Institution of Oceanography, 1947, "A statistical study of wave conditions at five sea localities along the California coast," University of California Wave Report No. 68.

Seymour, R.J., 1985, "Threshold effects on sediment transport by waves," J. Waterways, Port, Coastal, Ocean Engr., Proc. Amer. Soc. Civil Engrs., v 111, n 2, p 371-387.

Shibayama, T. and K. Horikawa, 1980, "Bed load measurement and prediction of two-dimensional beach transformation due to waves," Coastal Engr. in Japan, v 23, p 179-190.

Shields, A., 1936, "Anvendung der Aehnlichkeitsmechanik und der Turbulenzforschung auf die Geschiebebewegung," Mitteilungen der Preussischen Versuchsanstalt fuer Wasserbau und Schiffbau, Heft 26. See translation by W.P. Ott and J.C. van Uchelen, U.S. Dept. Agril., Soil Cons. Service Coop. Lab., Cal. Inst. Tech.

Sleath, J.F.A., 1970, "Velocity measurements close to the bed in a wave tank," J. Fluid Mech., v 42, p 111-123.

Sleath, J.F.A., 1978, "Measurements of bed load in oscillatory flow," J. Waterway, Port, Coastal and Ocean Div., Amer. Soc. Civil Engrs., v 104, n WW4, p 291-307.

Sleath, J.F.A., 1984, Sea Bed Mechanics, Wiley, New York, 335 pp.

Stive, M.J.F. and H.G. Wind, 1986, "Cross-shore mean flow in the surf zone," Coastal Engr., v 10, p 325-340.

Sunamura, T. and N.C. Kraus, 1985, "Prediction of average mixing depth of sediment in the surf zone," Marine Geology, v 62, p 1-12.

Svendsen, I.A., 1984, "Mass flux and undertow in a surf zone," Coastal Engr., v 8, p 347-365.

Svendsen, I.A. and C. Staub, 1981, "Horizontal particle velocities in long waves," J. Geophys. Res., v 86, n C5, p 4138-4148.

Taleki, P.G., 1966, "Fluorescent sand tracers," J. Sed. Petrol., v 36, n 2, p 468-485.

Thornton, E.B., 1970, "Variation of longshore current across the surf zone," Proc. 12th Coastal Engr. Conf., Amer. Soc. Civil Engrs., New York, p 291-308.

Watts, G.M., 1953, "Study of sand movement at South Lake Worth Inlet, Florida," U.S. Army Corps of Engineers, Beach Erosion Board Tech. Memo. No. 42, 24 pp.

White, T.E. and D.L. Inman, 1987a, "Application of tracer theory to NSTS experiments," Chapter 6B of the National Sediment Transport Study Monograph, R.J. Seymour, editor, Plenum Pub., New York.

White, T.E. and D.L. Inman, 1987b, "Measuring longshore transport with tracers," Chapter 13 of the National Sediment Transport Study Monograph, R.J. Seymour, editor, Plenum Pub., New York.

Yalin, M.S., 1963, "An expression for bed-load transportation," Proc. ASCE Hydr. Div., Amer. Soc. Civil Engrs., v 89, n HY3, p 221-250.

Yalin, M.S., 1972, Mechanics of Sediment Transport, 2nd edition, Pergamon Press, New York, 298 pp.

Yasso, W.E., 1966, "Formulation and use of fluorescent tracer coatings in sediment transport studies," Sedimentology, v 6, p 287-301.

Zampol, J.A. and B.W. Waldorf, 1987, "Discrete sampling of bedload and suspended load," Chapter 5A in The National Sediment Transport Study Monograph, R.J. Seymour, editor, Plenum Pub., New York.

APPENDIX 1: Measured versus Predicted Transport

For each of the bedload models tested in this study, the 30 data points of predicted versus measured transport are plotted. In some cases both the original model and the model with threshold criterion were tested. For these models, the original model data are plotted as solid dots, and the model with threshold criterion are plotted as open circles on the same figure.

A slope of one is indicated on the figures by the dashed line. How closely the data approach a slope of one is a measure of the accuracy of the model coefficients, but not of the functional form of the model. The functional form is tested with the correlation coefficients in Table 5-3.

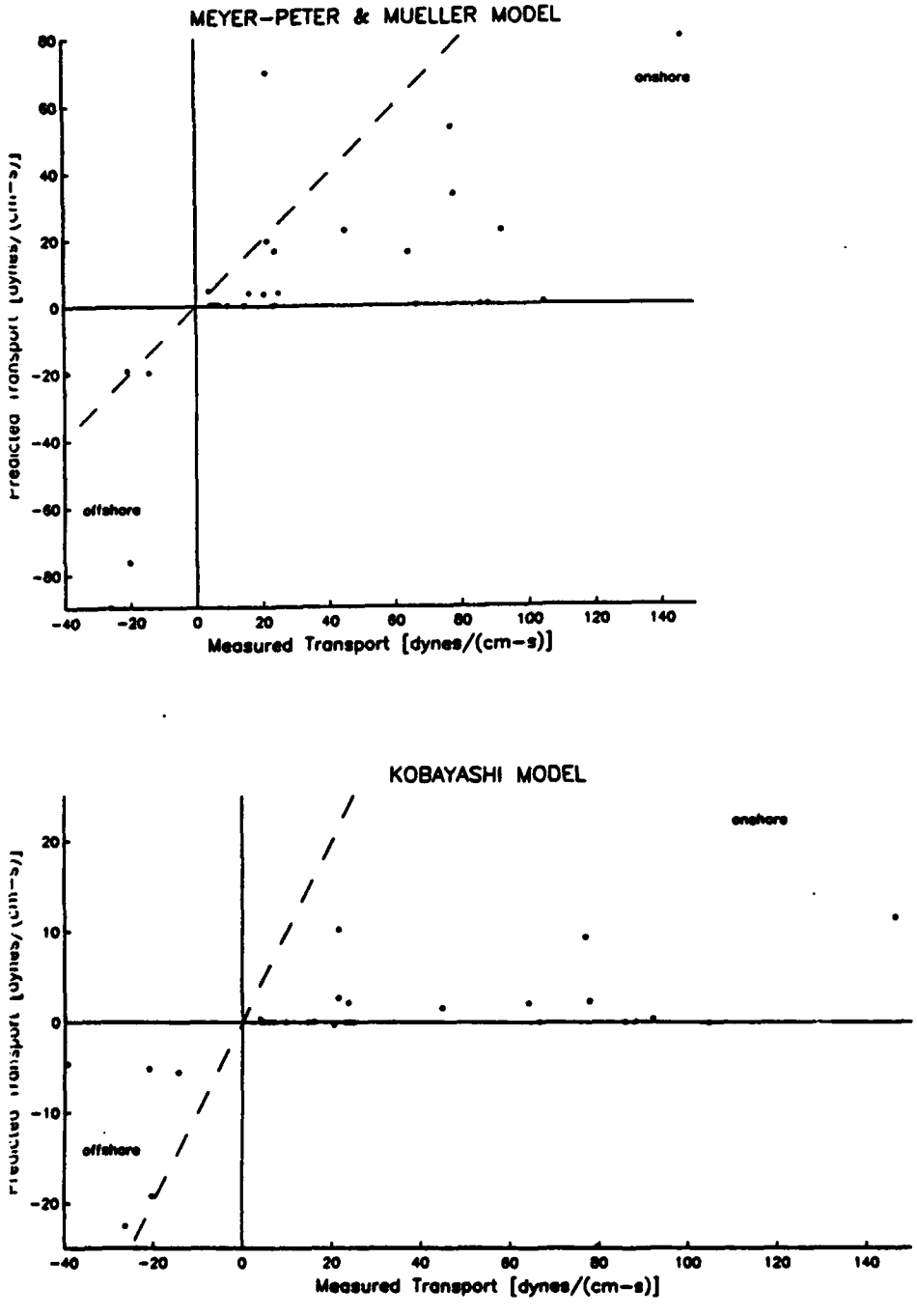

Figure 8-1. Meyer-Peter and Mueller (1948) and Kobayashi (1982) models.

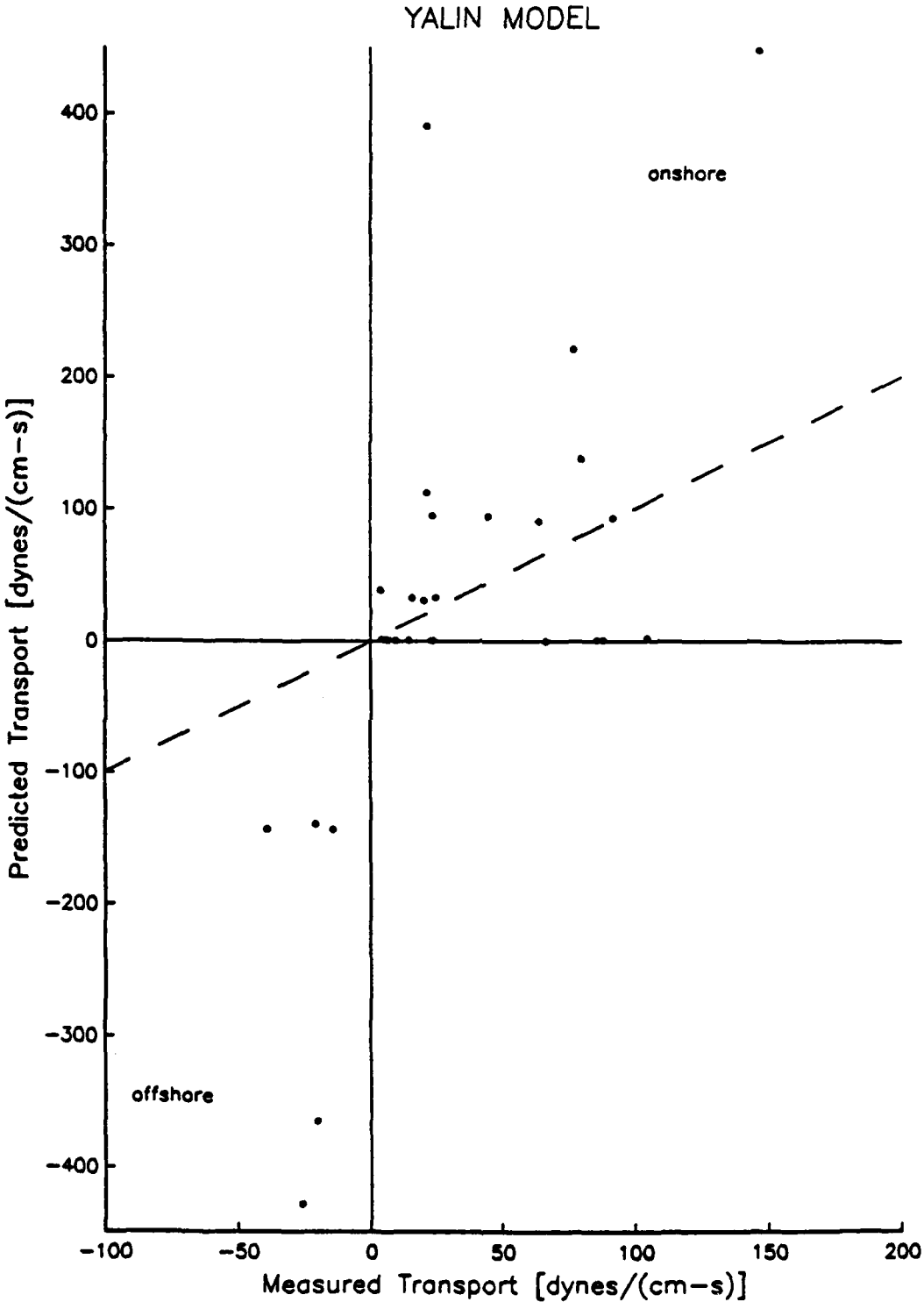

Figure 8-2. Yalin (1963) model.

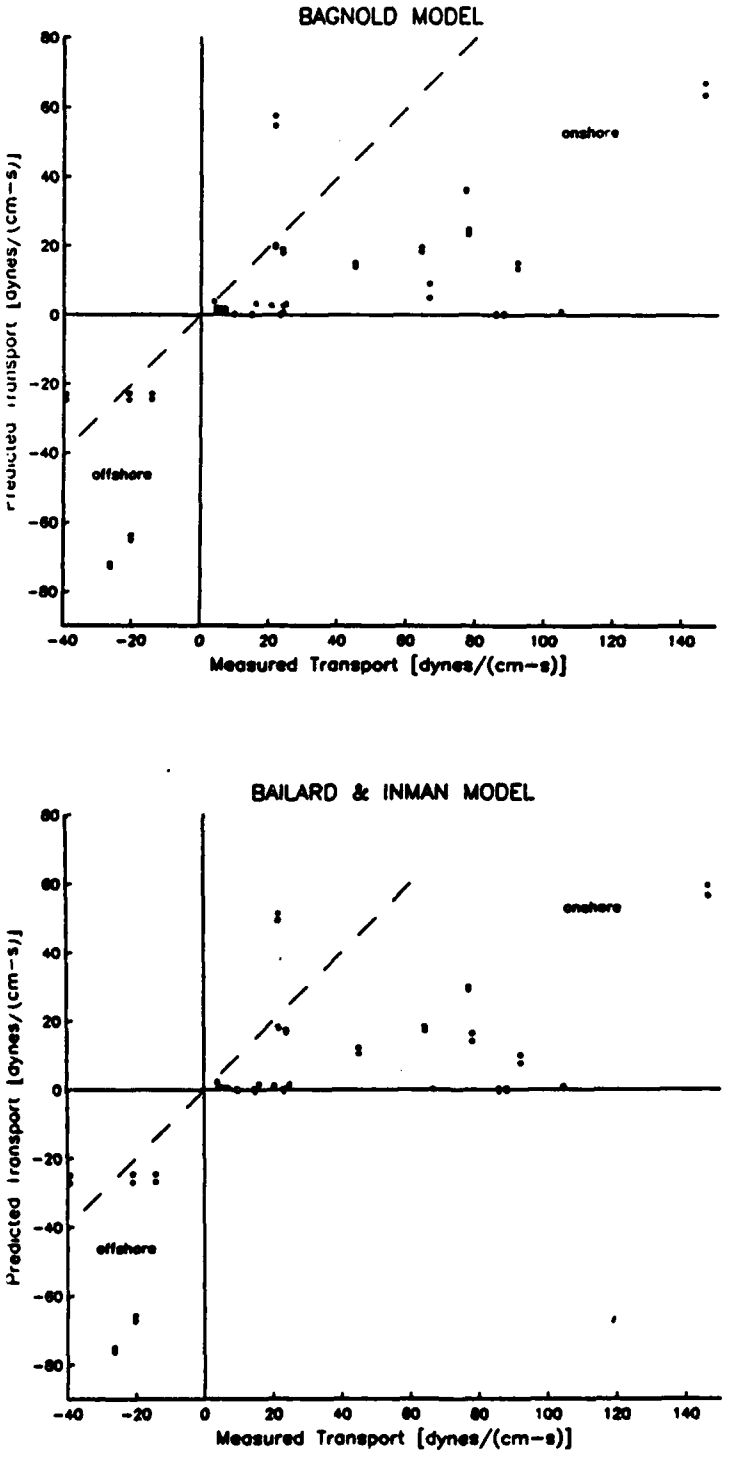

Figure 8-3. Bagnold (1963) and Bailard and Inman (1981) models.

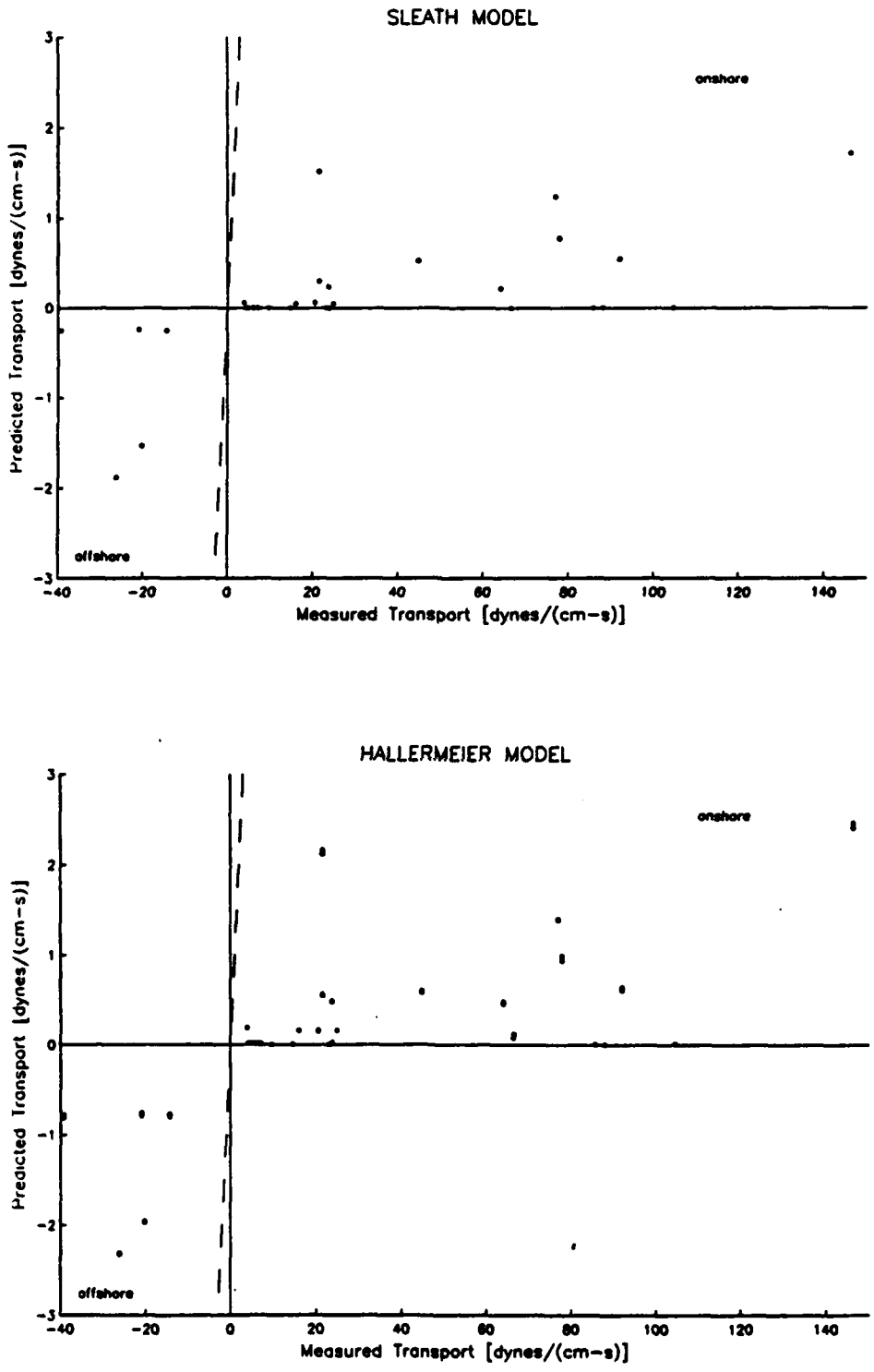

Figure 8-4. Sleath (1978) and Hallermeier (1982) models.

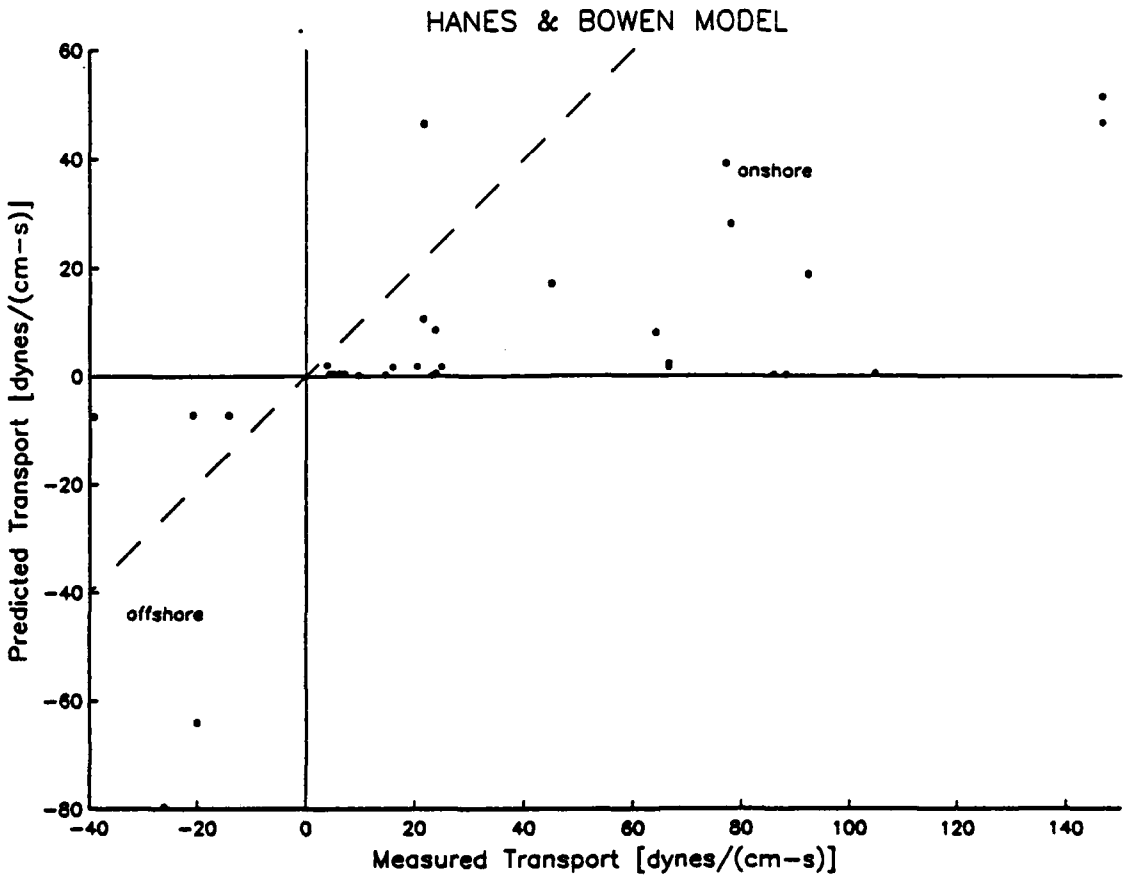

Figure 8-5. Hanes and Bowen (1985) model.

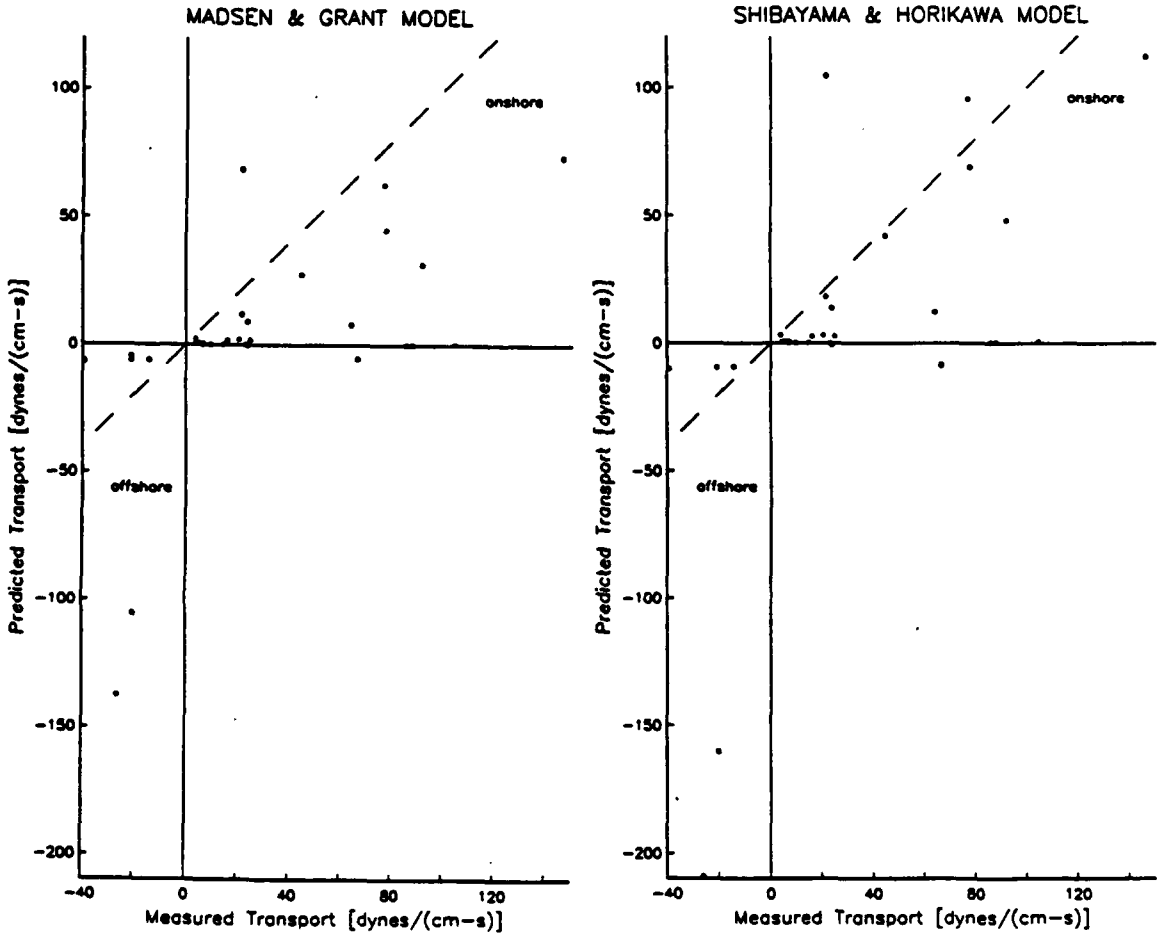

Figure 8-6. Madsen & Grant (1976) and Shibayama & Horikawa (1980) models.

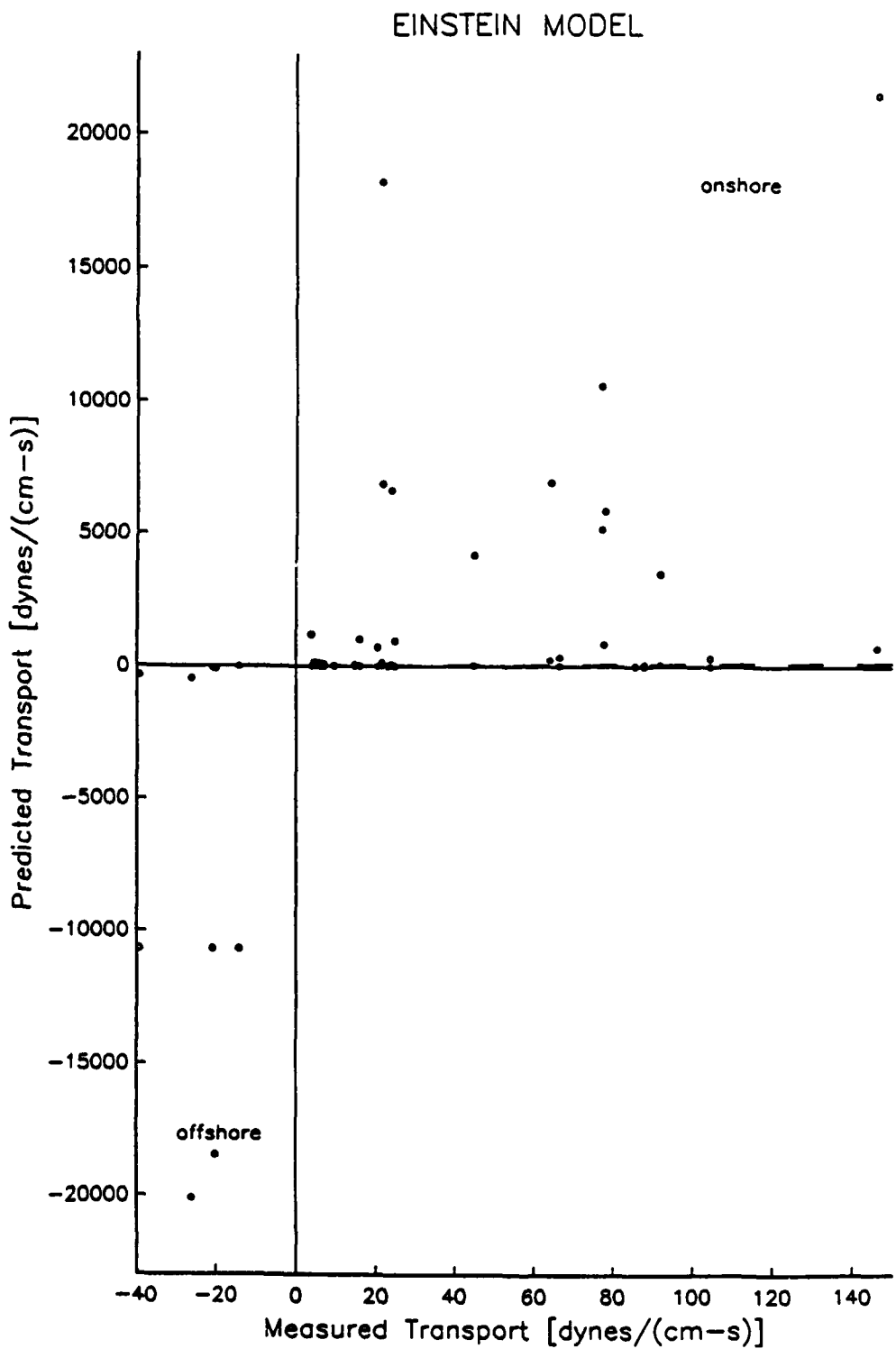

Figure 8-7. Einstein (1950) model.

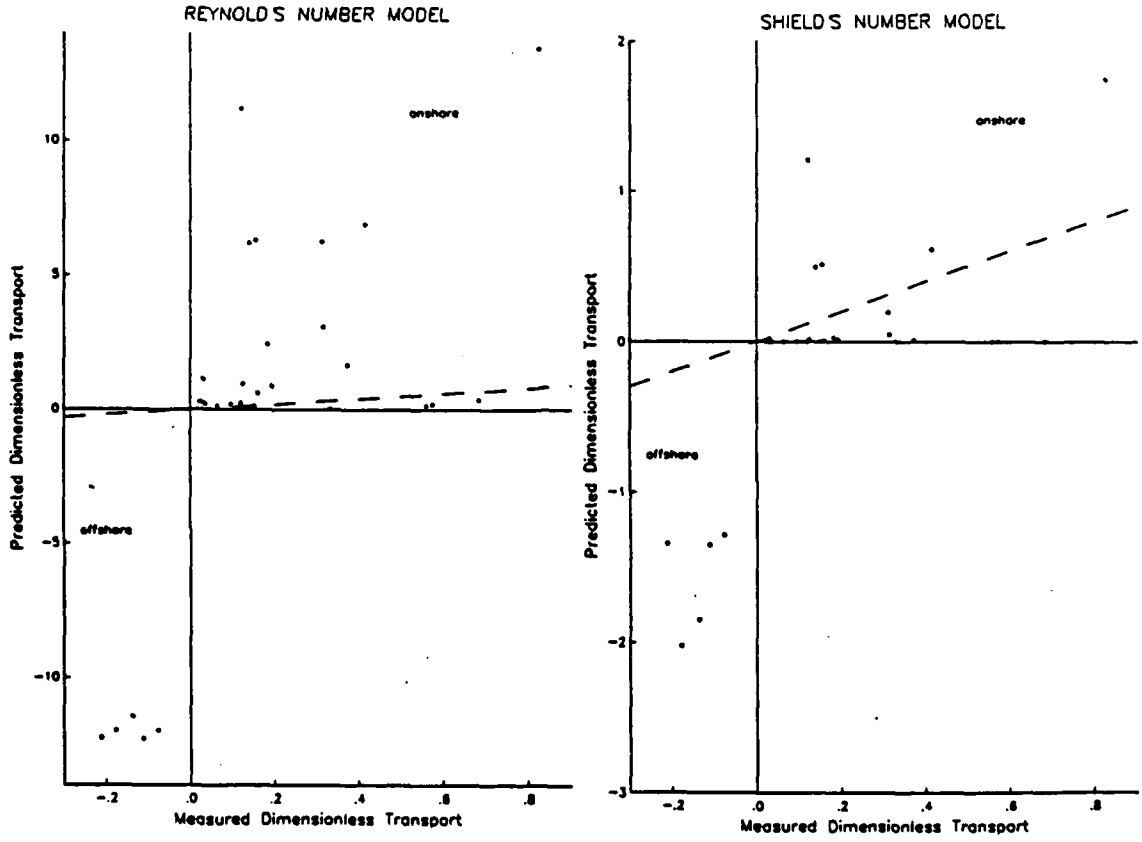

Figure 8-8. Reynold's number and Shields' number models.

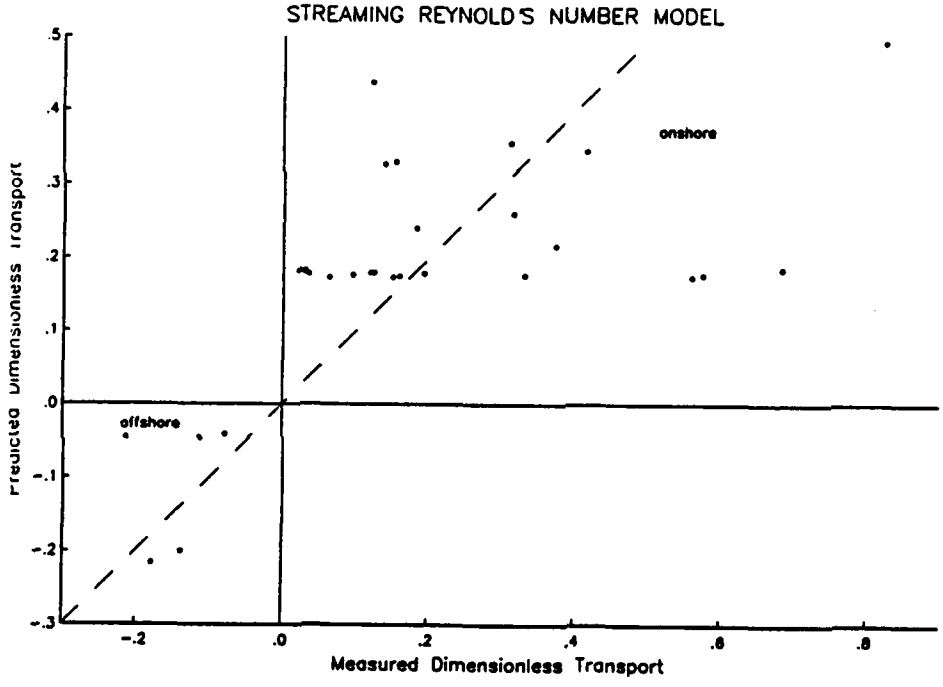

Figure 8-9. Streaming Reynold's number model.

APPENDIX 2: Transport Thickness

Both means (μ) and standard deviations (σ) of Z_o are listed for each of the following estimators:

"Crickmore profile" (no negative concentration gradients) applied to:

A: $Z_o = 2\Sigma[N(z)\ z]/\Sigma N(z)$ (White and Inman, 1987a)

B: $Z_o = \Sigma[N(z)\ \Delta z]/N_{max}$ (Crickmore, 1967)

Original concentration profile applied to:

C: 80% cutoff (Kraus et al, 1982)

D: 90% cutoff (Kraus et al, 1982)

E: 1.0 grains/gram penetration (Inman et al, 1980)

F: 0.5 grains/gram penetration (Inman et al, 1980)

G: $Z_o = 2\Sigma[N(z)\ z]/\Sigma N(z)$ (Inman et al, 1980)

H: Maximum penetration (King, 1951; Komar, 1969)

Table 8-1. Summary of Transport Thickness, Z_o, for Red Tracer (295 total samples)

Both means (μ) and standard deviations (σ) of Z_o are listed for each of the following estimators:

"Crickmore profile" (no negative concentration gradients) applied to:
A: $Z_o = 2\Sigma[N(z)\ z]/\Sigma N(z)$ (White and Inman, 1987a)
B: $Z_o = \Sigma[N(z)\ \Delta z]/N_{max}$ (Crickmore, 1967)
Original concentration profile applied to:
C: 80% cutoff (Kraus et al, 1982)
D: 90% cutoff (Kraus et al, 1982)
E: 1.0 grains/gram penetration (Inman et al, 1980)
F: 0.5 grains/gram penetration (Inman et al, 1980)
G: $Z_o = 2\Sigma[N(z)\ z]/\Sigma N(z)$ (Inman et al, 1980)
H: Maximum penetration (King, 1951; Komar, 1969)

Date	Number of Cores		Transport Thickness Estimates (cm) A	B	C	D	E	F	G	H
Part A: Red Tracer (295 total samples)										
23Jun80	29	μ	2.26	1.66	1.71	2.25	3.89	4.50	2.35	7.58
		σ	0.98	1.11	1.05	1.12	2.89	3.27	1.40	3.42
11Aug80	56	μ	2.06	1.65	1.57	1.92	2.93	3.36	2.18	7.35
		σ	1.63	2.31	2.24	2.43	3.93	3.99	3.04	3.99
12Sep80	53	μ	2.46	1.90	1.93	2.55	2.40	3.17	2.59	6.93
		σ	1.72	1.71	2.03	2.52	2.87	2.86	2.39	3.48
29Sep80	21	μ	3.45	2.52	2.28	4.14	0.60	2.11	3.16	9.43
		σ	1.75	1.97	1.67	3.30	0.82	2.65	1.86	2.76
3Aug84	19	μ	1.83	1.36	1.47	1.93	2.52	2.99	1.89	4.05
		σ	0.70	0.59	0.65	0.83	1.59	1.45	0.77	2.04
10Aug84	13	μ	1.38	0.99	1.20	1.47	1.38	1.88	1.42	2.54
		σ	0.61	0.45	0.57	0.84	1.55	1.49	0.57	1.88
23Aug84	44	μ	1.36	1.04	1.11	1.44	1.99	2.27	1.48	2.77
		σ	0.72	0.60	0.72	0.83	1.66	1.66	0.90	1.82
26Sep84	30	μ	1.92	1.31	1.41	1.87	3.34	3.96	1.89	6.45
		σ	0.79	0.72	0.77	0.93	2.40	2.43	0.97	2.68
30Oct84	30	μ	2.00	1.11	1.40	2.23	3.80	4.76	1.97	8.70
		σ	1.23	1.11	1.26	1.79	2.97	3.03	1.75	2.33

Table 8-2. Summary of Transport Thickness, Z_o, for Green Tracer (260 total samples)

Both means (μ) and standard deviations (σ) of Z_o are listed for each of the following estimators:

"Crickmore profile" (no negative concentration gradients) applied to:
A: $Z_o = 2\Sigma[N(z)\ z]/\Sigma N(z)$ (White and Inman, 1987a)
B: $Z_o = \Sigma[N(z)\ \Delta z]/N_{max}$ (Crickmore, 1967)
Original concentration profile applied to:
C: 80% cutoff (Kraus et al, 1982)
D: 90% cutoff (Kraus et al, 1982)
E: 1.0 grains/gram penetration (Inman et al, 1980)
F: 0.5 grains/gram penetration (Inman et al, 1980)
G: $Z_o = 2\Sigma[N(z)\ z]/\Sigma N(z)$ (Inman et al, 1980)
H: Maximum penetration (King, 1951; Komar, 1969)

Date	Number of Cores		Transport Thickness Estimates (cm) A	B	C	D	E	F	G	H
			Part B: Green Tracer (260 total samples)							
23Jun80	28	μ	2.22	1.62	1.66	2.17	4.14	5.20	2.27	8.42
		σ	0.90	1.13	1.03	1.15	3.31	3.38	1.35	2.80
11Aug80	70	μ	1.90	1.44	1.27	1.75	2.37	3.50	1.96	7.51
		σ	1.65	1.91	1.89	2.37	3.46	4.34	3.00	4.28
12Sep80	57	μ	3.16	2.67	2.83	3.46	2.87	3.83	3.60	7.81
		σ	1.85	2.79	2.59	2.83	3.17	3.40	3.33	3.19
29Sep80	25	μ	3.81	2.75	2.41	3.97	0.51	1.17	3.59	10.11
		σ	1.52	1.68	1.54	2.90	0.88	1.36	1.94	2.33
3Aug84	10	μ	1.47	1.14	1.15	1.50	2.09	2.52	1.49	3.71
		σ	0.80	0.68	0.78	0.89	1.47	1.58	0.85	2.24
10Aug84	2	μ	0.85	0.65	0.63	1.00	0.88	1.00	0.84	1.63
		σ	0.21	0.04	0.00	0.38	0.50	0.63	0.16	1.00
29Aug84	21	μ	1.27	0.92	1.08	1.39	1.55	1.82	1.39	2.23
		σ	0.87	0.67	0.92	1.04	1.26	1.48	1.14	1.83
26Sep84	24	μ	1.88	1.29	1.41	1.98	2.84	3.46	1.83	6.63
		σ	0.79	0.71	0.78	0.91	2.53	2.56	0.89	2.94
30Oct84	23	μ	1.44	0.79	1.05	1.44	4.10	4.63	1.37	7.28
		σ	0.70	0.38	0.76	0.96	2.52	2.80	0.73	3.03

Table 8-3. Transport Thickness: Red Tracer at Torrey Pines (295 total samples)

Experiment	No. of Cores		Transport Thickness Estimates (cm) A	B	C	D	E	F	G	H
23Jun80#1	8	μ	1.78	1.08	1.13	1.81	4.02	4.39	1.73	7.84
		σ	0.66	0.63	0.61	0.67	2.88	3.06	0.84	3.51
#2	4	μ	2.50	1.78	1.94	2.19	4.59	4.72	2.51	5.84
		σ	1.10	0.82	0.84	0.94	3.50	3.45	0.97	3.21
#3	10	μ	2.62	2.02	2.08	2.50	3.58	3.89	2.87	8.86
		σ	1.06	1.50	1.41	1.29	2.79	2.59	1.98	2.01
#4	7	μ	2.29	1.67	1.88	2.57	3.91	4.14	2.42	5.91
		σ	0.91	0.81	0.69	1.23	2.71	2.91	0.86	3.62
11Aug80#1	6	μ	1.99	1.28	1.33	1.83	0.81	0.85	1.76	6.83
		σ	1.16	1.02	0.82	1.17	0.69	0.72	1.07	4.04
#2	10	μ	2.17	1.92	1.91	2.36	1.96	2.39	3.06	6.71
		σ	1.88	2.65	2.89	3.12	3.21	3.08	4.81	3.61
#3	11	μ	2.51	2.42	2.17	2.60	3.36	4.15	2.67	7.85
		σ	2.36	3.73	3.57	3.63	4.67	4.75	3.89	4.23
#4	8	μ	2.01	2.04	1.92	2.23	2.69	2.81	2.63	7.22
		σ	1.94	2.81	2.57	2.93	3.16	3.24	3.73	4.00
#5	8	μ	1.79	1.12	1.09	1.25	2.84	3.09	1.46	7.75
		σ	0.92	0.70	0.74	0.97	3.60	3.67	0.85	4.17
#6	13	μ	2.06	1.22	1.18	1.53	4.31	4.87	1.72	8.33
		σ	0.89	0.66	0.51	0.71	4.72	4.53	0.72	3.19
12Sep80#1	6	μ	1.72	0.89	1.29	1.77	1.02	1.42	1.61	6.92
		σ	1.68	0.34	0.99	1.82	0.55	0.60	1.29	3.80
#2	9	μ	3.07	2.03	2.36	3.76	3.22	3.83	2.98	6.57
		σ	2.45	1.79	3.00	4.27	4.11	4.10	2.72	4.07
#3	9	μ	2.94	2.67	2.74	3.07	3.03	3.76	3.65	7.08
		σ	1.89	2.43	2.51	2.63	3.14	3.37	3.54	3.56
#4	9	μ	2.43	2.02	1.97	2.44	1.99	3.35	2.81	6.57
		σ	1.38	1.78	1.53	1.79	1.71	1.81	2.48	2.11
#5	8	μ	1.87	1.37	1.50	1.88	1.73	2.58	1.94	5.53
		σ	0.79	0.90	0.94	1.00	2.23	1.92	1.06	3.38
#6	12	μ	2.61	1.79	[illegible]	2.45	3.08	3.79	2.44	8.53
		σ	1.40	1.49	1.84	1.74	2.95	2.74	1.72	2.88
29Sep80#1	3	μ	2.10	1.07	0.96	2.29	0.71	0.71	1.55	4.88
		σ	1.05	0.61	0.24	1.33	0.31	0.31	0.68	3.12
#2	1									
#3	5	μ	3.12	2.49	2.25	3.60	0.38	1.20	2.70	10.30
		σ	1.69	1.92	1.92	3.19	0.52	0.93	1.66	1.47
#4	4	μ	2.85	1.60	2.53	2.97	0.59	1.94	2.83	7.81
		σ	1.07	0.97	1.47	1.50	0.53	0.65	1.40	1.71
#5	4	μ	4.58	2.46	4.74	3.72	5.94	0.84	1.84	10.50
		σ	2.21	1.30	2.05	1.74	3.90	1.46	1.98	1.22
#6	4	μ	4.31	2.07	2.38	6.41	0.50	2.56	4.09	11.25
		σ	1.68	0.56	0.95	3.67	0.80	1.63	1.72	1.09

Table 8-4. Transport Thickness:
Red Tracer at SIO
(295 total samples)

Experiment	No. of Cores		Transport Thickness Estimates (cm) A	B	C	D	E	F	G	H
3Aug84#1	11	μ	1.60	1.22	1.31	1.76	2.24	2.72	1.72	3.42
		σ	0.50	0.42	0.45	0.62	1.01	0.95	0.56	1.36
#2	8	μ	2.14	1.55	1.69	2.16	2.91	3.38	2.12	4.92
		σ	0.82	0.72	0.81	1.00	2.09	1.88	0.94	2.45
10Aug84#1	9	μ	1.57	1.13	1.40	1.71	1.81	2.31	1.65	2.97
		σ	0.60	0.43	0.55	0.87	1.70	1.59	0.51	2.09
#2	4	μ	0.93	0.63	0.75	0.94	0.44	0.94	0.89	1.56
		σ	0.35	0.10	0.28	0.45	0.21	0.48	0.26	0.60
29Aug84#1	11	μ	1.26	1.00	0.97	1.35	2.48	2.68	1.52	3.44
		σ	0.78	0.79	0.74	0.84	2.47	2.50	1.27	2.89
#2	18	μ	1.39	1.07	1.18	1.49	1.44	1.90	1.49	2.40
		σ	0.72	0.57	0.74	0.84	0.43	1.14	0.80	1.09
#3	15	μ	1.38	1.02	1.13	1.44	2.28	2.42	1.44	2.73
		σ	0.68	0.46	0.66	0.79	1.32	1.29	0.65	1.32
26Sep84#1	11	μ	1.91	1.01	1.40	2.03	3.20	3.83	1.73	6.51
		σ	0.88	0.67	0.79	1.05	2.23	2.33	0.95	1.93
#2	9	μ	1.80	1.30	1.26	1.57	2.81	4.07	2.01	6.12
		σ	0.75	0.87	0.85	0.92	2.42	2.57	1.31	3.42
#3	10	μ	2.06	1.55	1.55	1.95	3.98	4.00	1.96	6.68
		σ	0.71	0.53	0.64	0.72	2.41	2.40	0.48	2.59
30Oct84#1	6	μ	2.16	0.83	1.25	2.77	3.63	5.69	1.88	8.96
		σ	1.08	0.38	1.01	2.33	2.73	2.96	0.98	1.65
#2	6	μ	2.14	0.96	1.79	2.60	4.10	4.56	2.63	8.94
		σ	0.96	0.27	1.03	1.36	1.53	1.63	2.08	2.12
#3	9	μ	1.39	0.79	0.90	1.43	3.81	4.75	1.34	9.89
		σ	0.93	0.58	0.78	1.13	2.98	3.06	1.09	1.52
#4	9	μ	2.40	1.41	1.74	2.43	3.69	4.29	2.23	7.17
		σ	1.48	1.61	1.68	1.89	3.72	3.57	2.19	2.68

Table 8-5. Transport Thickness:
Green Tracer at Torrey Pines
(260 total samples)

Experiment	No. of Cores		Transport Thickness Estimates (cm) A	B	C	D	E	F	G	H
23Jun80#1	8	μ	1.93	1.11	1.28	1.78	4.70	5.94	1.79	8.16
		σ	0.49	0.59	0.64	0.71	3.87	3.72	0.79	3.87
#2	4	μ	2.47	2.00	1.94	2.38	4.91	5.78	2.61	7.69
		σ	0.95	1.00	0.94	1.00	3.35	3.16	1.04	1.87
#3	9	μ	2.34	1.85	1.83	2.19	3.10	4.56	2.54	8.36
		σ	1.07	1.56	1.48	1.36	2.81	3.10	1.98	1.43
#4	7	μ	2.36	1.69	1.80	2.57	4.32	4.93	2.39	8.63
		σ	0.89	0.85	0.58	1.22	3.10	3.46	0.78	2.84
11Aug80#1	6	μ	1.12	0.57	0.58	0.92	0.58	1.04	0.90	4.73
		σ	0.87	0.37	0.58	0.73	0.64	1.02	0.67	4.16
#2	10	μ	2.45	2.17	2.11	2.41	2.41	2.70	3.19	7.64
		σ	2.23	2.74	3.19	3.17	3.39	3.24	4.94	4.25
#3	11	μ	2.46	1.15	1.18	2.42	2.26	4.51	2.29	8.58
		σ	2.27	1.29	2.02	3.65	3.82	5.20	3.39	3.62
#4	11	μ	1.72	1.74	1.45	1.95	1.63	2.02	2.20	6.95
		σ	1.70	2.72	2.26	2.56	2.85	2.87	3.76	4.10
#5	9	μ	1.68	1.08	0.90	1.13	1.61	3.43	1.37	9.00
		σ	1.00	0.73	0.79	0.92	2.15	4.86	0.84	4.50
#6	13	μ	1.85	1.10	1.22	1.51	3.88	5.29	1.60	7.96
		σ	0.71	0.70	0.55	0.64	4.16	4.58	0.69	3.64
12Sep80#1	7	μ	2.56	0.85	1.96	3.05	1.39	1.77	2.43	6.41
		σ	1.88	0.30	1.92	2.56	1.16	1.57	2.07	3.04
#2	9	μ	3.45	3.67	3.29	3.68	2.79	4.69	4.44	7.93
		σ	2.68	4.51	4.23	4.58	4.04	4.49	5.50	3.35
#3	10	μ	3.70	3.16	3.59	4.19	2.49	3.21	4.72	8.64
		σ	1.79	2.81	2.74	3.11	2.81	3.07	3.75	2.73
#4	10	μ	3.35	2.41	2.79	3.52	3.98	5.45	3.52	8.29
		σ	1.36	1.66	1.37	1.56	3.41	3.69	2.06	3.46
#5	9	μ	2.70	1.56	2.18	2.81	1.86	2.49	2.63	7.90
		σ	0.91	0.36	0.95	1.01	1.74	1.65	0.77	3.14
#6	12	μ	3.34	2.72	3.22	3.78	3.57	4.32	3.9^	[illegible]5
		σ	1.78	2.56	2.56	2.66	3.19	2.89	3.10	2.87
29Sep80#1	3	μ	3.16	1.53	1.29	1.54	0.58	0.58	1.99	9.58
		σ	0.54	0.37	0.62	0.96	0.46	0.46	0.75	2.83
#2	2	μ	2.11	1.29	0.88	1.13	1.00	1.13	1.86	7.56
		σ	0.11	0.47	0.50	0.50	0.38	0.50	0.45	3.94
#3	4	μ	4.15	1.96	2.69	5.41	0.09	0.09	4.45	11.25
		σ	2.07	1.17	1.90	3.67	0.16	0.16	2.67	0.83
#4	5	μ	4.00	2.69	3.27	4.63	0.45	0.98	4.16	10.50
		σ	1.90	1.68	1.90	3.03	0.84	0.77	1.98	2.10
#5	6	μ	4.16	2.51	2.73	4.56	1.02	2.44	3.98	10.00
		σ	1.13	1.08	0.96	2.46	1.35	1.94	1.08	2.06
#6	5	μ	3.99	1.61	2.23	4.02	0.07	1.07	3.55	10.30
		σ	1.07	0.52	1.14	2.20	0.15	0.86	1.89	1.47

Table 8-6. Transport Thickness:
Green Tracer at SIO
(260 total samples)

Experiment	No. of Cores		Transport Thickness Estimates (cm) A	B	C	D	E	F	G	H
3Aug84#1	4	μ	1.48	1.07	1.13	1.56	2.03	2.44	1.57	3.75
		σ	0.66	0.48	0.53	0.69	1.62	1.32	0.73	1.78
#2	6	μ	1.46	1.18	1.17	1.46	2.13	2.58	1.44	3.69
		σ	0.89	0.78	0.91	1.00	1.36	1.73	0.91	2.50
10Aug84#1	2	μ	0.85	0.66	0.63	1.00	0.88	1.00	0.84	1.63
		σ	0.21	0.04	0.00	0.38	0.50	0.63	0.16	1.00
#2	0									
29Aug84#1	5	μ	1.22	0.95	0.93	1.27	1.48	1.90	1.50	2.80
		σ	0.83	0.87	0.73	0.73	1.33	2.00	1.59	2.88
#2	7	μ	1.13	0.90	0.94	1.19	1.09	1.44	1.17	1.95
		σ	0.82	0.73	0.93	0.97	0.80	1.11	0.98	1.28
#3	9	μ	1.43	0.85	1.29	1.63	2.00	2.11	1.53	2.17
		σ	0.92	0.47	0.95	1.18	1.39	1.36	0.93	1.35
26Sep84#1	8	μ	1.89	1.07	1.50	2.22	2.42	3.48	1.74	5.67
		σ	0.76	0.62	0.72	0.91	2.60	2.72	0.84	2.34
#2	9	μ	1.90	1.48	1.38	1.85	2.75	3.10	1.94	6.32
		σ	0.98	0.94	0.99	1.02	2.34	2.49	1.16	3.47
#3	7	μ	1.83	1.28	1.34	1.88	3.43	3.89	1.80	8.11
		σ	0.53	0.28	0.45	0.69	2.59	2.39	0.43	2.15
30Oct84#1	6	μ	1.20	0.69	0.63	0.88	2.60	3.06	1.02	7.67
		σ	0.53	0.29	0.38	0.61	1.85	2.00	0.42	2.50
#2	4	μ	1.27	0.71	0.88	1.50	3.94	4.75	1.18	6.66
		σ	0.49	0.27	0.53	0.57	2.39	2.95	0.49	3.49
#3	7	μ	1.64	0.98	1.30	1.59	5.43	5.79	1.69	7.13
		σ	0.86	0.49	0.87	1.03	2.51	2.95	0.93	3.17
#4	6	μ	1.55	0.72	1.29	1.79	4.15	4.77	1.47	7.48
		σ	0.65	0.27	0.81	1.12	2.34	2.45	0.67	2.94

APPENDIX 3: Measured Fluid Velocity

In Table 8-7 the seven fluid velocity moments used in this study are listed for the 30 experiments, along with dimensionfull transport, i, and dimensionless transport, Φ. For the 10 August 1984, 29 August 1984, and 26 September 1984 experiments the moments listed are averages for the two current meters.

In Table 8-8 the other six moments are correlated with the first moment to illustrate how well correlated the moments are with each other. Nevertheless, non-overlap of the 90% confidence intervals shows that the first through sixth moments are statistically distinct from each other.

Table 8-7. Fluid-velocity moments and transport
(Fluid velocities are in units of $[cm/s]^n$.)
(Dimensional transport, i, is in units [dynes/(cm-s)].)

Experiment	Transport i	Fluid-velocity moment $\langle u^n \rangle$ (Eq. 4.4)						
	#	n = 0.5	1	2	3 x10³	4 x10⁵	5 x10⁷	6 x10⁹
23 Jun 80								
#1	76.8	0.312	0.325	2.75	208.	16.0	12.6	10.1 8.28
#2	77.7	0.315	0.162	1.35	116.	9.45	7.64	6.19 5.08
#3	91.9	0.373	-0.0832	0.73	70.1	6.11	5.18	4.39 3.77
#4	44.8	0.182	0.227	1.07	84.4	6.66	5.29	4.28 3.53
11 Aug 80								
#1	66.4	0.096	-0.0066	0.096	3.70	.141	.052	.019 .0066
#2	23.8	0.119	-0.0033	0.125	5.28	.222	.093	.039 .0162
#3	4.2	0.021	0.176	0.149	7.21	.344	.165	.079 .0388
#4	4.9	0.024	0.110	0.147	7.17	.345	.166	.080 .0391
#5	6.0	0.030	-0.124	0.130	6.41	.309	.148	.071 .0343
#6	7.0	0.035	0.0123	0.106	5.26	.254	.121	.058 .0280
12 Sep 80								
#1	104.5	0.683	-0.000	0.221	10.0	.457	.209	.096 .0443
#2	85.6	0.559	0.0240	0.092	4.05	.178	.079	.035 .0158
#3	87.9	0.574	-0.000	0.125	5.23	.221	.095	.041 .0179
#4	9.6	0.063	-0.000	0.081	3.39	.144	.062	.027 .0118
#5	23.0	0.150	0.035	0.083	3.41	.143	.061	.026 .0114
#6	14.6	0.095	-0.000	0.120	5.02	.214	.093	.041 .0182
3 Aug 84								
#1	-26.2	-0.178	-0.725	-7.43	-420.	-26.5	-18.7	-14.7 -12.7
#2	-20.2	-0.138	-0.874	-7.10	-386.	-23.3	-15.7	-11.7 -9.67
10 Aug 84								
#1	146.3	0.824	0.948	7.33	421.	24.9	15.7	10.7 7.80
#2	21.5	0.121	0.418	6.11	357.	21.4	13.8	9.61 7.28
29 Aug 84								
#1	-39.2	-0.213	-0.788	-6.53	-234.	-8.92	-3.64	-1.58 -.725
#2	-20.9	-0.113	-1.25	-6.55	-233.	-8.83	-3.56	-1.52 -.683
#3	-14.3	-0.078	-0.482	-6.39	-231.	-8.87	-3.60	-1.53 -.675
26 Sep 84								
#1	64.0	0.415	0.869	4.14	161.	6.67	3.05	1.49 .775
#2	23.7	0.154	0.058	3.79	153.	6.66	3.14	1.60 .876
#3	21.5	0.139	0.583	3.72	158.	7.28	3.67	2.00 1.18
30 Oct 84								
#1	20.4	0.159	0.107	0.418	19.4	.987	.536	.307 .184
#2	3.8	0.030	0.274	0.775	31.1	1.37	.654	.336 .183
#3	15.9	0.124	0.488	0.650	26.5	1.16	.546	.276 .148
#4	24.8	0.193	0.338	0.597	25.2	1.14	.550	.282 .153

Table 8-8. Velocity Moment Correlations with <u>

(All correlations at 99.999999% significance level. Velocity moments are given by Eq. 4.4. Means, standard deviations, and intercepts are in units of [cm/s]^n.)

Velocity Moment	Mean	Standard Deviation	Slope m	Intercept b	Corr. Coef. r	Confidence Interval on Correlation 90%	80%	70%
$\langle u^{0.5} \rangle$	-5.93 $\times 10^{-4}$	4.68 $\times 10^{-1}$	6.17	-0.0338	0.811	.795 -.826	.800 -.821	.805 -.817
$\langle u \rangle$	3.02 $\times 10^{-2}$	3.56						
$\langle u^2 \rangle$	1.31 $\times 10^{1}$	1.76 $\times 10^{2}$	1.97 $\times 10^{-2}$	-0.228	0.974	.972 -.976	.972 -.976	.973 -.975
$\langle u^3 \rangle$	1.21 $\times 10^{3}$	1.02 $\times 10^{4}$	3.23 $\times 10^{-4}$	-0.362	0.925	.918 -.931	.921 -.929	.922 -.928
$\langle u^4 \rangle$	9.50 $\times 10^{4}$	6.71 $\times 10^{5}$	4.54 $\times 10^{-6}$	-0.401	0.856	.843 -.868	.848 -.864	.851 -.861
$\langle u^5 \rangle$	7.05 $\times 10^{6}$	4.96 $\times 10^{7}$	5.73 $\times 10^{-8}$	-0.373	0.798	.781 -.814	.787 -.809	.791 -.804
$\langle u^6 \rangle$	5.02 $\times 10^{8}$	4.03 $\times 10^{9}$	6.69 $\times 10^{-10}$	-0.306	0.757	.737 -.776	.744 -.769	.749 -.765

APPENDIX 4: Energy Spectra

Energy spectra are illustrated for the eight experiment days. Crossshore currents, longshore currents, and sea-surface elevation are listed separately. "C" indicates a current meter, "P" a pressure sensor, and "W" a wavestaff. Current meters measure current in cm/s, and their spectra are in units of $(cm/s)^2/Hz$. Pressure sensor measurements are converted to surface-corrected wave heights and then used to compute spectra with power densities of cm^2/Hz. Wavestaffs measure the mean surface elevation, and their spectra also have units of cm^2/Hz. Wave heights derived from wavestaffs and surface-corrected pressure are comparable.

The same scales and lower/upper limits for both abscissa and ordinate were kept for all spectra, for ease of comparison.

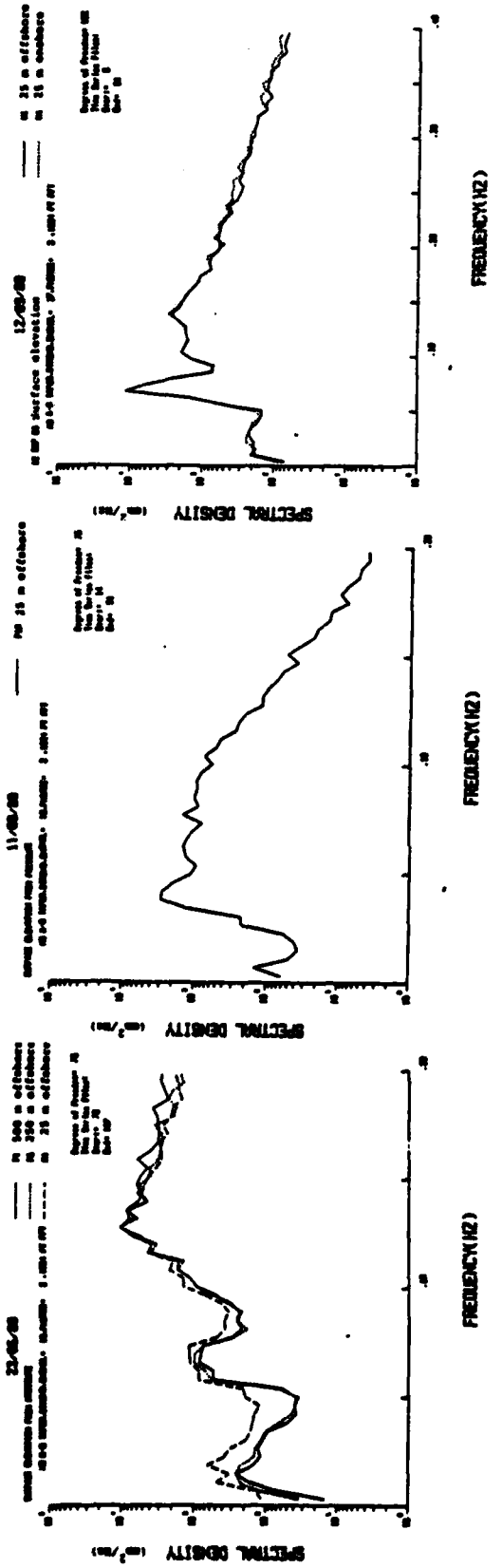

Figure 8-10. Surface-corrected wave energy spectra at Torrey Pines (1980).

Sensor locations are listed on each figure relative to the experiment site.

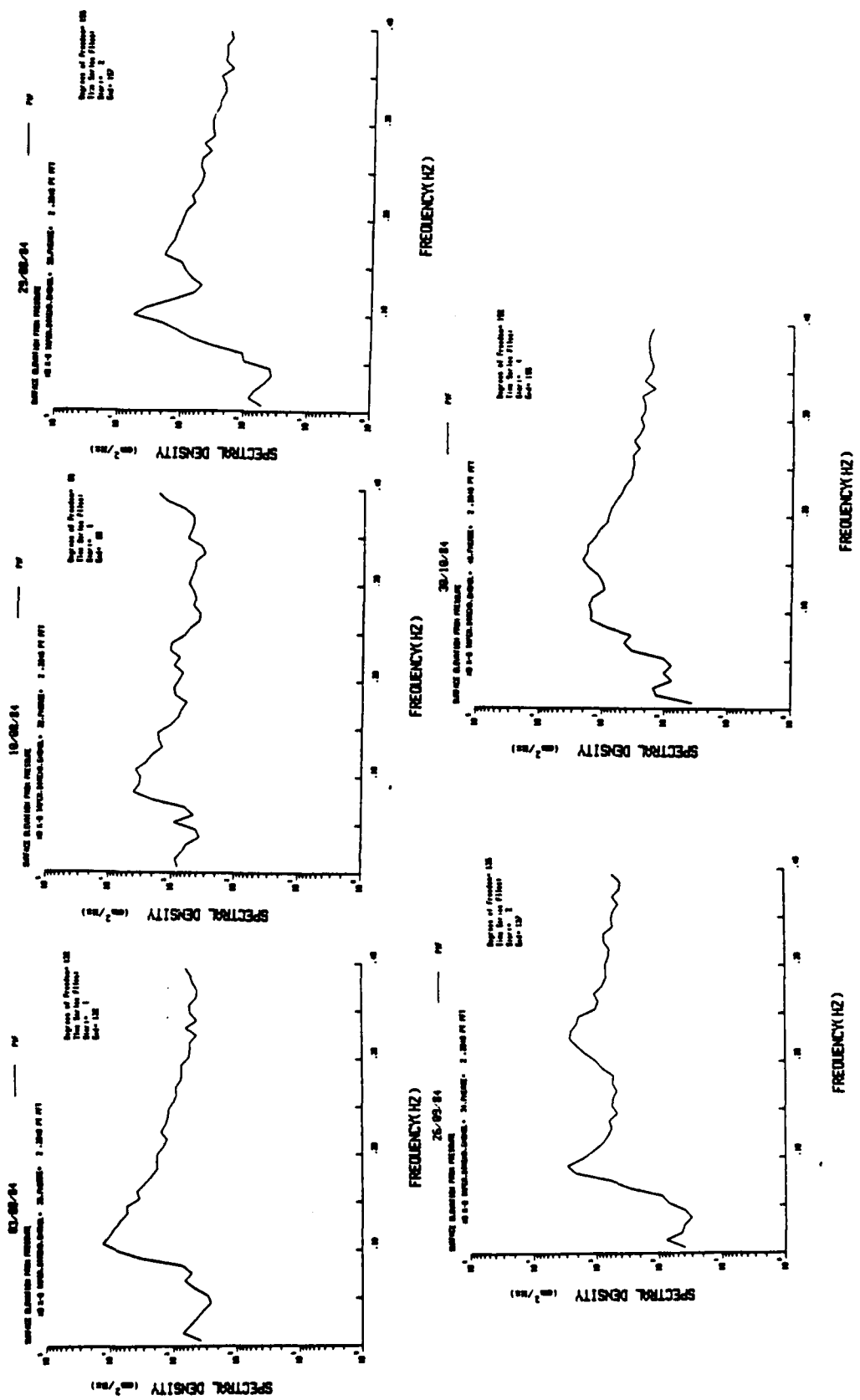

Figure 8-11. Surface-corrected wave energy spectra at SIO (1984). The pressure sensor was at the experiment site in all cases.

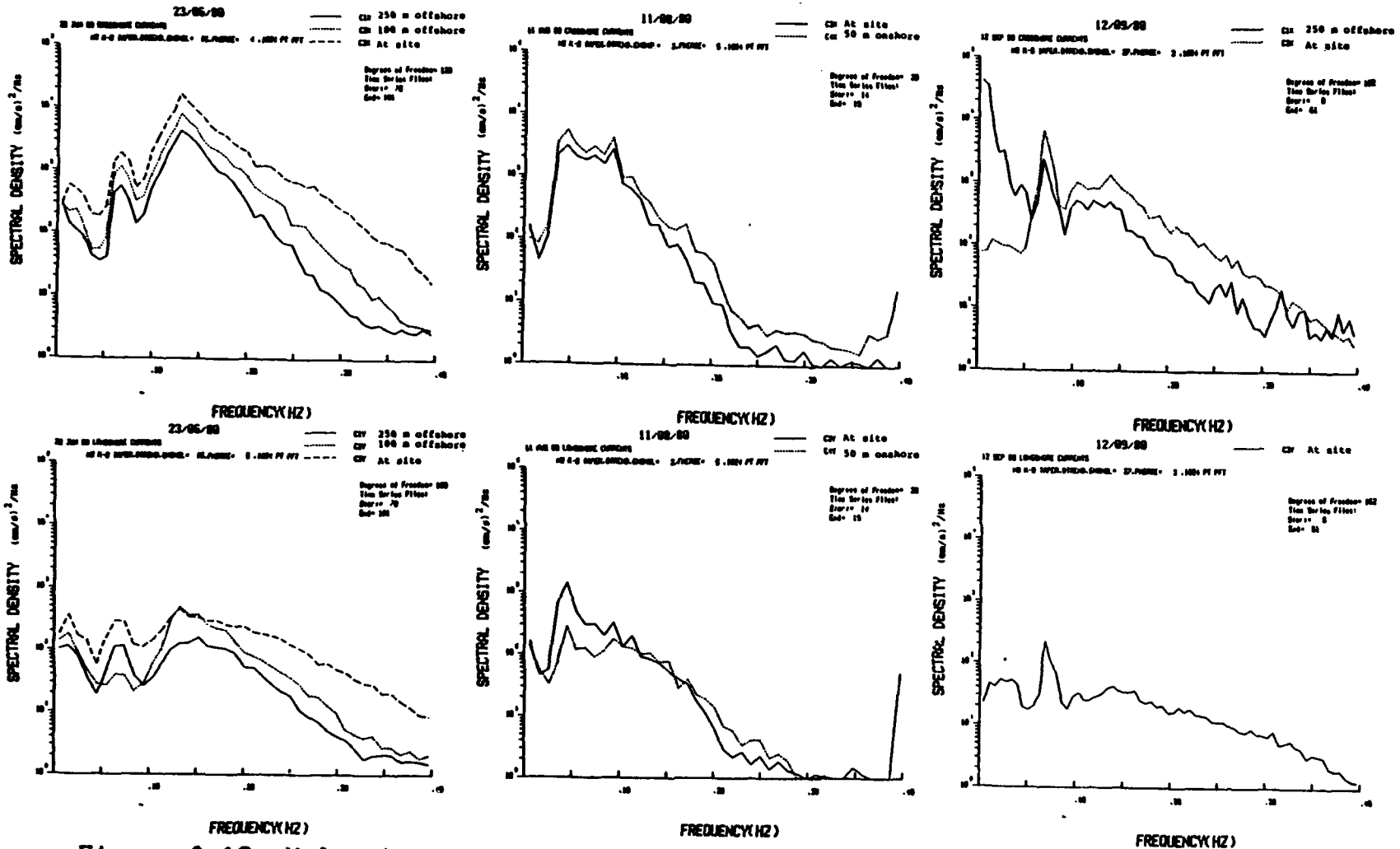

Figure 8-12. Velocity spectra at Torrey Pines (1980). Sensor locations are listed relative to the experiment site. Upper figures are crosshore currents, lower figures longshore currents.

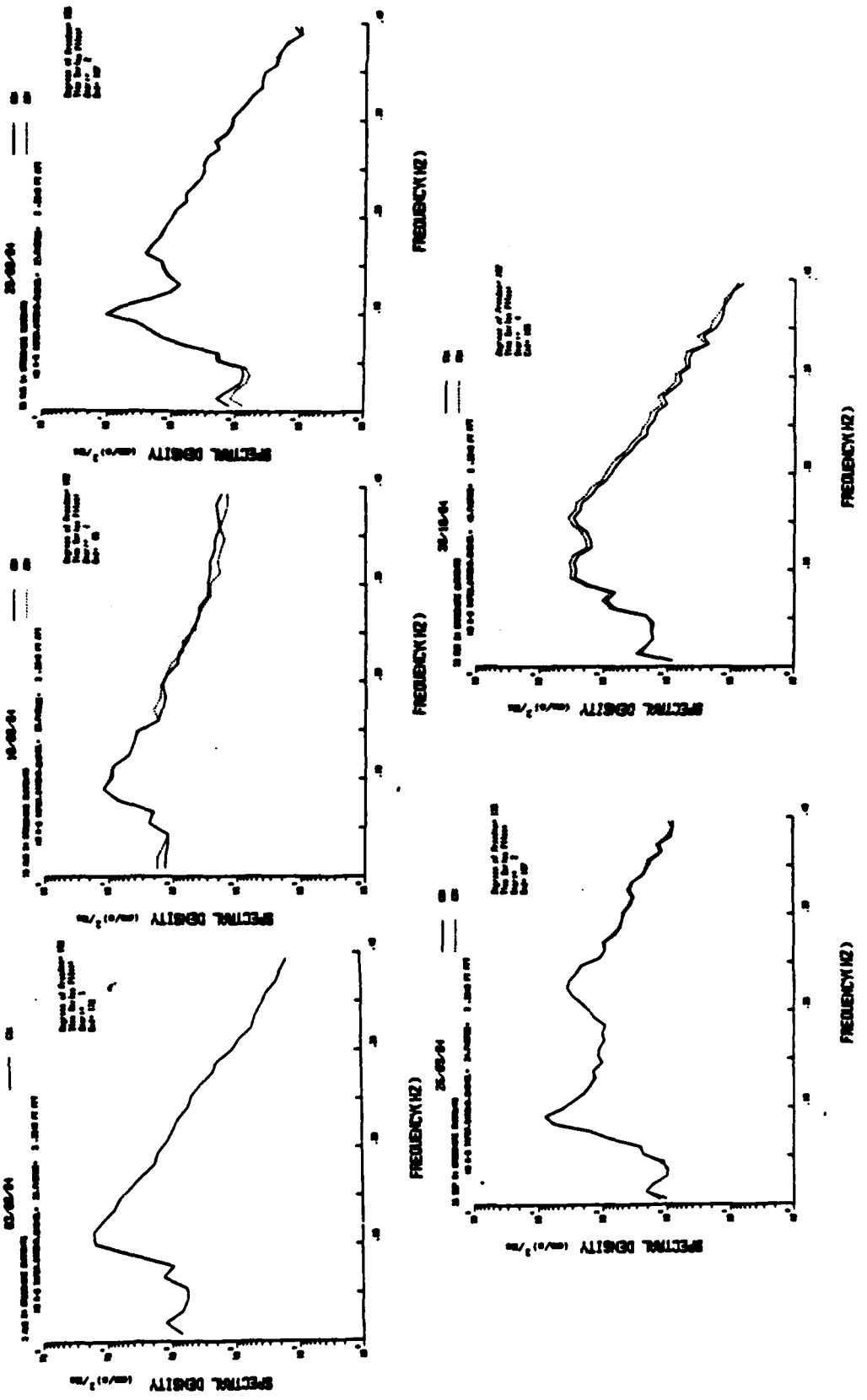

Figure 8-13. Crosshore velocity spectra at SIO (1984). All sensors were at the experiment site.

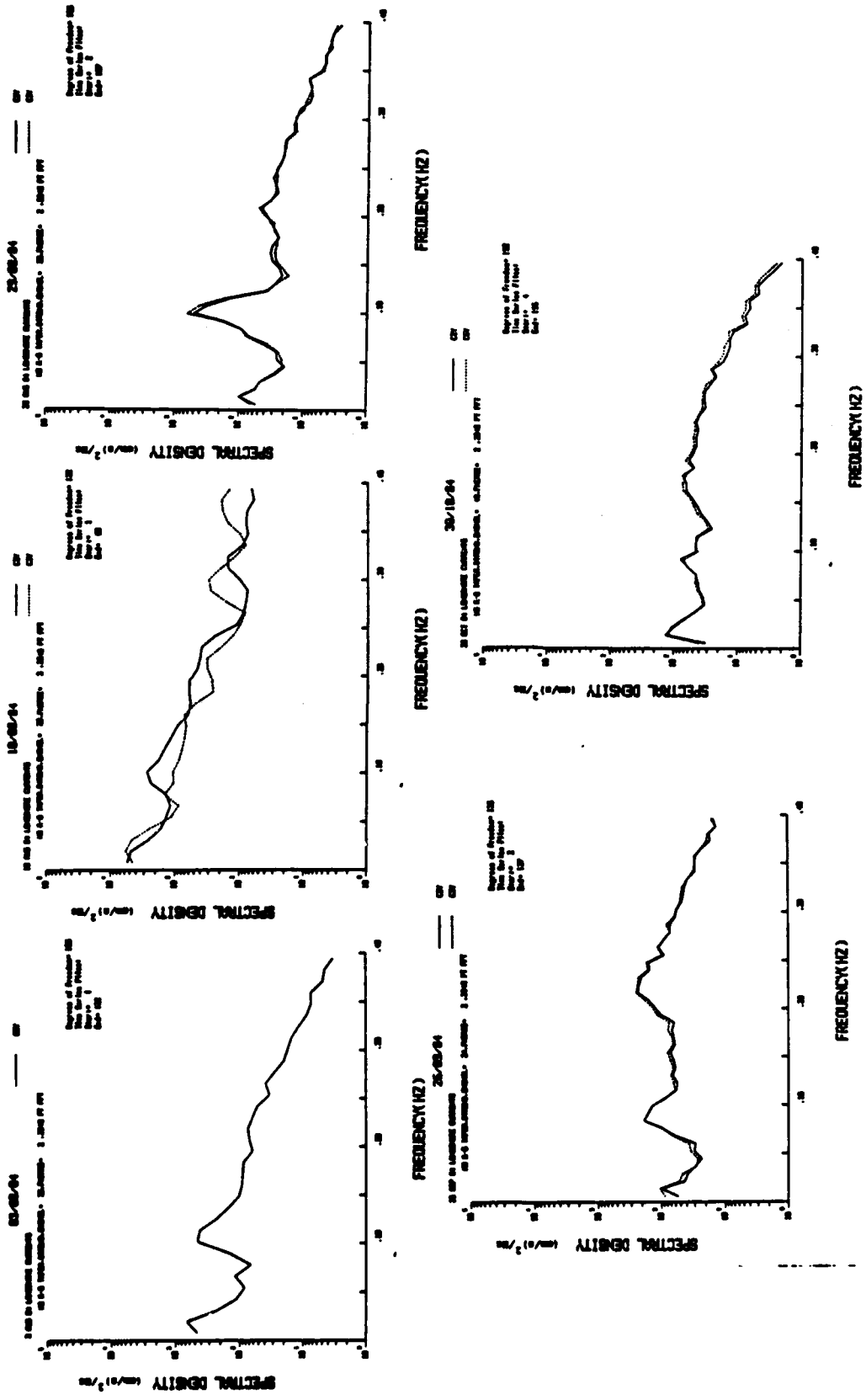

Figure 8-14. Longshore velocity spectra at SIO (1984). All sensors were at the experiment site.

APPENDIX 5: Correlations with Transport Thickness

Table 8-9. Correlation of Transport Thickness with Parameters from Surface-Corrected Wave Heights (d_o and u_m are from Table 4-1.)

Means and standard deviations are in units of cm for H_{sig} and $D(\theta-\theta_t)$ and cm/s for u_m. Intercepts are in cm.

Correlation with:	H_{sig}	$D(\theta-\theta_t)$	$\langle u_m \rangle^{0.5}$	$\langle u_m \rangle$	$\langle u_m \rangle^2$
Part A: Red Tracer (295 samples) (For Z_o, mean = 2.21 cm and st.dev. = 0.75 cm)					
Mean	71.5	.00378	6.24	39.8	1692
Standard Deviation	17.5	.00258	0.851	10.6	845
Slope, m	0.00159	3.553	0.240	0.0183	0.000219
Intercept, b	2.10	2.20	0.72	1.49	1.85
Correlation Coef.	0.037	0.012	0.272	0.259	0.247
90% Confidence Limits:					
(lower)	0.000	-0.035	0.235	0.222	0.210
(upper)	0.074	0.059	0.309	0.296	0.284
80% Confidence Limits:					
(lower)	0.013	-0.019	0.248	0.235	0.223
(upper)	0.061	0.043	0.296	0.283	0.271
70% Confidence Limits:					
(lower)	0.022	-0.007	0.257	0.244	0.232
(upper)	0.052	0.031	0.287	0.274	0.262
% Significance	16.8	4.8	89.0	87.2	85.2
Part B: Green Tracer (260 samples) (For Z_o, mean = 2.28 cm and st.dev. = 0.96 cm)					
Mean	71.5	0.00378	6.24	39.8	1692
Standard Deviation	17.5	0.00258	0.851	10.6	845
Slope, m	0.00702	30.27	0.502	0.0386	0.000435
Intercept, b	1.78	2.17	-0.84	0.76	1.56
Correlation Coef.	0.128	0.081	0.445	0.426	0.383
90% Confidence Limits:					
(lower)	0.091	0.034	0.408	0.389	0.347
(upper)	0.165	0.128	0.482	0.463	0.420
80% Confidence Limits:					
(lower)	0.104	0.050	0.421	0.402	0.359
(upper)	0.152	0.112	0.469	0.450	0.407
70% Confidence Limits:					
(lower)	0.113	0.062	0.430	0.411	0.368
(upper)	0.143	0.100	0.460	0.441	0.398
% Significance	54.0	32.2	99.4	99.0	98.0
Mean correlation coefficient for the two colors:	0.083	0.047	0.359	0.343	0.315

Table 8-10. Correlation of Transport Thickness with Maximum Orbital Velocity from Current Measurements (u_m is from Table 4-2.)
Means and standard deviations are in units of cm/s.
Intercepts are in cm.

Correlation with:	$\langle u_m \rangle^{0.5}$	$\langle u_m \rangle$	$\langle u_m \rangle^2$
Part A: Red Tracer (295 samples) (For Z_o, mean = 2.02 cm and st.dev. = 0.49 cm)			
Mean	6.46	42.9	2039
Standard Deviation	1.064	14.12	1308
Slope, m	-0.164	-0.0117	-0.000111
Intercept, b	3.08	2.52	2.24
Correlation Coef.	-0.356	-0.307	-0.296
90% Confidence Limits:			
(lower)	-0.403	-0.384	-0.343
(upper)	-0.309	-0.290	-0.249
80% Confidence Limits:			
(lower)	-0.387	-0.368	-0.327
(upper)	-0.325	-0.306	-0.265
70% Confidence Limits:			
(lower)	-0.375	-0.356	-0.315
(upper)	-0.337	-0.318	-0.277
% Significance	94.2	92.6	88.0
Part B: Green Tracer (260 samples) (For Z_o, mean = 2.01 cm and st.dev. = 0.75 cm)			
Mean	6.46	42.9	2039
Standard Deviation	1.064	14.12	1308
Slope, m	-0.344	-0.0241	-0.000223
Intercept, b	4.22	3.03	2.45
Correlation Coef.	-0.488	-0.454	-0.389
90% Confidence Limits:			
(lower)	-0.535	-0.501	-0.436
(upper)	-0.441	-0.407	-0.342
80% Confidence Limits:			
(lower)	-0.519	-0.485	-0.420
(upper)	-0.457	-0.423	-0.358
70% Confidence Limits:			
(lower)	-0.507	-0.473	-0.408
(upper)	-0.469	-0.435	-0.370
% Significance	99.3	98.8	96.3
Mean correlation coefficient for the two colors:	-0.422	-0.396	-0.343

Table 8-11. Correlation of Transport Thickness with Orbital Diameter and Total Velocity (from current-meter measurements, Table 4-2)

Means and standard deviations are in units of cm for d_o and cm/s for u_T. Intercepts are in cm.

Corr. with:	$\langle d_o \rangle^{0.5}$	$\langle d_o \rangle$	$\langle d_o \rangle^2$	$\langle u_T \rangle^{0.5}$	$\langle u_T \rangle$	$\langle u_T \rangle^2$
Part A: Red Tracer (295 samples) (For Z_o, mean = 2.02 cm and st.dev. = 0.49 cm)						
Mean	12.4	158	27065	4.20	18.4	369
Standard Dev	1.93	47.5	15261	.638	5.62	222
Slope, m	-.0518	-.00206	-5.83×10^{-6}	-.306	-.0301	-.000696
Intercept, b	2.66	2.34	2.17	3.30	2.57	2.27
Cor. Coef.	-0.204	-0.200	-0.182	-0.398	-0.345	-0.315
90% Confidence Limits:						
(lower)	-0.249	-0.245	-0.227	-0.445	-0.392	-0.362
(upper)	-0.159	-0.155	-0.137	-0.351	-0.298	-0.268
80% Confidence Limits:						
(lower)	-0.234	-0.230	-0.212	-0.429	-0.376	-0.346
(upper)	-0.174	-0.170	-0.152	-0.367	-0.314	-0.284
70% Confidence Limits:						
(lower)	-0.222	-0.218	-0.200	-0.417	-0.364	-0.334
(upper)	-0.186	-0.182	-0.164	-0.379	-0.326	-0.296
% Sig.	71.6	70.8	66.0	96.8	93.4	90.4
Part B: Green Tracer (260 samples) (For Z_o, mean = 2.01 cm and st.dev. = 0.75 cm)						
Mean	12.4	158	27065	4.20	18.4	369
Standard Dev	1.93	47.5	15261	.638	5.62	222
Slope, m	-.0877	-.00388	-.0000132	-.323	-.0610	-.00137
Intercept, b	3.09	2.62	2.36	3.32	3.11	2.50
Cor. Coef.	-0.226	-0.246	-0.269	-0.275	-0.457	-0.406
90% Confidence Limits:						
(lower)	-0.271	-0.291	-0.314	-0.322	-0.50[illegible]	-0.453
(upper)	-0.181	-0.201	-0.224	-0.228	-0.410	-0.359
80% Confidence Limits:						
(lower)	-0.256	-0.276	-0.299	-0.306	-0.488	-0.437
(upper)	-0.196	-0.216	-0.239	-0.244	-0.426	-0.375
70% Confidence Limits:						
(lower)	-0.244	-0.264	-0.287	-0.294	-0.476	-0.425
(upper)	-0.208	-0.228	-0.251	-0.256	-0.438	-0.387
% Sig.	76.6	80.8	84.8	85.0	98.8	97.2
Mean correlation coefficient for the two colors:	-0.215	-0.223	-0.226	-0.337	-0.401	-0.361

APPENDIX 6: Measured Transport

Table 8-12. Crosshore Transport

Experiment	Sample Time (min.)	--green tracer-- U (cm/s)	Z_o (cm)	i (dynes/(cm-s))	--red tracer-- U (cm/s)	Z_o (cm)	i	Transport Mean <i> (dynes/(cm-s))	Dif. Δi
23Jun80#1	18.1	.0443	1.93	81.4	.0425	1.78	72.1	76.8	9.3
#2	39.8	.0321	2.47	75.5	.0335	2.50	79.8	77.7	-4.3
#3	62.0	.0380	2.34	84.7	.0397	2.62	99.1	91.9	-14.4
#4	131.1	.0194	2.36	43.6	.0211	2.29	46.0	44.8	-2.4
11Aug80#1	18.6	.0838	1.12	89.4	.0229	1.99	43.4	66.4	46.0
#2	46.0	.0256	2.45	59.7	-.0059	2.17	-12.2	23.8	71.9
#3	72.8	.0167	2.46	39.1	-.0129	2.51	-30.8	4.2	69.9
#4	105.4	.0041	1.72	6.7	.0016	2.01	3.1	4.9	3.6
#5	133.0	.0079	1.68	12.6	-.0004	1.79	-0.6	6.0	13.2
#6	160.2	.0096	1.85	16.9	-.0015	2.06	-2.9	7.0	19.8
12Sep80#1	25.1	.0771	2.56	188.0	.0128	1.72	21.0	104.5	167.0
#2	55.5	.0335	3.45	110.1	.0209	3.07	61.1	85.6	49.0
#3	87.0	.0386	3.70	136.0	.0142	2.94	39.8	87.9	96.2
#4	131.7	.0093	3.35	29.7	-.0046	2.43	-10.6	9.6	40.3
#5	180.7	.0112	2.70	28.8	.0096	1.87	17.1	23.0	11.7
#6	227.1	.0038	3.34	12.1	.0068	2.62	17.0	14.6	-4.9
29Sep80#1	19.5	.0950	3.16	286.0	-.0293	2.10	-58.6	113.7	344.6
#2	36.6	-.0489	2.11	-98.3	-.0883	3.00	-252.3	-175.3	154.0
#3	67.8	.0171	4.15	67.6	-.0088	3.12	-26.2	20.7	93.8
#4	110.0	.0112	4.00	42.7	-.0094	2.85	-25.5	8.6	68.2
#5	137.2	.0254	4.16	100.7	.0088	4.74	39.7	70.2	61.0
#6	168.4	.0106	3.99	40.3	-.0074	4.31	-30.4	5.0	70.7
3Aug84#1	66.3	-.0134	1.48	-18.9	-.0220	1.60	-33.5	-26.2	14.6
#2	141.3	-.0076	1.46	-10.6	-.0146	2.14	-29.8	-20.2	19.2
10Aug84#1	55.3	.0815	0.85	66.0	.1515	1.57	226.6	146.3	-160.6
#2	120.0	.0069		5.6	.0421	0.93	37.3	21.5	-31.7
29Aug84#1	50.9	-.0233	1.22	-27.1	-.0427	1.26	-51.2	-29.3	24.1
#2	105.5	-.0137	1.13	[illegible]	.0205	1.39	-27.1	-20.9	12.4
#3	167.3	-.0125	1.43	-17.0	-.0088	1.38	-11.6	-14.3	-5.4
26Sep84#1	50.9	.0104	1.89	18.7	.0572	1.91	109.3	64.0	-90.6
#2	100.6	-.0034	1.90	-6.2	.0312	1.80	53.5	23.7	-59.7
#3	145.2	.0152	1.83	26.5	.0084	2.06	16.5	21.5	10.0
30Oct84#1	82.3	.0104	1.20	11.9	.0140	2.16	28.8	20.4	-16.9
#2	135.5	.0088	1.27	10.6	-.0015	2.14	-3.1	3.8	13.7
#3	176.4	.0119	1.64	18.6	.0100	1.39	13.2	15.9	5.4
#4	206.8	.0061	1.55	9.0	.0177	2.40	40.5	24.8	-31.5

Table 8-13. Longshore Transport

Experiment	Sample Time (min.)	green tracer U (cm/s)	green tracer Z_o (cm)	green tracer i (dynes/cm-s)	red tracer U (cm/s)	red tracer Z_o (cm)	red tracer i (dynes/cm-s)	Transport Mean <i> (dynes/cm-s)	Transport Dif. Δi
23Jun80#1	18.1	-.0187	1.93	-34.4	-.0196	1.78	-33.2	-33.8	-1.2
#2	39.8		2.47			2.50			
#3	62.0	-.0036	2.34	-8.0	-.0039	2.62	-9.7	-8.9	1.7
#4	131.1	-.0027	2.36	-6.1	-.0022	2.29	-4.8	-9.5	-1.3
11Aug80#1	18.6	-.1172	1.12	-125.0	-.0945	1.99	-179.1	-152.1	54.1
#2	46.0	-.00009	2.45	-0.2	-.0010	2.17	-2.1	-1.1	1.9
#3	72.8	-.00003	2.46	-0.06	.00001	2.51	0.03	-0.05	-0.1
#4	105.4	-.0040	1.72	-6.6	-.0040	2.01	-7.7	-7.1	1.1
#5	133.0	-.0003	1.68	-0.4	-.00001	1.79	-0.02	-0.2	-0.4
#6	160.2	-.00003	1.85	-0.04	.000001	2.06	0.00	-0.02	-0.04
12Sep80#1	25.1	-.0194	2.56	-47.3	-.0014	1.72	-2.3	-24.8	-45.0
#2	55.5	-.0003	3.45	-1.1	-.0005	3.07	-1.6	-1.3	0.4
#3	87.0	.00009	3.70	-0.3	-.00001	2.94	-0.04	-0.18	-0.3
#4	131.7	.0002	3.35	-0.6	-.00002	2.43	-0.05	-0.33	-0.6
#5	180.7	-.00008	2.70	-0.2	-.00007	1.87	-0.12	-0.17	-0.1
#6	227.1	-.00006	3.34	-0.2	-.00009	2.62	-0.22	-0.21	0.0
29Sep80#1	19.5	.0533	3.16	160.4	.0692	2.10	138.4	149.4	22.0
#2	36.6	.00006	2.11	0.1	.0063	3.00	18.0	9.1	-17.9
#3	67.8	.0018	4.15	7.1	.0075	3.12	22.3	14.7	-15.2
#4	110.0	.0225	4.00	85.7	.0204	2.85	5.4	70.6	80.4
#5	137.2	.0180	4.16	71.3	.0187	4.74	84.4	77.9	-13.1
#6	168.4	.0150	3.99	57.0	.0034	4.31	14.0	35.5	43.1
3Aug84#1	66.3	.00002	1.48	0.03	-.0006	1.60	-0.9	-0.5	1.0
#2	141.3	-.00007	1.46	-0.09	-.0002	2.14	-0.5	-0.3	0.4
10Aug84#1	55.3	.0004	0.85	0.31	.0051	1.57	7.6	4.0	-7.3
#2	120.0	.0139		11.3	.0165	0.93	14.6	12.9	-3.4
29Aug84#1	50.9	.0009	1.22	1.1	-.0064	1.26	-7.7	-3.3	8.8
#2	105.5	.0004	1.13	0.4	-.00032	1.39	-0.4	-0.02	0.8
#3	167.3	.0040	1.43	5.4	.0046	1.38	6.1	5.7	-0.7
26Sep84#1	50.9	.00008	1.89	0.15	.00045	1.91	0.8	0.5	-0.7
#2	100.6	-.0000051	1.90	-0.01	-.00003	1.80	-0.05	-0.03	0.04
#3	145.2	.0003	1.83	0.59	.00016	2.06	0.31	0.45	0.28
30Oct84#1	82.3		1.20			2.16			
#2	135.5		1.27			2.14			
#3	176.4		1.64			1.39			
#4	206.8		1.55			2.40			

APPENDIX 7: Computed Transport

Transport computed from each of the bedload models is listed for each of the 30 tracer experiments for which current meter data were available. Transport is dimensional in units of dynes/(cm-s). Transport for the 10 August 1984, 29 August 1984, and 26 September 1984 experiments is the average for the two current meters.

Table 8-14. Crosshore Transport Predicted by the u^3 Models

(Positive transport is onshore.)

Experiment		Transport [dynes/(cm-s)]						
		Bailard & Inman		Bagnold		Meyer-Peter & Mueller	Yalin	Kobayashi
			with u_t		with u_t			
23Jun80	#1	29.20	29.95	36.25	35.92	53.15	220.91	9.34
	#2	14.07	16.43	23.40	24.78	33.22	137.90	2.24
	#3	7.61	10.00	13.51	15.19	22.47	93.05	0.41
	#4	10.47	12.17	13.93	15.12	22.71	94.40	1.55
11Aug80	#1	0.23	0.15	9.13	5.09	-0.01	-0.02	-0.01
	#2	0.44	0.34	2.67	0.98	0.11	0.41	0.01
	#3	0.67	0.60	2.08	0.78	0.39	1.44	0.05
	#4	0.83	0.58	2.11	0.76	0.41	1.52	0.05
	#5	0.65	0.49	1.95	0.68	0.35	1.32	0.04
	#6	0.48	0.35	1.86	0.55	0.28	1.04	0.04
12Sep80	#1	0.27	0.97	0.66	1.08	0.67	2.48	0.03
	#2	-0.64	0.35	-0.17	0.50	0.23	0.84	-0.02
	#3	-0.48	0.45	-0.04	0.55	0.24	0.89	-0.01
	#4	-0.41	0.28	0.02	0.36	0.16	0.60	-0.01
	#5	-0.62	0.28	-0.16	0.35	0.15	0.55	-0.01
	#6	-0.55	0.43	-0.11	0.51	0.25	0.90	-0.02
3Aug84	#1	-76.31	-75.01	-72.91	-71.93	-89.73	-428.49	-22.51
	#2	-67.35	-65.79	-65.07	-63.79	-76.28	-364.72	-19.21
10Aug84	#1	59.31	56.34	66.96	63.55	79.89	447.14	11.59
	#2	51.31	49.28	57.73	54.88	69.76	390.41	10.25
29Aug84	#1	-27.32	-25.06	-24.79	-23.17	-19.80	-143.12	-4.66
	#2	-27.01	-24.61	-24.77	-22.92	-19.25	-139.12	-5.17
	#3	-26.82	-24.64	-24.61	-22.94	-19.83	-143.31	-5.56
26Sep84	#1	18.29	17.20	19.65	18.38	15.78	90.69	2.11
	#2	17.37	16.63	19.02	18.08	16.53	94.83	2.12
	#3	18.32	17.85	20.40	19.70	19.61	112.22	2.67
30Oct84	#1	1.09	1.36	2.73	2.81	3.65	30.94	0.32
	#2	2.14	2.37	3.89	3.92	4.61	38.96	0.45
	#3	1.47	1.71	3.28	3.33	3.90	32.97	0.03

Table 8-15. Crosshore Transport Predicted by the u^4 and u^5 Models

(Positive transport is onshore.)

Experiment		Transport [dynes/(cm-s)]				
		Sleath with u_t	Hallermeier	with u_t	Hanes & Bowen	with u_t
23Jun80	#1	1.24	1.40	1.39	39.10	39.00
	#2	0.78	0.97	0.99	27.89	28.08
	#3	0.55	0.61	0.64	18.61	18.86
	#4	0.53	0.58	0.60	16.87	17.04
11Aug80	#1	-0.000	0.12	0.08	2.27	1.60
	#2	0.001	0.029	0.014	0.61	0.33
	#3	0.003	0.022	0.012	0.56	0.37
	#4	0.003	0.022	0.011	0.56	0.37
	#5	0.003	0.020	0.010	0.52	0.32
	#6	0.002	0.019	0.008	0.47	0.26
12Sep80	#1	0.006	0.013	0.015	0.48	0.51
	#2	0.002	0.003	0.007	0.16	0.22
	#3	0.002	0.004	0.007	0.17	0.23
	#4	0.001	0.003	0.005	0.13	0.15
	#5	0.001	0.002	0.005	0.11	0.14
	#6	0.002	0.003	0.007	0.17	0.22
3Aug84	#1	-1.88	-2.32	-2.31	-79.54	-79.43
	#2	-1.53	-1.97	-1.96	-64.07	-63.93
10Aug84	#1	1.72	2.46	2.41	46.56	51.35
	#2	1.52	2.16	2.12	46.56	46.28
29Aug84	#1	-0.25	-0.81	-0.78	-7.52	-7.41
	#2	-0.24	-0.79	-0.76	-7.26	-7.13
	#3	-0.25	-0.80	-0.77	-7.29	-7.18
26Sep84	#1	0.22	0.48	0.46	7.98	7.88
	#2	0.24	0.49	0.48	8.54	8.47
	#3	0.30	0.56	0.55	10.59	10.53
30Oct84	#1	0.06	0.15	0.16	1.81	1.82
	#2	0.06	0.19	0.19	2.00	2.00
	#3	0.05	0.16	0.16	1.64	1.64
	#4	0.05	0.16	0.16	1.68	1.68

Table 8-16. Crosshore Transport Predicted by the u^6 and u^n Models

(Positive transport is onshore.)

Experiment		Transport [dynes/(cm-s)]					
		Madsen & Grant	with u_t	Shibayama & Horikawa	with u_t	Einstein	with u_t
23Jun80	#1	62.87	62.87	95.56	95.44	5172.	10591.
	#2	45.19	45.19	68.68	68.85	837.	5862.
	#3	31.53	31.53	47.92	48.14	88.7	3498.
	#4	27.57	27.57	41.91	42.07	32.0	4187.
11Aug80	#1	-5.40	-5.20	-8.20	-8.79	351.	23.1
	#2	-0.29	-0.28	-0.44	-0.67	88.4	71.3
	#3	0.41	0.39	0.62	0.46	25.1	142.6
	#4	0.45	0.43	0.68	0.52	8.63	142.6
	#5	0.41	0.39	0.62	0.46	1.85	110.4
	#6	0.36	0.35	0.54	0.37	0.44	71.3
12Sep80	#1	0.45	0.45	0.68	0.70	-0.00	306.2
	#2	0.17	0.17	0.26	0.30	-0.92	38.3
	#3	0.17	0.17	0.26	0.30	-0.00	84.2
	#4	0.12	0.12	0.19	0.20	-0.00	23.7
	#5	0.12	0.12	0.18	0.19	-0.00	23.7
	#6	0.18	0.18	0.27	0.29	-0.00	75.0
3Aug84	#1	-137.45	-137.45	-208.92	-208.84	-484.	-20097.
	#2	-105.41	-105.41	-160.22	-160.12	-120.	-18453.
10Aug84	#1	73.69	73.34	112.01	111.79	728.	21472.
	#2	68.86	68.53	104.67	104.47	163.	18204.
29Aug84	#1	-6.63	-6.48	-10.08	-10.02	-368.	-10684.
	#2	-6.26	-4.62	-9.52	-9.45	-82.9	-10684.
	#3	-6.16	-6.02	-9.37	-9.30	-19.5	-10684.
26Sep84	#1	8.12	7.92	12.34	12.27	247.	6944.
	#2	9.12	8.90	13.85	13.80	29.3	6635.
	#3	12.11	11.82	18.40	18.36	7.72	6866.
30Oct84	#1	2.17	2.13	3.30	3.30	0.00	720.
	#2	2.18	2.14	3.31	3.31	0.00	1195.
	#3	1.76	1.73	2.68	2.68	0.00	1015.
	#4	1.81	1.78	2.76	2.76	0.00	964.

Table 8-17. Longshore Transport Predicted by the u^3 Models

(Positive transport is to the north.)

Experiment		Transport [dynes/(cm-s)]		
		Bailard & Inman	Bailard & Inman with u_t	Kobayashi
23Jun80	#1	0.76	2.04	-5.32
	#2	-0.68	0.80	-5.68
	#3	0.20	1.06	-3.04
	#4	4.14	3.73	1.74
11Aug80	#1	-1.79	-0.08	-0.11
	#2	-2.22	-0.02	-0.07
	#3	-2.02	0.05	-0.05
	#4	-1.87	0.03	-0.08
	#5	-1.95	-0.02	-0.07
	#6	-2.17	-0.09	-0.08
12Sep80	#1	-1.32	-0.03	-0.08
	#2	-1.66	-0.06	-0.06
	#3	-1.82	-0.07	-0.05
	#4	-1.96	-0.08	-0.04
	#5	-2.06	-0.10	-0.04
	#6	-1.66	-0.07	-0.03
3Aug84	#1	-5.16	-3.94	-7.29
	#2	-6.63	-5.21	-7.24
10Aug84	#1	9.51	3.18	12.58
	#2	5.09	-0.32	11.20
29Aug84	#1	-9.14	-6.97	-2.87
	#2	-7.75	-5.97	-2.62
	#3	-7.28	-5.60	-2.85
26Sep84	#1	10.74	6.82	2.96
	#2	13.02	8.84	4.40
	#3	14.57	10.50	5.83
30Oct84	#1	2.13	1.46	2.89
	[illegible]	1.24	0.83	1.71
	#3	0.71	0.43	0.93
	#4	0.31	0.12	0.49

END

12-87

DTIC